©2021 Society of Economic Geologists, Inc.
Economic Geology, v. 116, no. 2, pp. 285–321

Geology, Structural Analysis, and Paragenesis of the Arrow Uranium Deposit, Western Athabasca Basin, Saskatchewan, Canada: Implications for the Development of the Patterson Lake Corridor

Sean Hillacre,[1,†] Kevin Ansdell,[1] and Brian McEwan[2]

[1]*Department of Geological Sciences, University of Saskatchewan, Saskatoon, Saskatchewan S7N 5E2, Canada*

[2]*NexGen Energy Limited, Suite 200, 475 2nd Avenue South, Saskatoon, Saskatchewan S7K 1P4, Canada*

Abstract

Recent significant discoveries of uranium mineralization in the southwestern Athabasca basin, northern Saskatchewan, Canada, have been associated with a series of geophysical conductors along a NE- to SW-trending structural zone, termed the Patterson Lake corridor. The Arrow deposit (indicated mineral resource: 256.6 Mlb U_3O_8; grade 4.03% U_3O_8) is along this trend, hosted exclusively in basement orthogneisses of the Taltson domain, and is the largest undeveloped uranium deposit in the basin. This study is the first detailed analysis of a deposit along this corridor and examines the relationships between the ductile framework and brittle reactivation of structures, mineral paragenesis, and uranium mineralization. Paragenetic information from hundreds of drill core samples and thin sections was integrated with structural analysis utilizing over 18,000 measurements of various structural features. The structural system at Arrow is interpreted as a partitioned, strike-slip–dominated, brittle-ductile fault system of complex Riedel-style geometry. The system developed along subvertical, NE- to SW-trending dextral high-strain zones formed syn- to post-D_3 deformation, which were the focus of extensive premineralization metasomatism (quartz flooding, sericitization, chloritization), within the limb domain of a regional-scale fold structure. These zones evolved through post-Athabasca dextral and sinistral reactivation events, creating brittle fault linkages and dilation zones, allowing for hydrothermal fluid migration and resulting uraninite precipitation and associated alteration (white mica, chlorite, kaolinite, hematite, quartz veins). This study of the structural context of Arrow is important as it emphasizes that protracted reactivation of deep-seated structures and their subsidiaries was a fundamental control on uranium mineralization in the southwestern Athabasca basin.

Introduction

The Proterozoic Athabasca basin in northern Saskatchewan is the primary location of uranium deposits and mines in Canada. Unconformity-related uranium deposits in the basin are among the highest-grade uranium deposits in the world, some of which are one hundred times the world average grade (World Nuclear Association, 2018). Although there have been past-producing mines in the western basin (i.e., Cluff Lake), most of the uranium exploration and mining activity over the last 50-plus years has been focused in the eastern portion of the basin (Fig. 1). Since the discovery of Rabbit Lake by Gulf Minerals Ltd. in 1968 (Sibbald, 1985), unconformity-related uranium deposits in the eastern Athabasca basin, such as the Cigar Lake, Eagle Point, and McArthur River deposits, have been well studied (e.g., Hoeve and Sibbald, 1978; Hoeve et al., 1980; Sibbald, 1985; Fayek and Kyser, 1993; Kotzer and Kyser, 1995; Quirt, 1999; Fayek et al., 2002; Jefferson et al., 2007; Alexandre et al., 2009; Mercadier et al., 2010; Cloutier et al., 2011). Unconformity-related uranium deposits conventionally host pods of mineralization just above, below, or along the unconformable contact between Proterozoic Athabasca Supergroup sandstones and the underlying basement rock and are typically associated with major graphitic structures that intersect the unconformity surface.

Although fewer in abundance, a number of significant deposits and prospects have been discovered in the western portion of the basin, including the Kianna deposit on the Shea Creek property south of Cluff Lake and Maybelle River in the far west (Fig. 1). Since 2012, exploration projects led by several companies in the southwestern part of the basin has been focused along the Patterson Lake corridor, which is a NE- to SW-trending geophysical feature delineated by a sequence of deep-seated conductors (Figs. 2, 3). This led to the discovery of the high-grade Triple R deposit in 2012 (87.76 Mlb at a grade of 1.82% U_3O_8 indicated; Fission Uranium Corp., 2018) and, subsequently the Arrow deposit by NexGen Energy Ltd., the latter being the focus of this study. In addition, the Bow, South Arrow, Cannon, Harpoon, and Spitfire prospects have been identified along the corridor. The Arrow deposit is the most significant recent discovery in the southwestern Athabasca basin and is the flagship discovery within NexGen Energy's Rook I property, approximately 75 km south of the past-producing Cluff Lake uranium deposits. The 21st hole drilled by NexGen Energy at the Rook I property, AR-14-001, intersected high-grade uranium at the Arrow target. AR-14-001 encountered multiple structural zones containing uranium mineralization, and at the time of drilling, no other holes existed within a 4-km radius. Akin to the Eagle Point uranium deposit in the eastern Athabasca basin, Arrow is a structurally controlled deposit, hosted entirely by crystalline basement rocks below the Athabasca Supergroup sedimentary rocks. The mineralized area of Arrow, as currently defined, is 308 m wide by 970 m in strike length, with mineralization starting at 110 m below surface and extending to 980 m. The Arrow deposit has an indicated mineral resource estimate of 256.6 Mlb U_3O_8 contained within 2.89 million tonnes (Mt) grading 4.03% U_3O_8, including a high-grade core of 181 Mlb U_3O_8 contained within 0.46 Mt grading 17.85% U_3O_8, and

†Corresponding author: e-mail, sean.hillacre@gmail.com

 Submitted: August 28, 2019 / Accepted: May 21, 2020

Downloaded from http://pubs.geoscienceworld.org/segweb/economicgeology/article-pdf/116/2/285/5245035/4797_hillacre_et_al.pdf
by Univ Nebraska Lincoln user

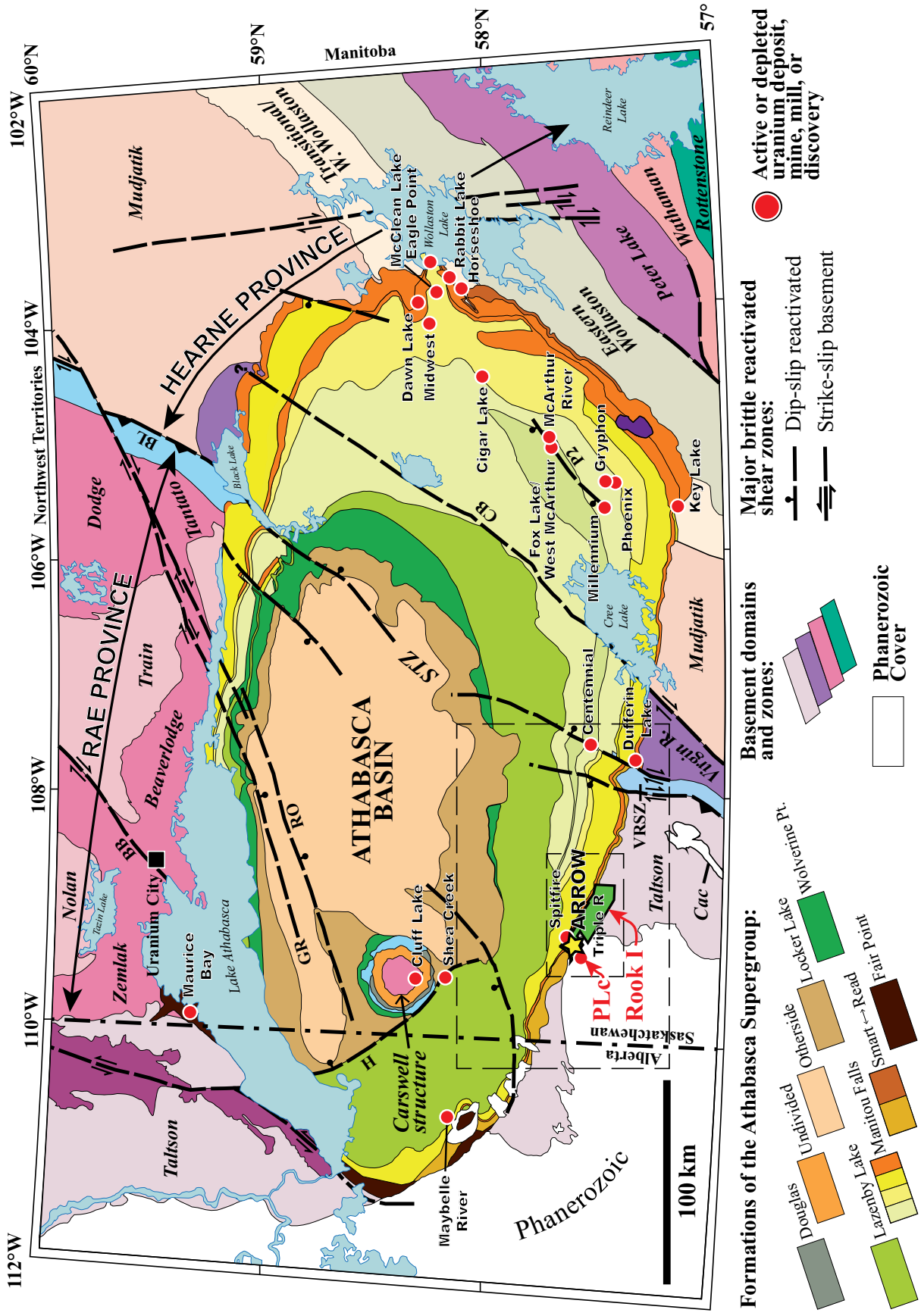


Fig. 1. Lithostructural domains of northern Saskatchewan and Alberta illustrating major components of the Churchill structural province of the Precambrian Shield, Athabasca basin geology, and overlying Phanerozoic cover. Note the location of the Rook I property and Clearwater anorthosite complex (Cac) within the Taltson domain, and with respect to the Snowbird tectonic zone (STZ), the Virgin River shear zone (VRSZ), the Grease River shear zone (GR), and the Cable Bay shear zone (CB). Athabasca basin unconformity-related uranium deposits are shown, with the Arrow deposit (yellow star) along the Patterson Lake corridor (PLc), as well as major brittle reactivated shear zones: BB = Black Bay, BL = Black Lake, CB = Cable Bay, GR = Grease River, H = Harrison, RO = Robillard, VRSZ = Virgin River shear zone. Modified from Jefferson et al. (2007). The locations of Figures 2 and 3 are shown as large and small dashed boxes, respectively.

Downloaded from http://pubs.geoscienceworld.org/segweb/economicgeology/article-pdf/116/2/285/5245035/4797_hillacre_et_al.pdf
by Univ Nebraska Lincoln user

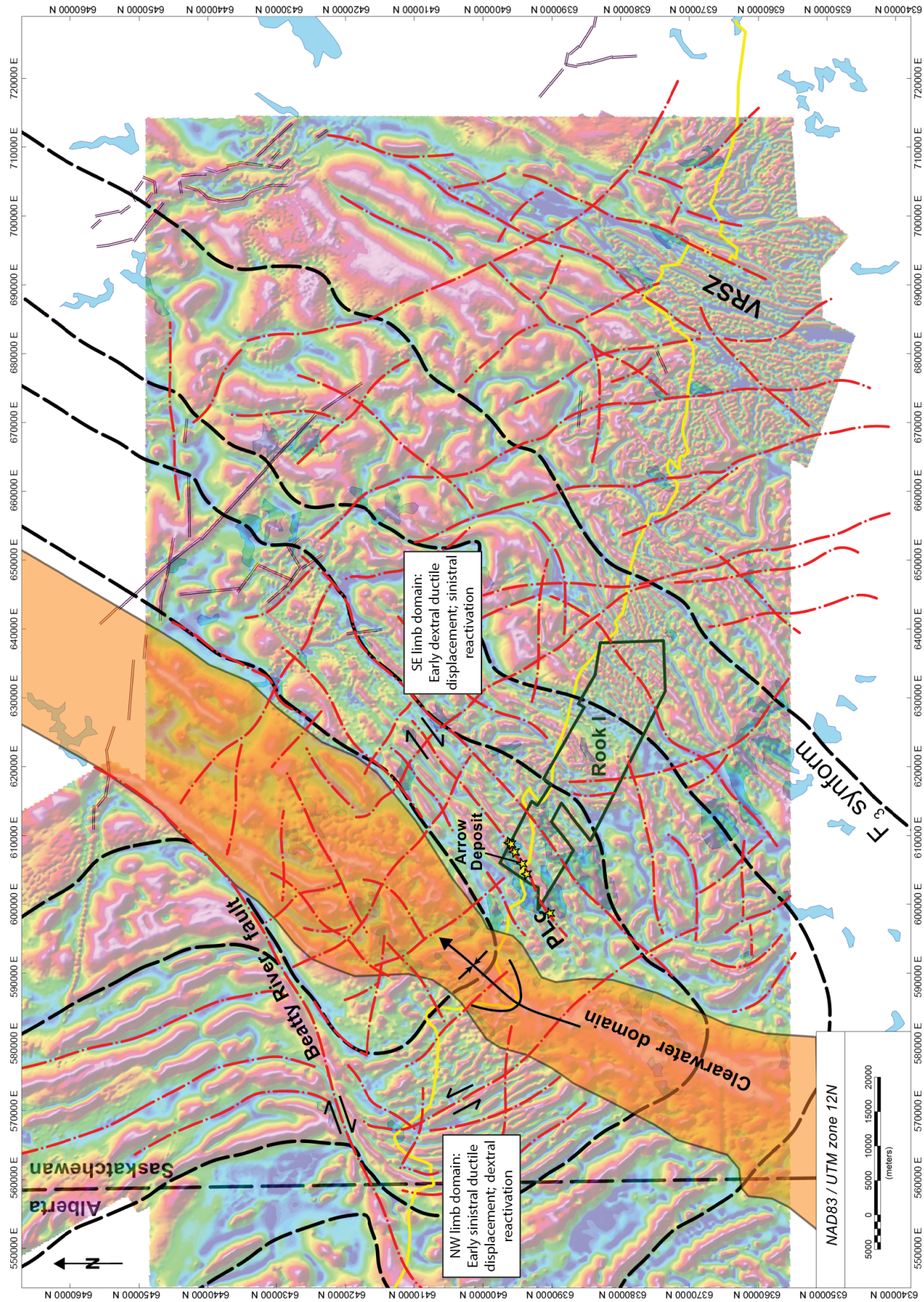


Fig. 2. Map illustrating regional structural geology interpretation based on stitched magnetic tilt geophysical surveys. Note the regional F_3 fold form lines (NE-plunging box-style synform; black dashed lines), interpreted crustal-scale structural corridors (conformable to or crosscutting fold limbs, and axial-planar; red dashed lines), dikes (purple double lines), Athabasca basin outline (yellow line), and the Clearwater domain (orange) following the interpreted F_3 synform axial trace (black line with arrow). NexGen's Rook I property is outlined in dark green. Note the aeromagnetic signature of the Virgin River shear zone (VRSZ), and the Arrow and Triple R deposits, and the South Arrow, Harpoon, Bow, and Spitfire discoveries (yellow stars) along the Patterson Lake corridor (PLc).

Downloaded from http://pubs.geoscienceworld.org/segweb/economicgeology/article-pdf/116/2/285/5245035/4797_hillacre_et_al.pdf
by Univ Nebraska Lincoln user

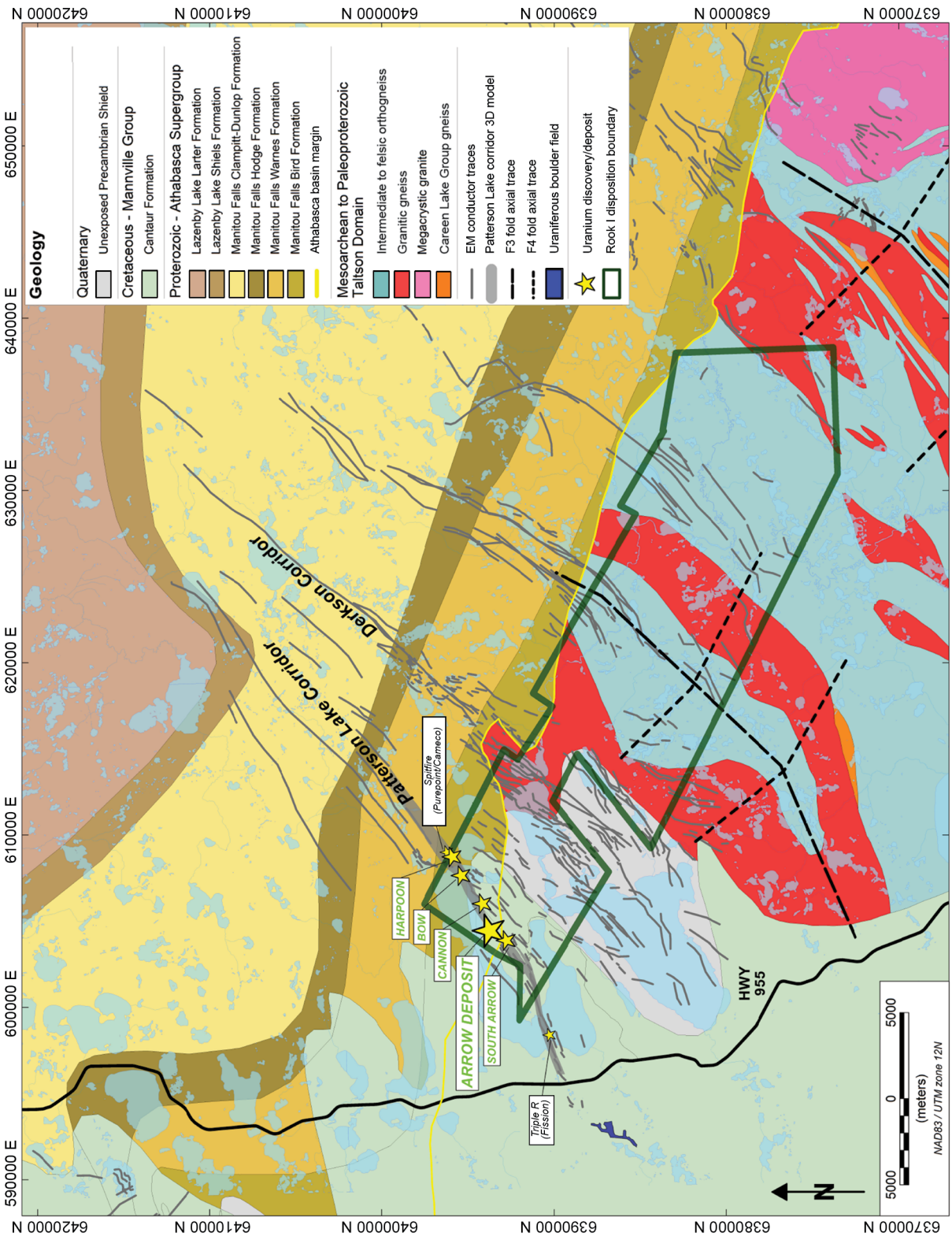


Fig. 3. Geologic map showing Taltson domain basement geology with generalized fold axial traces, as well as the overlying Athabasca Supergroup and Phanerozoic sedimentary geology of the southwestern Athabasca basin region. Geophysical electromagnetic (EM) conductors are shown, defining the Patterson Lake and Derkson corridors. The Arrow deposit lies along the Patterson Lake corridor, northeast along strike from the South Arrow uranium discovery and the Triple R deposit, and southwest along strike from the Harpoon, Bow, Cannon, and Spitfire uranium discoveries. Bedrock geology 1:250,000 shape files obtained from Saskatchewan Ministry of Energy and Resources (2019).

Downloaded from http://pubs.geoscienceworld.org/segweb/economicgeology/article-pdf/116/2/285/5245035/4797_hillacre_et_al.pdf
by Univ Nebraska Lincoln user

an inferred mineral resource estimate of 91.7 Mlb U_3O_8 contained within 4.84 Mt grading 0.86% U_3O_8 (O'Hara et al., 2018). It is thus the largest undeveloped uranium resource in the Athabasca basin and is currently second only to the McArthur River deposit in size.

The southwestern Athabasca basin has been the focus of intense exploration activity in the last few years; however, the characteristics and setting of uranium mineralization in the area are only beginning to be understood. This study examines the relationship between the ductile framework and brittle reactivation of structures, mineral paragenesis, and uranium mineralization at the Arrow deposit. A main goal of this study is to describe and characterize the effects and control of deep-seated structures and metasomatism on the development of these deposits. This study is the first comprehensive analysis of the structural and hydrothermal-metasomatic history, and paragenetic relationships of the largest known uranium deposit along the Patterson Lake corridor and may provide constraints on the origin and evolution of basement-hosted unconformity-related uranium deposits across the Athabasca basin.

Regional Geology

The Athabasca basin is situated in the Western Churchill structural province of the Canadian Shield, which is divided into the Rae province to the west and the Hearne province to the east, separated by the Snowbird tectonic zone (Fig. 1). Historically, the basement rocks south of the Athabasca basin and west of the Virgin River shear zone, where the Rook I property lies, have been termed the Western Granulite domain (Lewry and Sibbald, 1977) and the Lloyd domain (e.g., Card, 2009) and considered to be Archean in age. However, recent mapping, geochronology, and geophysical analysis in the Lloyd domain (e.g., Card, 2012a; Card et al., 2014) suggest that the rocks, and their metamorphic and structural history, are correlative with the 2460 to 1985 Ma rocks present within the Paleoproterozoic Taltson magmatic zone in Alberta and that these rocks extend below the southwest Athabasca basin (Fig. 1). This package of Taltson-aged rocks and plutons terminate against the MacDonald fault along the eastern shore of Great Slave Lake in the Northwest Territories and reemerge south of the southwest Athabasca basin, extending to the east where they are truncated by the Virgin River shear zone (Fig. 1; Hoffman, 1988; Ashton et al., 2009; Card et al., 2014, Tschirhart et al., 2020).

The Virgin River shear zone is a NE- to SW-trending segment of the Snowbird tectonic zone south of the Athabasca basin that separates the rocks of the Taltson and Virgin River domains and is demarcated by a 5- to 7-km-wide zone of mylonitic rocks (Fig. 2; Card, 2002; Card and Bosman, 2007). Rocks of the Taltson domain lie within the hanging wall of the Virgin River shear zone and are dominated by NNE- to ENE-striking, subvertical oriented granulite facies (M_1) intermediate orthogneisses (Card, 2009). A sample of a quartz dioritic orthogneiss from Lloyd Lake, southeast of the Rook I property, was dated by Card et al. (2014) using U-Pb SHRIMP analysis on zircon and yielded an interpreted crystallization age of 2459 ± 14 Ma, with a concordia age of 1899 ± 26 Ma, interpreted as a metamorphic overprint coincident with M_2 amphibolite facies metamorphism. Historically, Taltson domain rocks have been interpreted to be intercalated with gneissic charnockitic granites and Paleoproterozoic-aged metasedimentary psammitic and pelitic gneisses of the Careen Lake Group (Fig. 3; Card, 2009). However, more recent studies (e.g., Card et al., 2018) suggest that many of these metasedimentary rocks previously described in outcrop are of metasomatic origin and that true metasedimentary rocks may only comprise a few percent of the Taltson domain.

The Clearwater domain lies immediately west of the Rook I property, identifiable as a massive curvilinear NNE-trending aeromagnetic high feature that truncates the western boundary and overprints magnetic trends of the Taltson domain (Fig. 2; Tschirhart et al., 2020). It is interpreted as a structurally bound zone of weakly deformed K-feldspar–rich porphyritic granite and older granitoid gneiss (Sibbald, 1974; Card, 2002; Jefferson et al., 2007). U-Pb zircon geochronology on zircons from the porphyritic granites yielded a crystallization age of 1843 ± 4 Ma (Stern et al., 2003), suggesting that they are contemporaneous with the emplacement of Hudson granites ca. 1.85 to 1.82 Ga into the orthogneisses of the Taltson domain (Bickford et al., 1994; Peterson et al., 2002; Card, 2018).

As aforementioned, the basement rocks under the southwestern Athabasca basin were subjected to a protracted metamorphic and deformational history, involving multiple thermotectonic events. Taltson domain rocks underwent a high-grade metamorphic event of undefined age (M_0) prior to the emplacement of the Clearwater anorthosite complex ("Cac" in Fig. 1) ca. 2110 Ma (Card et al., 2014). Subsequently, a high-temperature metamorphic event (M_1) Paleoproterozoic in age, ca. 1.94 to 1.93 Ga (Stern et al., 2003; Card et al., 2018), reached upper amphibolite to granulite facies conditions in most parts of the Taltson domain in Saskatchewan and was accompanied by formation of a regional S_1 gneissosity (Card et al., 2007, 2014). The S_1 foliation is folded by isoclinal, intrafolial F_2 folds with an axial planar S_2 cleavage, resulting in the formation of a regional composite S_1-S_2 foliation. Characterizing the bulk of the domain is a gently SE-dipping S_1 foliation (Card et al., 2008, 2014), with a composite gneissic S_1-S_2 foliation defined by preferred orientation of pyroxene, biotite, and hornblende, supporting that it was imparted during M_1 metamorphism under granulite facies. This transposition foliation represents the dominant regional gneissosity of the Taltson domain. The presence of a garnet-clinopyroxene assemblage and a lack of hornblende in the least altered rocks suggest that these anhydrous granulites would have formed at temperatures above 850°C and at pressures below approximately 5 to 7 kbar (Card et al., 2014). The composite S_1-S_2 foliation has been subsequently folded and transposed into NE- to ENE-striking F_3 folds (Figs. 2, 3; Card, 2009). Realignment with the F_3-axial planar foliation resulted in a steeply dipping transposition foliation, which is intensified proximal to and within high-strain corridors such as the Virgin River shear zone. D_3 deformation was generally weak in the central Taltson domain but, where more intense within high-strain zones, it is accompanied by a significant amphibolite facies metamorphic (M_2) overprint (Card, 2009). The second phase of metamorphism (M_2) is interpreted to be synchronous with D_3 deformation at ca. 1.92 to 1.90 Ga (Stern et al., 2003; Card et al., 2014), resulting in amphibolite facies retrogression indicated by replacement

Downloaded from http://pubs.geoscienceworld.org/segweb/economicgeology/article-pdf/116/2/285/5245035/4797_hillacre_et_al.pdf
by Univ Nebraska Lincoln user

of granulite facies assemblages in the country rocks (i.e., replacement of orthopyroxene by biotite and magnetite in the quartz dioritic gneisses (Card, 2009) and replacement of pyroxene by amphibole (Card et al., 2014)). Furthermore, a lack of partial melt component (Card et al., 2014) corroborates that M_2 metamorphism occurred under amphibolite facies conditions below 650° to 700°C (e.g., Bucher and Frey, 1994). A third major thermotectonic event records midgreenschist facies metamorphism (M_3) coincident with the Trans-Hudson orogeny.

The Virgin River shear zone contains outcrop evidence for multiple displacement episodes under ductile, brittle-ductile, and brittle conditions. Brittle reactivation of the Virgin River shear zone along the Dufferin Lake fault is interpreted to have played a role in the formation of uranium deposits at the base of the Athabasca basin along this trend (Card et al., 2007; Reid et al., 2014). West from the Virgin River shear zone, lineaments trending in several orientations, including northeast, northwest, and west, likely represent late, brittle-ductile, and brittle fault zones with unknown displacements (Fig. 2; Card et al., 2014). Shear zone development linked to F_3 folding is widespread in the Cable Bay straight belt (Fig. 1), and analogous structures are common in the Taltson domain (Figs. 2, 3) as described by Card (2009).

The present-day Athabasca basin is an erosional remnant, which covers most of northern Saskatchewan and extends into northern Alberta, of a large Paleoproterozoic-Mesoproterozoic sedimentary basin (Fig. 1; Ramaekers et al., 2007). At the center of the basin, the Athabasca Supergroup sandstones have a preserved maximum depth of approximately 1,500 m thick (Ramaekers, 1979, 1980; Tremblay, 1982). The basin consists of a series of mainly continental, unmetamorphosed siliciclastic sedimentary rocks, predominantly sandstone, of the Athabasca Supergroup (Fig. 1; Bosman and Ramaekers, 2015). They were deposited during the period of ca. 1710 to 1500 Ma, accommodated by subsidence of three spatially overlapping subbasins: Jackfish, Cree, and Mirror (Ramaekers et al., 2007; Jeanneret et al., 2017). The oldest subbasin, Jackfish, is defined by a NE-trending trough in the westernmost Athabasca basin, whereas the above-lying Cree and Mirror subbasins are recognized as EW-trending saucer-shaped basins (Ramaekers et al., 2007). Below the Athabasca basal nonconformity with crystalline basement rock, basement rocks commonly exhibit a bleached zone (white zone), red hematite-stained zone (red zone), mixed hematite- and chlorite-altered zone (red-green zone), and a chlorite zone (green zone) where mafic and feldspathic minerals have been altered to chlorite. This has been interpreted to represent a paleoregolith and/or paleoweathering profile that has been overprinted by diagenetic and/or hydrothermal fluids (MacDonald, 1980; Adlakha et al., 2014).

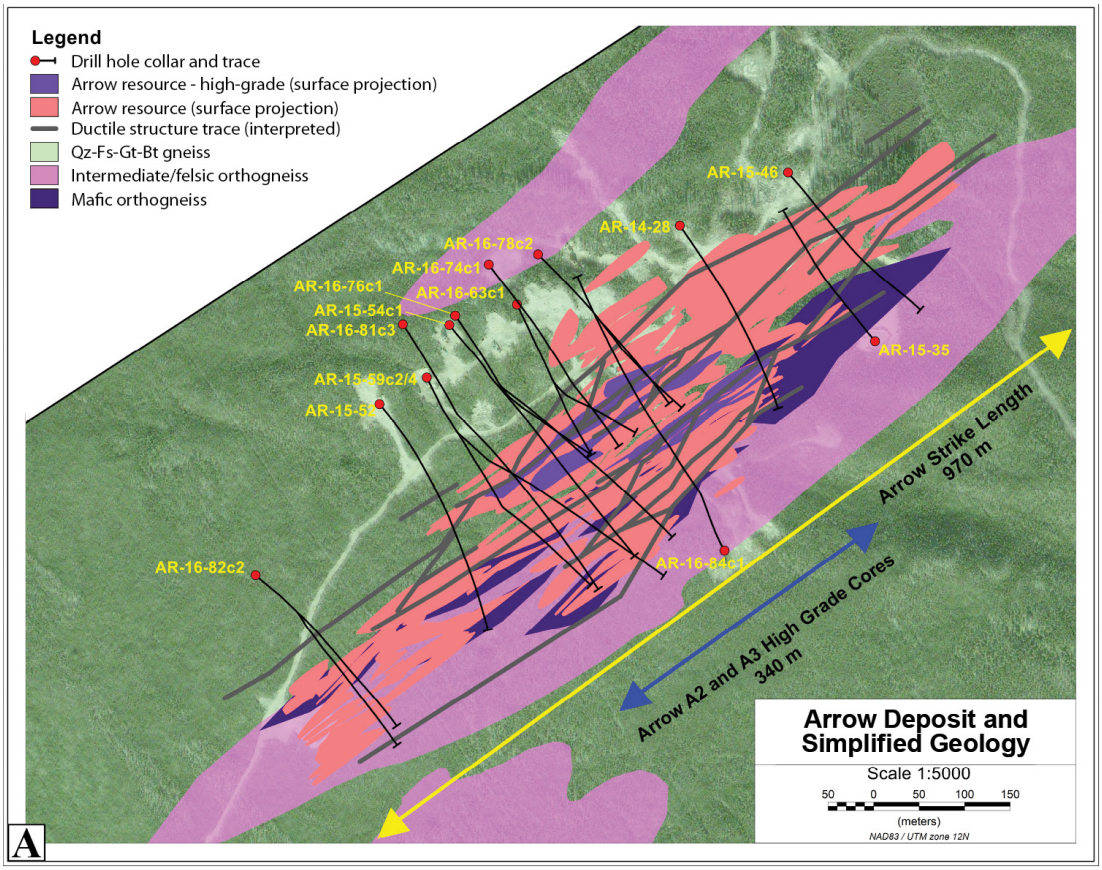
Patterson Lake Corridor and Arrow Deposit Geology

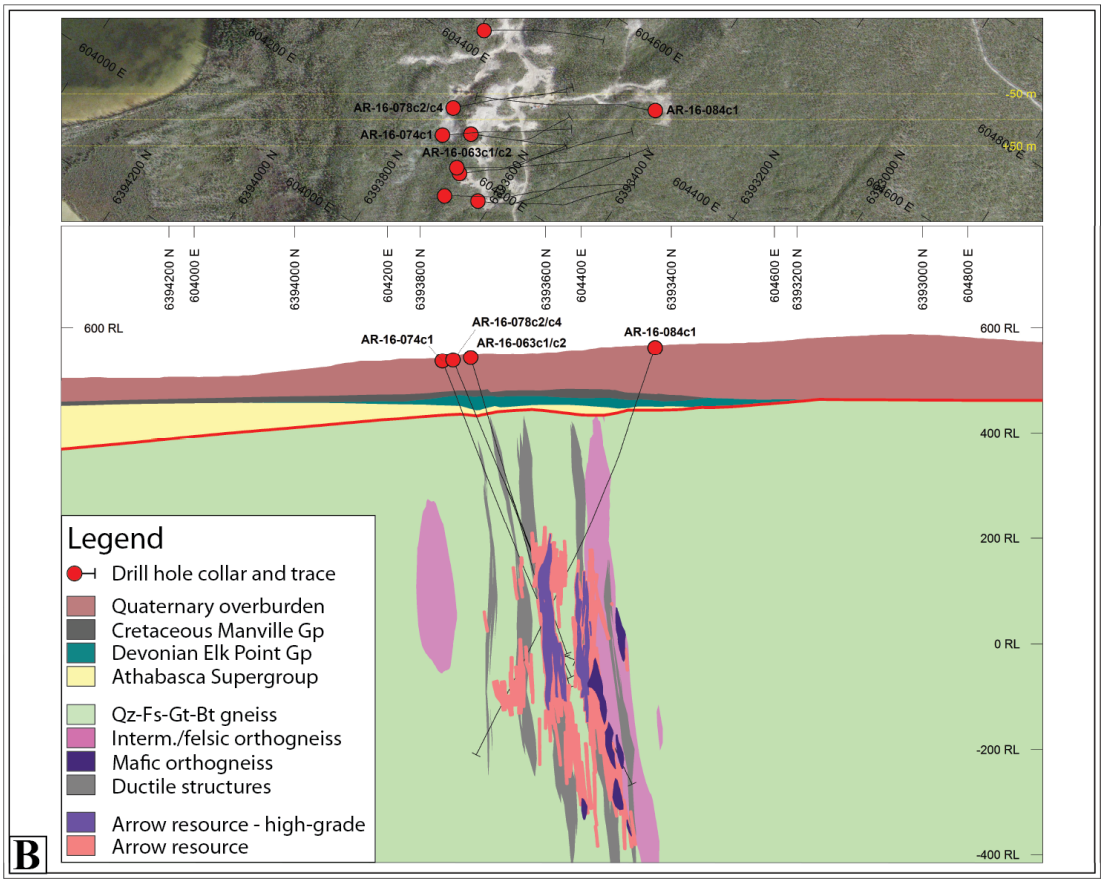
The Arrow deposit is hosted within Paleoproterozoic basement rocks of the Taltson domain, consisting dominantly of upper amphibolite to granulite facies orthogneiss (Fig. 3; e.g., Card, 2017). The crystalline basement rocks, in which the Patterson Lake corridor is rooted, comprise a spectrum of variably altered mafic to ultramafic, intermediate, and local alkaline rock types. Fresh examples of any of these rock types are notably rare, as they are overprinted by protracted episodes of deformation and metasomatism. The most abundant basement rock types consist of gneissic, metasomatized feldspar-rich granitoid rocks and dioritic to quartz dioritic and quartz monzodioritic gneiss, with subordinate granodioritic and tonalitic gneiss (Card et al., 2018). Localized minor rock types encountered along the Patterson Lake corridor include weakly foliated or schistose ultrabasic rocks, amphibolite, porphyroblastic feldspar-rich syenite, granitic and syenitic anatectic pegmatite, migmatite, and relatively young mafic and alkaline intrusive rocks (Card and Noll, 2016). The latter have been identified in drill core along the Patterson Lake corridor to the northeast of the Arrow deposit, including calcite-rich, xenolith-bearing carbonatite-like rocks (Card, 2017) and medium- to coarse-grained, white-green clinopyroxenite (Card, 2018). These form part of the Patterson Lake Alkaline Igneous Complex, which postdate regional metamorphism and is typically associated with alkalic metasomatism of wall rocks, resulting in halos of fenitic alteration (Card, 2018; Hillacre, 2018). The spatial association of the dike rocks and associated alteration with discrete high-strain zones indicates a link to these structures, suggesting that the alteration zones acted as nucleating sites for high-strain zones and/or that alkaline magma flowed along these conduits, reusing them as the path of least resistance.

The dominant host rock of the Arrow deposit is porphyroblastic, weakly to moderately gneissic and/or augen textured, pervasively quartz-flooded quartz-feldspar-garnet-biotite ± graphite gneiss (Fig. 4A, B), which has historically been called "semipelitic gneiss" in the region. It consists of approximately 30 to 80% blue quartz, 15 to 20% potassium feldspar (commonly replaced by white mica), 10 to 30% garnet (commonly replaced by chlorite), 1 to 10% graphite, and 1 to 5% biotite (Fig. 5A). Accessory minerals include sillimanite, tourmaline, and rutile/anatase. This rock type is extensive within the Arrow locality, hosting over 50% of the deposit (Fig. 4A, B), and exhibits a wide range of alteration styles and intensities (Fig. 5A, B). The origin of this rock type has been a recent topic of study, with both metasedimentary and metasomatic origins proposed. Historically, the rock has been interpreted to be of metasedimentary origin, as the mineral assemblage resembles that observed in metapelites (i.e., presence of garnet, graphite, sillimanite). Based on more recent studies (e.g., Card, 2017,

Fig. 4. A) Arrow plan map showing simplified basement geology projected to the unconformity surface (red horizon in Fig. 4B), simplified graphitic structure traces, and drill hole collars and traces for 18 representative holes selected for components of this study. Resource outline from O'Hara et al. (2018). B) Schematic northwest-southeast cross section looking northeast (057°) showing orthogneisses unconformably overlain by Athabasca Supergroup sandstones, Devonian rocks, Cretaceous rocks, and Quaternary glacial deposits, along with the Arrow deposit resource outline (O'Hara et al., 2018) and 3-D modeled ductile structural zones. The wide extent of the quartz-feldspar-garnet-biotite gneiss reflects limited drilling peripheral to Arrow, and the vast influence metasomatism has played along the Patterson Lake corridor. Abbreviations: Bt = biotite, Fs = feldspar, Gt = garnet, Qz = quartz.

Downloaded from http://pubs.geoscienceworld.org/segweb/economicgeology/article-pdf/116/2/285/5245035/4797_hillacre_et_al.pdf
by Univ Nebraska Lincoln user





Downloaded from http://pubs.geoscienceworld.org/segweb/economicgeology/article-pdf/116/2/285/5245035/4797_hillacre_et_al.pdf
by Univ Nebraska Lincoln user

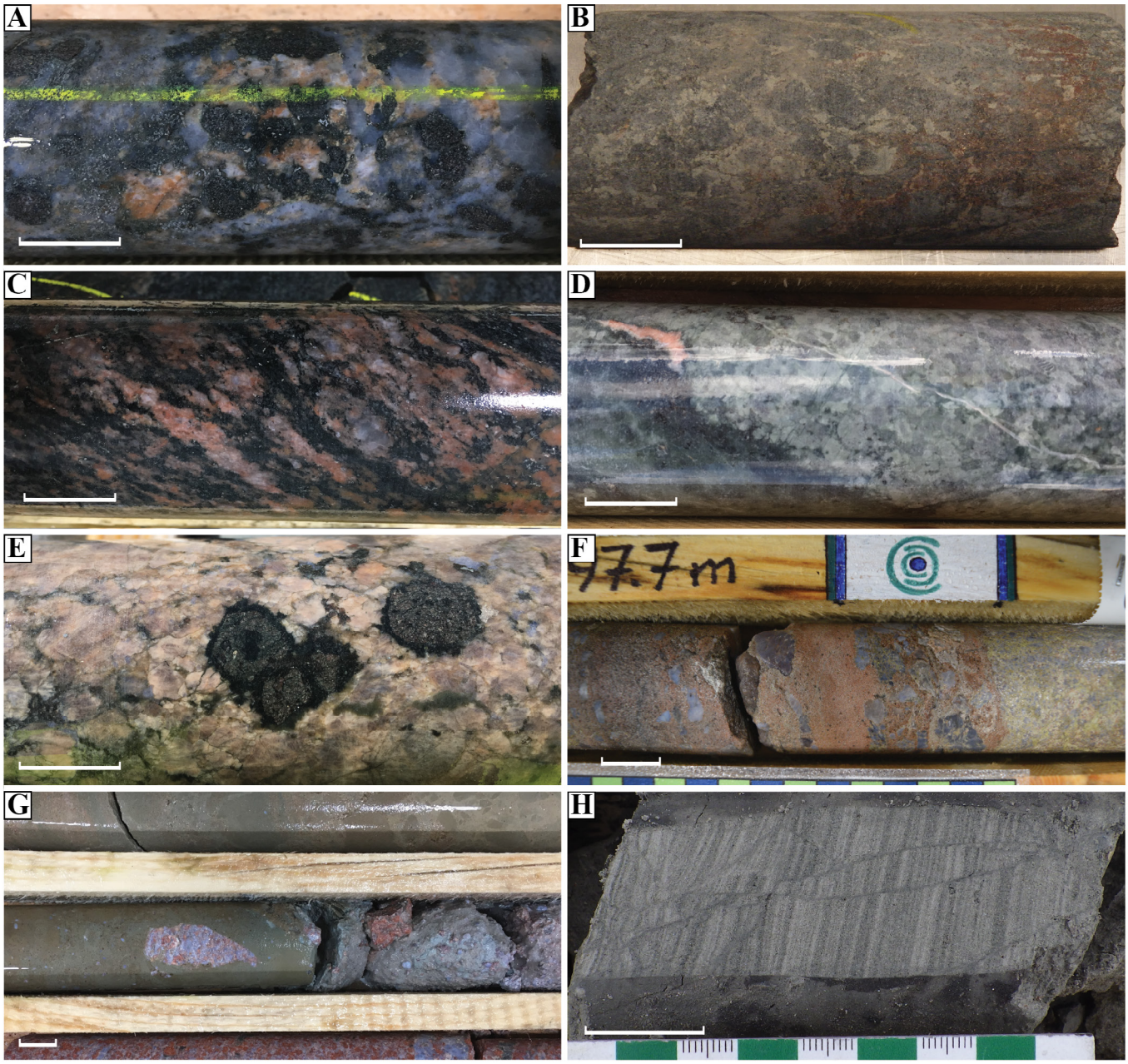


Fig. 5. A) NQ (47.6 mm diam) drill core photo of porphyroblastic quartz-feldspar-garnet-biotite gneiss exhibiting weak chloritization of garnets and trace albitization of K-feldspar (NQ, GAR-18-008, 580.9 m). B) Strongly sericite and chlorite altered quartz-feldspar-garnet-biotite gneiss lacking silicification proximal to the A2 shear, hosting U mineralization and associated hematite alteration (NQ, AR-15-059c2, 506.8 m). C) Relatively unaltered quartz monzonitic gneiss (AR-18-215c1, 647.0 m). D) Contact of a massive, medium-grained green-white clinopyroxenite associated with alkali alteration related to fenitization (NQ, HP-16-020, 251.2 m). E) Coarse-grained syenitic rock with biotite masses replacing perthitic K-feldspar. Subhedral to euhedral garnet porphyroblasts are overgrowing secondary biotite masses (NQ, HP-16-018, depth not recorded). F) Conglomeratic unconformity between Athabasca Supergroup sandstone and Taltson basement rock (NQ, AR-18-212c1, 97.7 m). G) Unconformable contact between Devonian Meadow Lake Formation sandstone and Taltson basement rock (NQ, AR-18-211c1, 102.5 m). H) HQ (63.5 mm diam) core photo of planar, interbedded Cretaceous Cantuar Formation sandstones and mudstones with normal microfaults (GAR-18-010, 30.1 m). White scale bars are 20 mm.

2018; Onstad et al., 2017) and work detailed in this study, more comprehensive observation of the paragenetic and textural relationships suggests a metasomatic origin through alteration and overprinting of a feldspathic igneous protolith (i.e., the metapelite mineral assemblage was not in equilibrium, evidenced by crosscutting and grain boundary relationships). Such relationships include red-purple garnet porphyroblasts, possibly of almandine to pyrope composition, clearly overgrowing primary feldspar grains or secondary prismatic sillimanite, and graphite, which is strongly controlled by structure

Downloaded from http://pubs.geoscienceworld.org/segweb/economicgeology/article-pdf/116/2/285/5245035/4797_hillacre_et_al.pdf
by Univ Nebraska Lincoln user

and overgrows other minerals. Although this rock type, which comprises the dominant uranium mineralization host rock at the Arrow deposit, has been referred to as semipelitic gneiss in the past, the best interpretation is that the rocks that host the Arrow deposit are dominated by orthogneisses.

The other rocks in the vicinity of the Arrow deposit include intermediate orthogneisses (Fig. 5C) consisting of quartz monzodioritic to quartz dioritic gneiss with subordinate tonalitic, granodioritic, and granitic gneiss, mafic orthogneisses, and minor alkaline clinopyroxenite (diopsidite; Fig. 5D), syenite, and granitic pegmatites (Fig. 5E). The main fabrics and contacts of crystalline basement rocks in the Arrow deposit area are all steeply dipping (Fig. 4B), with a northeast to southwest strike.

Northeast- to SW-striking, relatively quartz poor, low- to medium-grade mylonites and phyllonites (termed the A1 to A5 shears within the Arrow deformation zone; "ductile structures" in Fig. 4B) correlate with interpreted geophysical electromagnetic (EM) conductors across the property (Fig. 2) and locally host uranium mineralization within the Arrow deposit (Fig. 4A, B). They exhibit variable deformational textures and a range of mineralogical composition, consisting of variable proportions of chlorite, biotite, white mica, graphite, sulfides, and deformed quartz.

The crystalline basement rocks that host the Arrow deposit are unconformably overlain by flat-lying Athabasca Supergroup sandstones (Fig. 4B). The Athabasca sandstones are planar and crossbedded, poorly sorted, medium- to coarse-grained, quartz arenite to conglomeratic sedimentary layers of the Bird Formation of the Manitou Falls Group (Fig. 5F; Bosman and Ramaekers, 2015) and exhibit a variety of alteration features such as bleaching (i.e., depletion of Fe content), quartz dissolution and complete friability, silicification, and clay alteration. The alteration profiles in the Athabasca Supergroup in the Patterson Lake area are similar to alteration halos observed above and around uranium deposits in the eastern section of the basin, although they are generally not as intense or widespread due to the depth of mineralization relative to the unconformity. Directly above the Arrow deposit, alteration in the sandstones increases with proximity to the upward propagation of structures into the overlying Athabasca Supergroup.

The Athabasca Supergroup sandstones are overlain by a series of Phanerozoic and Quaternary rock types and deposits of variable thickness (Fig. 4B). Where Athabasca sandstone cover is thin toward the southern edge of the Rook I property, basement rocks are unconformably overlain by Devonian (Fig. 5G) or Cretaceous sedimentary rocks.

The Lower to Middle Devonian Elk Point Group sequences are made up of two distinct units. The most basal Devonian rocks are of the La Loche Formation, consisting of regolithic, poorly sorted breccia with clasts of older Athabasca sandstone and/or basement rock and fine- to coarse-grained, white to medium brown-gray arkosic sandstone and conglomeratic sandstones (Norris, 1963; Bosman et al., 2018). The La Loche Formation grades into the Meadow Lake Formation, which consists of poorly sorted, green to red, fine- to coarse-grained sandstones with carbonate cement (Bosman et al., 2018; Fig. 5G).

Cantuar Formation rocks of the Lower Cretaceous Mannville Group overlie Devonian sequences where present. They consist of green-gray to black, very fine to medium-grained sandstone interbedded with fissile mudstones, and fine- to coarse-grained, crossbedded beige sandstone with minimal mudstone (Bosman et al., 2018; Fig. 5H). The latter is commonly saturated with bitumen and often contains centimeter- to decimeter-scale coal beds. The distribution of the Cretaceous strata in the area is widespread; however, the Devonian sequences appear to be somewhat restricted to areas overlying the known uranium deposits in the area (i.e., Arrow, Triple R) suggesting that underlying structural controls affected deposition well into the Phanerozoic (Bosman, 2017). Furthermore, elevated uranium concentrations and clay alteration within the Phanerozoic stratigraphy may indicate the presence of late mobile uranium in the Patterson Lake area, thus allowing for the potential for lower-grade sandstone-hosted deposits (Bosman, 2017).

The geologic sequence of the Patterson Lake corridor is capped with Pleistocene glacial till overburden (Fig. 4B). The glacial tills are typically 20 to 50 m thick and contain variable amounts of sand and clay minerals. NE- to ENE-trending drumlins are common, as are outwash plains and hummocky terrain. Glacial striations on exposed outcrops in the Rook I area also indicate a general ice direction movement to the southwest (Sykes et al., 2014).

Methods and Sampling

Structural data—oriented diamond drill core measurements

The methods used for structural analysis include interpretations of individual structural measurements obtained from 139 oriented diamond drill holes completed during drill programs up to the end of 2016. Measurements are comprised of alpha, beta, and gamma angles of structural features, following the techniques outlined by Holcombe Coughlin and Associates (2007). The working data set is composed of more than 18,000 measurements in total, with an average of one foliation and at least one brittle and/or ductile structural measurement taken every 3 m of drill core, with more structures measured in areas of importance (e.g., fault zones, high-strain zones) and fewer structures measured in structurally quiescent areas.

For quality assurance (QA), the working data set was composed of measurements taken from a minimum of two consecutive 3-m-long drill core runs that were oriented with a bottom-of-hole reference line and an allowable range of ±30° beta rotation from either reference line. The beta rotation criterion was put in place to ensure data used in this study were as reliable as possible without bias or mistakes introduced by human error during the orientation process at the drill site (i.e., core barrel rotation) and/or data collection by field geologists. Any oriented structural data that did not comply with the QA stipulations were disregarded for use in this study. All 139 drill holes included in the working structural data set were created as borehole traverses in RocScience DIPS v.06 software (DIPS), which allows for application of Terzaghi weighting to oriented structural data and can eliminate the need to convert alpha and beta measurements to strike and dip prior to stereographic projection. The Terzaghi method involves application of a correction factor to each feature and subsequent stereographical analysis on the weighted data set

Downloaded from http://pubs.geoscienceworld.org/segweb/economicgeology/article-pdf/116/2/285/5245035/4797_hillacre_et_al.pdf
by Univ Nebraska Lincoln user

(Terzaghi, 1965), resulting in more representative structural trends through noise reduction and accounting for drill hole bias. Following QA filtering and confidence level assignment, structural data was stereographically assessed with DIPS software on lower hemisphere Schmidt equal-area stereonets. Statistical contouring of orientation clustering, mean orientation and confidence calculation, cluster variability, kinematic analysis, and qualitative and quantitative feature attribute analysis were computed in DIPS software.

Mineralogical and textural data—hand sample, thin section, and backscattered electron (BSE) microscopy

Approximately 400 samples of unaltered, altered, and mineralized rocks were collected from 18 representative drill holes that intersect the deposit (Fig. 4A, B). A combination of hand sample examination, thin section microscopy, and electron microprobe analysis (EMPA) has been used to generate a detailed paragenesis of the Arrow deposit. A suite of 50 thin sections containing representative paragenetic relationships were examined using transmitted and reflected optical microscopes. Select thin sections were also examined using BSE microscopy on a JEOL 8600 Superprobe electron microprobe analyzer, housed at the Electron Microscopy Laboratory in the Department of Geological Sciences, University of Saskatchewan. Uraniferous minerals and certain silicate and sulfide minerals were analyzed using wavelength dispersive spectrometry. Mineral abbreviations used throughout the paper are from Whitney and Evans (2010).

Radioactivity measurements quoted in all figures and captions were made with Radiation Solutions RS-120 and RS-125 handheld gamma-ray scintillometers and spectrometers, respectively, and are reported in counts per second (cps). Both the RS-120 scintillometers and RS-125 spectrometers feature large detectors for high sensitivity, using a large 2.0 × 2.0 Nal crystal (103 cm^3) and provide a direct survey readout of gamma-ray radiation in counts per second. Additionally, the RS-125 spectrometer also provides a direct assay readout in % K, ppm U, and ppm Th, and is autostabilizing on naturally occurring radioactive elements (K, U, and Th), eliminating the requirement for test sources.

Structural Analysis

Regional structural context

Multiple phases of deformation and related sets of structures have been recognized in the Taltson domain rocks hosting the Arrow deposit. As discussed above, D_1 through D_3 events resulted in formation of a broadly NE-striking and SE-dipping structural grain, multiple generations of folds, and ductile to brittle-ductile high-strain zones postpeak metamorphism and syn- to late-D_3. Subsequent post-Athabasca deformation episodes reactivated ductile basement structures and formed brittle structures also affecting Athabasca Supergroup sedimentary rocks. Along the Patterson Lake corridor, known zones of uranium mineralization are hosted within reactivated basement structures both outside (e.g., Triple R deposit) and just within the southwestern margin of the Athabasca basin (e.g., Arrow deposit).

Regionally, the Arrow deposit lies within the southeast limb domain of a regional NE-plunging box fold-style synform (Fig. 2), and thus general gneissosity and basement lithological contacts at Arrow dominantly dip southeast with a general northeast strike. In contrast to the gently dipping S_1-S_2 foliation observed across the Taltson, the composite foliation at Arrow is transposed subparallel to the S_3 fabric contemporaneous with D_3 deformation, manifested through the Arrow deformation zone as a subvertical and anastomosing, steeply SE-dipping S_1-S_3 transposition foliation. Taltson S_1-S_2 foliations were transposed during deformation events along the Patterson Lake corridor, creating the steeply dipping, F_3 axial planar foliations observed through the Arrow deformation zone (Arrow stereonet in Fig. 6). Variability in the dip direction of the S_1-S_3 fabric increases through the core of the deposit, shifting locally to the northeast and thus creating the mirrored pole distribution of Arrow foliation measurements, visible on the Arrow deposit stereonet in Figure 6. Along strike of the Patterson Lake corridor, foliation dip angles shallow out, dipping moderately to the southeast at the Harpoon (northeast along strike) and South Arrow (southwest along strike) discoveries (Fig. 6), illustrating a higher degree of structural disturbance and thus transposition at Arrow. Oblique axial-planar brittle fracturing or crenulations are observable within drill core-scale F_3 folding and local high-strain folds; however, in most cases axial planar foliation in these folds cannot be distinguished from the main foliation.

The composite foliation observed at Arrow contains a subhorizontal stretching lineation related to deformation, parallel to the longest axis (X) of the finite strain ellipsoid related to high strain along the Arrow shear zones. Figure 7A is a stereographic projection of true stretching lineations measured from foliation surfaces throughout the Arrow deformation zone. The stereonet defines clusters of shallow-plunging lineations dominantly to the northeast and southwest, with weaker trends to the northwest and southeast. The term "stretching lineation" has genetic implications, as it refers to aggregates or single crystals that have been deformed by stretching. Since elongate crystals can also form normal to the stretching direction through boudinage or vein formation (Passchier and Trouw, 2005), care has been taken to distinguish true stretching lineations, which represent the strain x-axis (Fig. 7B, C). In addition to ductile lineations, a variety of fold structures are observable at drill core scale, fractally reflecting deposit- and regional-scale structures, as well as providing information about the formation of the Arrow high-strain zones.

Arrow deformation zone geometry—A1 to A5 high-strain zones

The high-grade uranium lenses at Arrow are situated below the Athabasca basement unconformity in variably metasomatized and hydrothermally altered orthogneisses cut by a series of heterogeneous ductile to semiductile shears. These high-strain zones, which constitute the portion of the Patterson Lake corridor that hosts the Arrow deposit, are named the A1 through A5 shears in the deposit locality. The A1 through A5 shear zones are defined by a series of stacked, near-vertical, NE-striking low- to medium-grade mylonites and phyllonites, extending to at least a kilometer depth below surface. The major high-strain zones (047°/86°) are separated by relatively unstrained, silicified blocks of wall rock, and connected by NE-SW– (239°/89°) and NNE-SSW–trending (208°/86°)

Downloaded from http://pubs.geoscienceworld.org/segweb/economicgeology/article-pdf/116/2/285/5245035/4797_hillacre_et_al.pdf
by Univ Nebraska Lincoln user

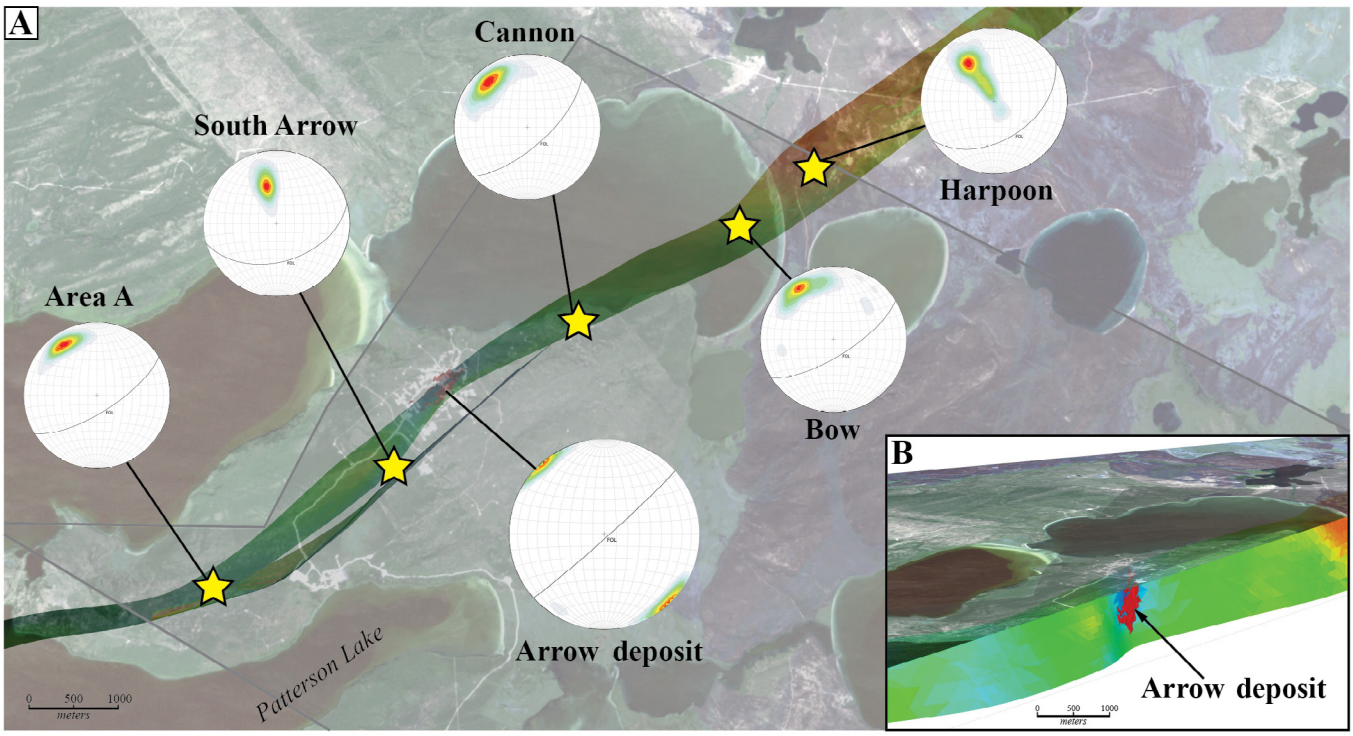


Fig. 6. Plan view (A) and perspective view (B) looking north-northwest (013°) of a 3-D structural model of the Patterson Lake corridor constructed using 3-D Maxwell plate electromagnetic geophysical data and oriented drill core data from the Arrow deposit, and South Arrow, Harpoon, Bow, Cannon, and Area A uranium showings (stereonets shown). Variability in dip angles along the corridor is highlighted by warm colors (shallow dip) and cool colors (steep dip). The geometry of the corridor illustrates the steepening of regional S_1-S_2 foliation at Arrow due to transposition with S_3 foliation during deformation. The Rook I property boundary is outlined in gray. Mean dip and dip direction: Area A (n = 617) = 71°/148°; South Arrow (n = 1,882) = 46°/164°; Arrow Deposit (n = 3,513) = 87°/138°; Cannon (n = 425) = 68°/138°; Bow (n = 354) = 71°/148°; Harpoon (n = 546) = 45°/147°.

oblique shear bends and flexures (Fig. 8). The prevailing ductile structural grain defining the Arrow high-strain zones is subvertical and anastomosing subparallel to the S_1-S_3 transposition foliation and contains a well-defined subhorizontal stretching/extension lineation, as discussed above. Restraining (transpressional) and releasing (transtensional) bends of the Arrow strike-slip deformation zone are evident in the 3-D modeled structural geometry (Fig. 8). Stereographic projection of all high-strain zone shear fabric measurements taken from Arrow drill core also reveals a weaker west-northwest to east-southeast trend (Fig. 8), reflecting local folding of shear fabrics, S fabrics, and linkages between shear zones. The principal flattening surfaces of the A1 through A5 shear zones shift in strike along the length of the deposit while dip remains subvertical, and zones of uranium mineralization are largely bound by oblique shears (Fig. 8).

Shear zone classification, characteristic fabrics, and shear sense indicators

The heterogeneous strike-slip deformation zone hosting the Arrow deposit contains a spectrum of highly strained rocks. Different authors have classified highly deformed rocks in different ways, based on mineralogy (e.g., quartz-feldspar mylonite), on the metamorphic grade at which the structure formed (e.g., high-grade mylonite), or on relative porphyroclasts and matrix percentages (e.g., Schmid and Handy, 1991). Problems with these classifications are attributed to the variety of different mylonitic rocks that can be formed under the same conditions from different parent rocks and the arbitrary choice of matrix percentages between mylonite classes. For the purposes of this paper, the highly strained rocks within the Arrow deformation zone will be described based on type and completeness of recrystallization, matrix content, and micaceous mineral content. The Arrow A1 through A5 high-strain zones are dominantly composed of low- to medium-grade mylonites, with local high-grade mylonites and phyllonites. These strongly deformed rocks are overprinted by abundant brittle fault rocks, described in the "Brittle Fault Rocks" section of this paper.

The mylonitized rocks comprising the A1 through A5 shears are characterized by the presence of a moderate to strong LS fabric, a relatively fine grained matrix with porphyroclasts, close to isoclinal high-strain and parasitic folding (e.g., Fig. 9A), mantled porphyroclasts (Fig. 9A, B), asymmetric structures including C-type (cisaillement) and C'-type shear bands (Fig. 9C-E), augen texture (Fig. 9A, B), stair-stepping and oblique foliations, and ribboned, folded, and variably recrystallized quartz (Fig. 9E). The high-strain zones at Arrow trend northeast to southwest, with zones of highest strain (i.e., C fabrics) oriented subparallel and oblique to the main S_1-S_3 transposition foliation. Like the main foliation, the shear fabric measurement poles exhibit a distribution across the stereonet due to their subvertical, anastomosing nature (Fig. 8). C-type shear bands observed in drill core are relatively straight

Downloaded from http://pubs.geoscienceworld.org/segweb/economicgeology/article-pdf/116/2/285/5245035/4797_hillacre_et_al.pdf
by Univ Nebraska Lincoln user

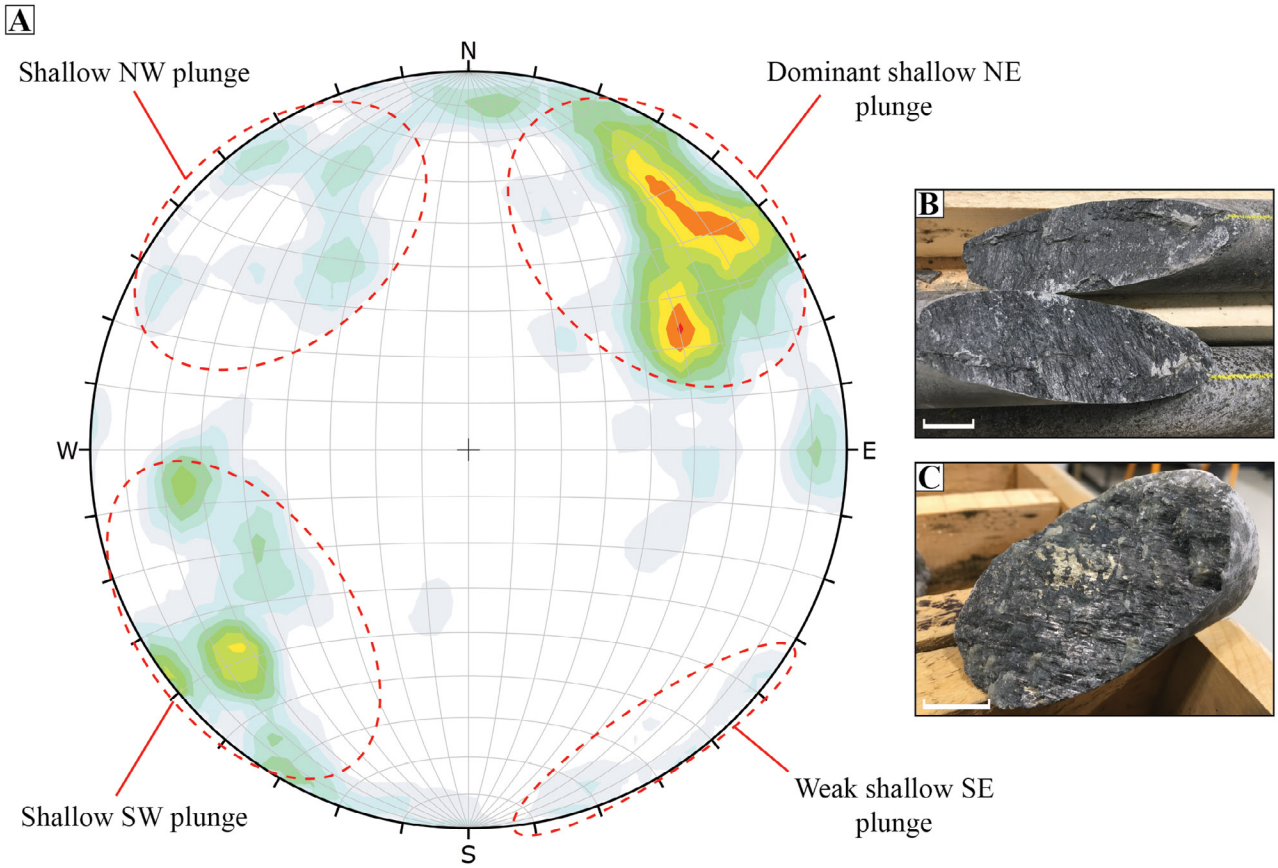


Fig. 7. A) Schmidt equal-area stereographic projection of all ductile stretching/extension lineations measured from oriented Arrow drill core within foliation planes. n = 367. B) Subhorizontal ductile lineations in chlorite along a foliation plane in Arrow NQ drill core (AR-18-210c3, 560.0 m). C) Oblique ductile lineations in chlorite along a foliation plane in Arrow NQ drill core. Relatively late, undeformed sulfide mineralization is present along foliation-parallel fracture (GAR-18-007, 489.4 m). Both drill holes were collared at approximately –70° dip orthogonal to the structural grain containing the lineation. Yellow line on core is bottom-of-hole orientation mark. Scale bars in B and C are 20 mm.

and lie parallel to the shear zone boundary, dipping steeply and often subparallel or oblique to core axis (Fig. 9D). C'-type shear bands are oblique to shear zone boundaries and the older foliation (S fabrics), and commonly form within more micaceous mylonites (Fig. 9C; Passchier and Trouw, 2005).

The kinematic relationships resulting from the prolonged structural evolution of the Patterson Lake corridor are exceeding complex. Overall, early ductile structures are defined by a right-lateral sense of movement, informed by both deposit- and drill core-scale shear geometries (Figs. 8, 9F, respectively). The most common examples of sinistral movement within the portion of the Patterson Lake corridor hosting the Arrow deposit are recorded within brittle structures, which frequently mask or destroy early dextral kinematic indicators. The importance of late, sinistral reactivation of the corridor in the locality of Arrow is crucial to the deposit formation and is discussed in the latter sections of this paper.

The foliations within the Arrow high-strain zones have been subject to high-strain folding, resulting in drill core-scale structures ranging from relatively open to isoclinal folds with variably inclined axial planes or surfaces (Fig. 10A). In general, these folds are asymmetric, gently to moderately plunging and moderately to steeply inclined; however, axial surfaces have locally been rotated, resulting in recumbent and nearly reclined folds (Fig. 10B-D). Many of these folds are asymmetric, cylindrical curtain folds, with a relatively straight, subhorizontal fold axis parallel to the lineation. A loss of cylindricity may occur where the curtain fold axial planes are rotated or curved (Fig. 10B). In cases where the fold axes are rotated toward the shear direction rather than remaining normal to shear direction, as in a cylindrical fold, folds with curvilinear hinge lines such as sheath folds may form. Within the Arrow high-strain zones, high-strain sheath folds have been evidenced in drill core by eye-fold interference patterns, which represent a y-z cross section through the body of the sheath fold (Fig. 10C, D). Oriented measurements of fold axial surfaces and hinge lines also indicate the curvilinear nature of sheath fold hinge lines, with the hinge measurements generally plotting along the fold axial trace (stereonet in Fig. 10A). Most of the high-strain folds at Arrow decrease in amplitude vertically due to the steeply dipping geometry of the high-strain zones (as illustrated in Fig. 10A), while mylonitic foliations decrease in intensity laterally away from the core of the shear zone. Quartz ribbons very commonly exhibit isoclinal and ptygmatic folding (Fig. 9E), due to the relative competency contrast between the quartz (high competency) and the

Downloaded from http://pubs.geoscienceworld.org/segweb/economicgeology/article-pdf/116/2/285/5245035/4797_hillacre_et_al.pdf
by Univ Nebraska Lincoln user

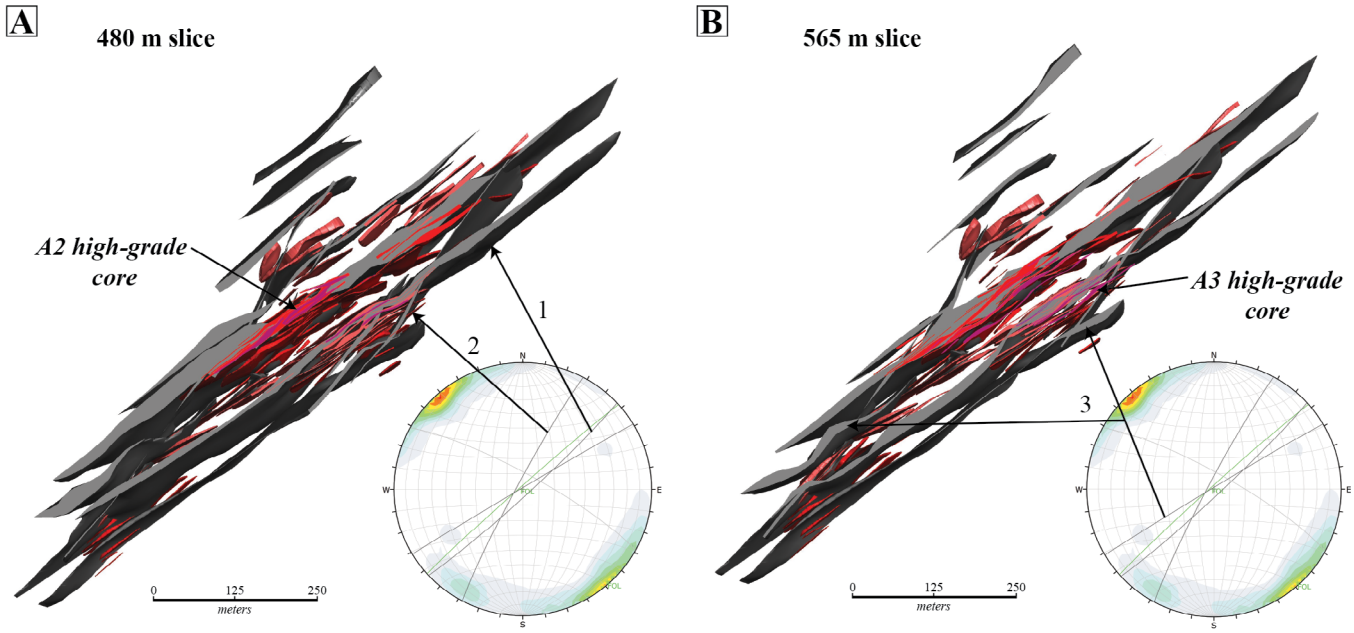


Fig. 8. Plan view depth slices of 3-D modeled Arrow ductile structural zones (gray) at A) 480 m and B) 565 m, illustrating orientations of major shear trends (1, 2, 3) identified from Schmidt equal-area stereographic projections of all high-strain zone shear fabric measurements taken from oriented Arrow drill core (n = 555). Note the shift in strike of the principal flattening surfaces while dip remains subvertical, and how mineralization lenses (red and purple) are largely bound by oblique shears. Trend 1 (047°/86°) is the most prominent, representing anastomosing ductile shear fabrics subparallel to S_1-S_3 transposition foliation. Trends 2 (208°/86°) and 3 (239°/89°) represent shears oblique to and connecting the main structural grain as restraining and releasing bends. A weaker trend illustrating internal (drill core-scale) high-strain and folded (F4) shear fabrics and linkages is also identifiable. Mean foliation plane (S_1-S_3) is shown in green on stereonets for reference.

chloritic, sericitic, and/or graphitic matrix (low competency) of the shear zone.

Shear zone mineralogy, alteration, and recrystallization

The Arrow high-strain zones exhibit a range of alteration types replacing matrix-forming minerals (i.e., phyllonites) and are variable in their mineralogy and extent of recrystallization (e.g., Figs. 9, 10). Dominant alteration assemblages include white mica (commonly fine-grained or sericitic white mica), chlorite (sudoite, clinochlore), and clay minerals (kaolinite, illite; often associated with mineralization), forming the sheared groundmass or present within crosscutting structures. Quartz-rich mylonitic rocks are also observed locally within the Arrow deformation zone. The A1 through A5 high-strain zones are locally overprinted by structurally controlled, postchlorite graphite and iron sulfides. These minerals are dominantly observed as stringer veins, along fractures or foliation planes, and as disseminated masses in voids or interstitially between other minerals. Graphite and sulfides are also frequently observed to crosscut each other, indicating graphite remobilization and multiple sulfide mineralization episodes. The sulfide mineralogy through the Arrow deformation zone is strongly dominated by iron-rich sulfides (pyrite, chalcopyrite, pyrrhotite).

The quartz grains and porphyroclasts within the mylonitized rocks at Arrow exhibit a range of characteristics, which are associated with the high strain imposed on these rocks during shear zone genesis. Feldspar porphyroclasts within low-grade mylonites at Arrow commonly exhibit fracturing by cataclasis; however, quartz is usually deformed via crystal-plastic processes, evidenced through undulose extinction and change in crystal shape and boundaries (Fig. 11A, B). In medium-grade mylonites at Arrow, quartz is dominantly recrystallized through subgrain rotation (Fig. 11B), growing to a polygonal crystalloblastic fabric of strain-free grains exceeding 50 μm (Trouw et al., 2009). Subgrain rotation recrystallization appears to be dominant in the samples examined; however, higher-temperature grain boundary migration recrystallization, and lower-temperature bulging recrystallization have both been observed (Fig. 11A).

Brittle fault rocks

Deformation in rocks is not homogeneously distributed. In general, shear zones can be subdivided into brittle zones or faults at higher crustal levels and ductile shear zones at lower crustal levels, which generate characteristic fabrics and mineral assemblages that reflect the pressure-temperature (P-T) conditions and flow type of the structural environment (Passchier and Trouw, 2005). The Arrow deformation zone contains abundant brittle fault rocks, including incohesive fault breccias, cataclasites, and fault gouge, with rare cohesive cataclasites, typical of low temperatures within the upper 10 km of the Earth's crust (Imber et al., 2008). Meter-scale extensional fault-fill veins also overprint ductile strain and are encompassed by fault damage zones of Riedel shear fractures and linkages, tension gashes, and hydraulic (fluid overpressuring) breccias. These brittle structures overprint the ductile to brittle-ductile high-strain zones at Arrow and crosscut relatively unstrained wall rock in the hanging-wall and footwall

Downloaded from http://pubs.geoscienceworld.org/segweb/economicgeology/article-pdf/116/2/285/5245035/4797_hillacre_et_al.pdf
by Univ Nebraska Lincoln user

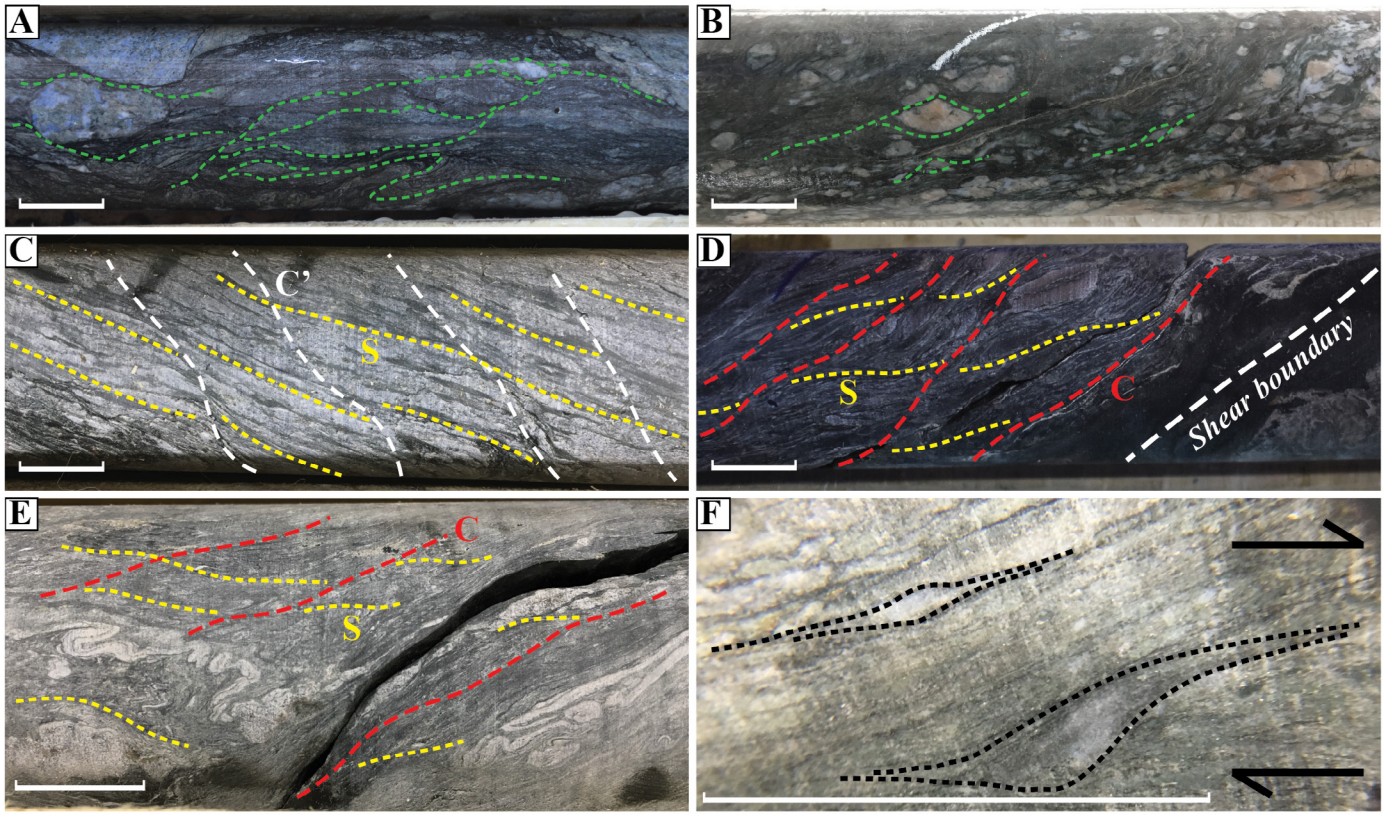


Fig. 9. A) Low-grade graphitic mylonite with wall-rock porphyroclasts, quartz augen, and local isoclinal folding. Shear foliations are highlighted by green dashed lines (AR-15-058c1, 430.1 m). B) Medium-grade mylonite in granitic rock containing σ-type porphyroclasts and quartz-feldspar augen, traced with green dashed lines (AR-18-210c3, 580.1 m). C) Chloritic-graphitic mylonite exhibiting moderately developed C'-S fabrics (AR-18-216c1, 350.4 m). D) Mineralized graphitic mylonite with porphyroclasts, late quartz veining, and sigmoidal curvature of shear bands (AR-17-167c2, 467.1 m, up to 54,500 cps). E) Graphitic mylonite with C-S fabric and intrafolial quartz ribbons exhibiting ptygmatic and isoclinal folding (AR-18-214c1, 255.3 m). F) Hand-lens photograph of a surface cut perpendicular to subvertical shear foliation, looking downdip. Asymmetric quartz σ porphyroclasts indicate early dextral strike-slip movement. The same core sample is overprinted with brittle fractures containing slickenstriae, which exhibit sinistral sense of shear. (AR-17-156c1, 731.8 m). White scale bars are 20 mm.

blocks, often at low angles relative to the near-vertical ductile to semiductile shear zones. Post-Athabasca brittle shear fractures and breccias are among the most frequently mineralized structures within the Arrow deformation zone.

During reactivation of preexisting structural weaknesses, strain may be accommodated by a variety of en echelon structures, including Riedel shear fractures, thrusts, or normal faults. In this case, individual fractures may remain active or become reactivated after other types have developed, so that simultaneous movement on all fractures accommodates strain within a strike-slip deformation zone. Drill core-scale examples of these types of shear fractures are common in a variety of orientations at the Arrow deposit, conformable to and crosscutting foliation at oblique and high angles (Figs. 12A-F, 13A-G). Sets of NNE- to NE-striking subsidiary extensional and ENE-striking contractional shear fractures are most prominent (Figs. 12D, 13B, C) and are associated with NW-, NNW-, and N-striking conjugate shear fractures, faults, cataclasites, fault breccias, and gouge (Figs. 12B, E, F, 13D-F). All of these sets of structures chiefly exhibit steep dip (~70°–85°); however, there are notable sets of relatively shallow dipping (~30°–60°) reverse faults and transtensional shear fractures that appear to have taken up strain later in structural evolution as evidenced by crosscutting relationships observed in drill core (e.g., Fig. 12C). These shallow structures exhibit variability in their dip direction, with south, north, southeast, and northeast directions being dominant (Fig. 13G). Local subhorizontal faults and fractures are also present in the Arrow data and dip chiefly southwest, south, and southeast. Rare EW-striking cross structures have been observed, with moderate dip to the north or south. Due to the competent, quartz-rich nature of the host rock at Arrow, these interconnected networks of shear fractures, faults, and tension gashes are preferential fluid pathways and thus are frequently filled or lined with variable alteration minerals and/or uranium mineralization; especially within the hanging-wall and footwall block damage zones separating the A1 to A5 shears. Gently dipping structures at Arrow frequently contain alteration minerals that are interpreted to be late in paragenesis, such as tourmaline. Fractures and faults filled with uranium result in mineralized veins with thickness (Fig. 12A-E), some of which may be crosscut by other veins or fractures containing uranium and/or other minerals (Fig. 12B-D).

Downloaded from http://pubs.geoscienceworld.org/segweb/economicgeology/article-pdf/116/2/285/5245035/4797_hillacre_et_al.pdf
by Univ Nebraska Lincoln user

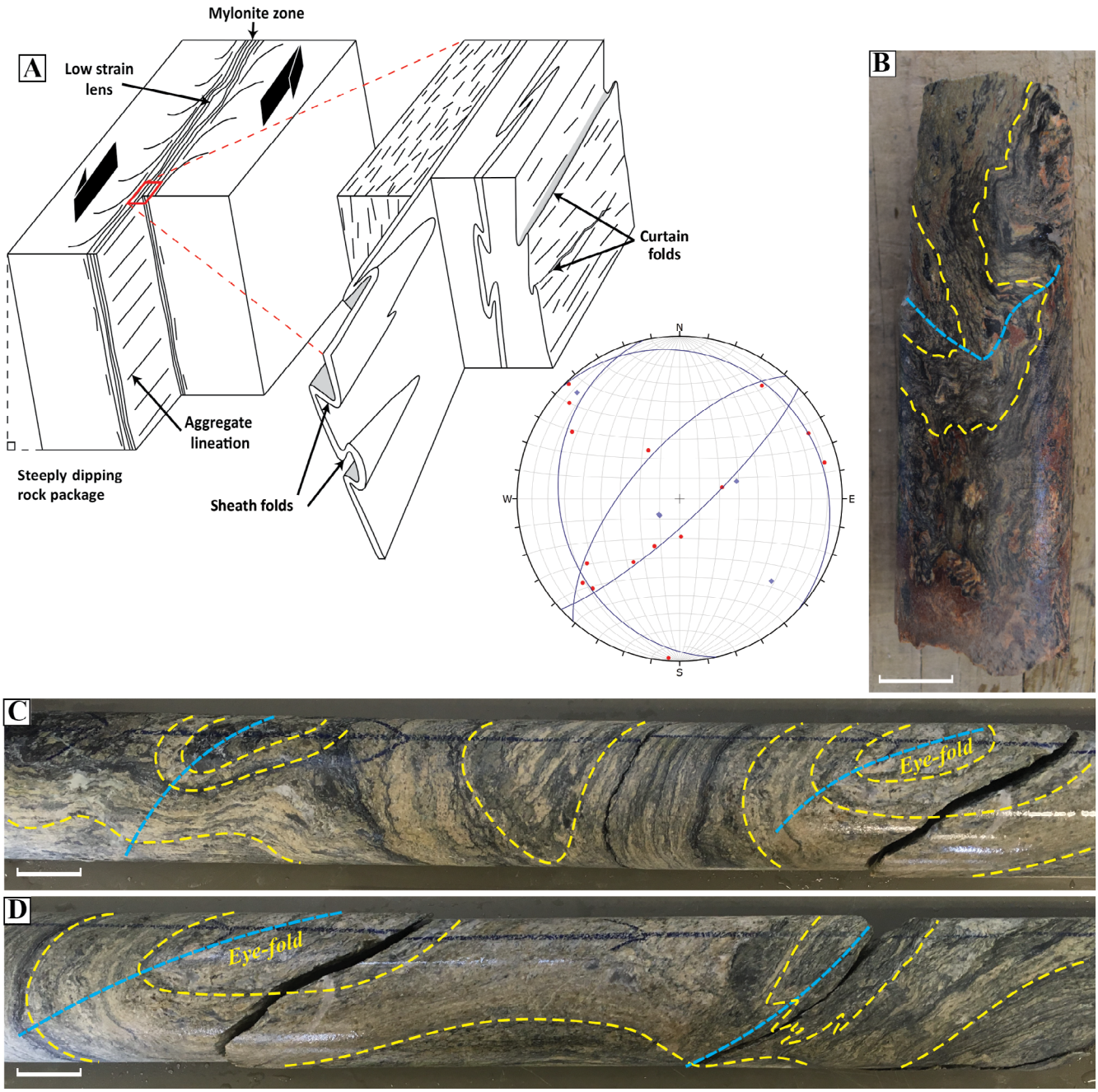


Fig. 10. A) Schematic of high-strain curtain and sheath fold geometry within a steeply dipping mylonite zone (modified after Passchier and Trouw, 2005), with an equal-area projection of axial plane (blue diamonds; $n = 5$) and fold hinge (red circles; $n = 15$) data from select high-strain folds at Arrow showing curvilinear fold hinges. B) Uranium mineralization precipitated along an asymmetrical, recumbent curtain fold with a rotated and curved axial surface (blue line) and smaller-scale parasitic folding (AR-16-093c1, 461.8–461.95 m, up to 26,000 cps). C) Possible sheath folds in chloritic-sericitic phyllonite indicated by eye-fold interference patterns in drill core (AR-17-115c1, 678.8 m). D) Plunging inclined high-strain folds in chloritic-sericitic phyllonite with local parasitic folding (AR-17-115c1, 679.1 m). Yellow lines are shear foliation traces. White scale bars are 20 mm.

Brittle fault rocks can broadly be subdivided into cohesive and incohesive types. Cohesive fault rocks comprise cohesive breccia, cohesive cataclasite, and pseudotachylyte, and are thought to form under brittle-dominant P-T conditions, with lithostatic pressure up to approximately 3 kbar and temperatures up to 300°C (Trouw et al., 2009). Incohesive fault rocks are usually found in faults that have been active up to shallow crustal levels and are subdivided into incohesive breccia, incohesive cataclasite, and fault gouge (Passchier and Trouw, 2005). Contrary to cohesive breccias and cataclasites, the wall-rock contacts and embedded fragments in incohesive fault rocks frequently exhibit polished surfaces with slickensides or slickenfibers (Passchier and Trouw, 2005). In some cases, these linear features may be used to determine the di-

Downloaded from http://pubs.geoscienceworld.org/segweb/economicgeology/article-pdf/116/2/285/5245035/4797_hillacre_et_al.pdf
by Univ Nebraska Lincoln user

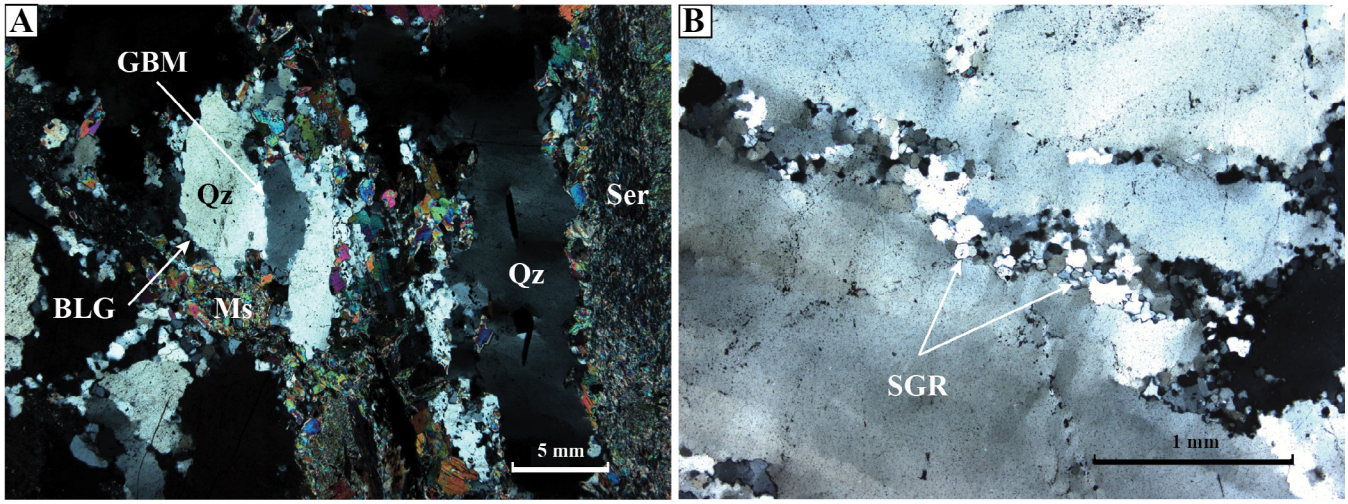


Fig. 11. A) Cross-polarized light (XPL) photomicrograph of quartz grains within the northeastern portion of the A2 shear zone exhibiting a spectrum of dynamic recrystallization textures including grain boundary migration (GBM) and bulging (BLG) indicative of a transition from high to low temperature and a corresponding decrease in strain rate (A2 shear, AR-16-078c2, 437.0 m). B) XPL photomicrograph of quartz grains within the A3 shear footwall showing evidence for crystal-plastic deformation through well-developed undulose extinction and subgrain rotation recrystallization (SGR) (A3 shear, AR-16-074c1, 630.3 m). Mineral abbreviations: Ms = muscovite, Qz = quartz, Ser = sericite.

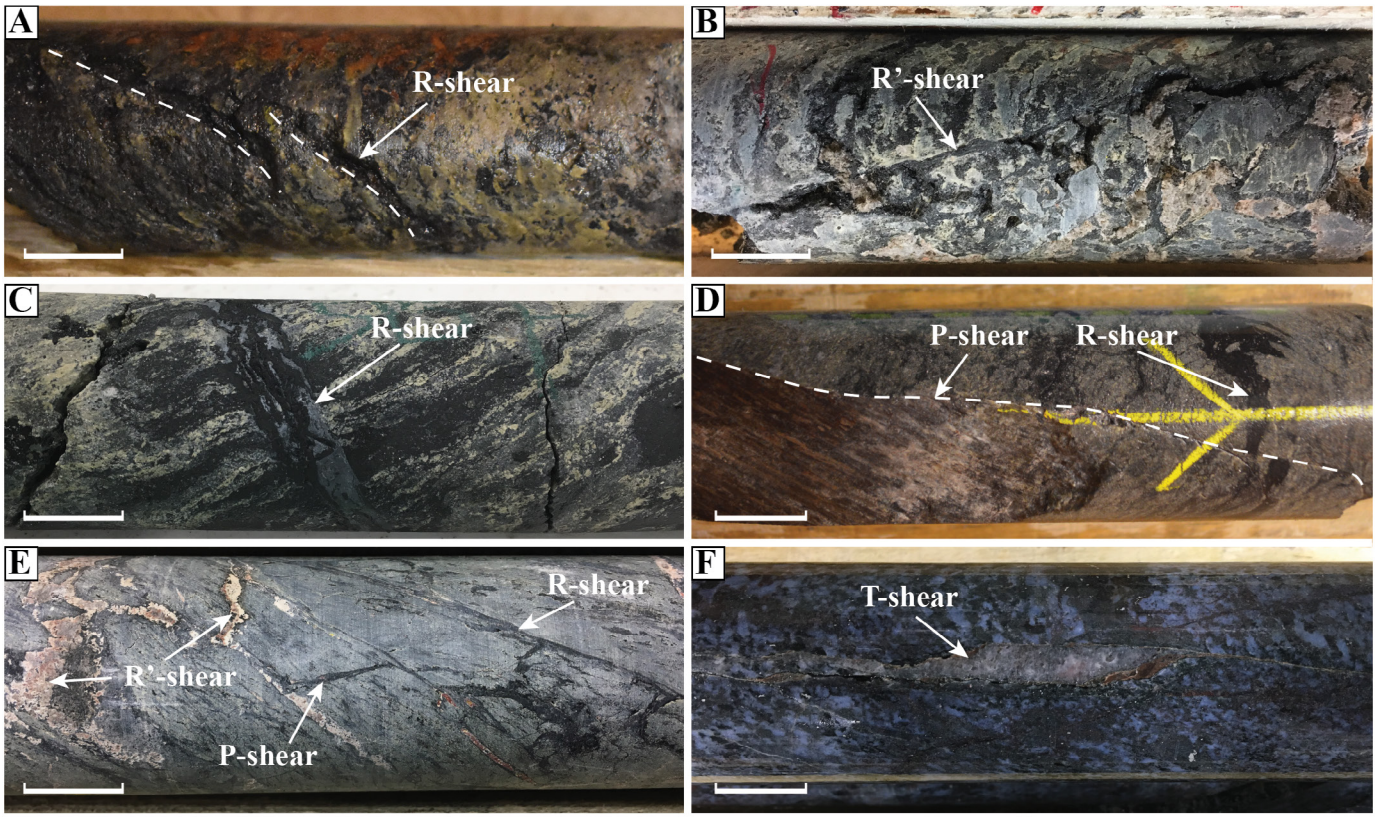


Fig. 12. A) Uraninite-filled R-shear fractures oblique to shear foliation (AR-18-186c2, 462.5–462.6 m, up to >61,000 cps). B) Steeply dipping uraninite-healed R'-shear crosscutting chemical replacement mineralization along foliation at high angle (AR-18-186c2, 463.5–463.6 m, up to >61,000 cps). C) Mineralized, shallow NE-dipping R-shear fracture with reverse offset (AR-19-226c1, 514.95 m, up to >61,000 cps). D) Uraninite mineralization within a gently SE-dipping transtensional R-shear fracture, crosscut and offset (normal) by a steeply dipping, striated transpressional P shear. (AR-17-129c1, 913.8–914.0 m, up to >61,000 cps). E) Uraninite mineralization reusing a quartz-filled network of shear fractures, illustrating the linkage of R, R', and P fractures and resulting rhomb-shaped geometry (AR-18-186c2, 456.5–456.6 m, up to 41,000 cps). F) Steeply dipping rhomb-shaped T-shear fracture filled with quartz and crosscutting foliation. Top-to-the-left movement is indicated. White scale bars are 20 mm.

Downloaded from http://pubs.geoscienceworld.org/segweb/economicgeology/article-pdf/116/2/285/5245035/4797_hillacre_et_al.pdf
by Univ Nebraska Lincoln user

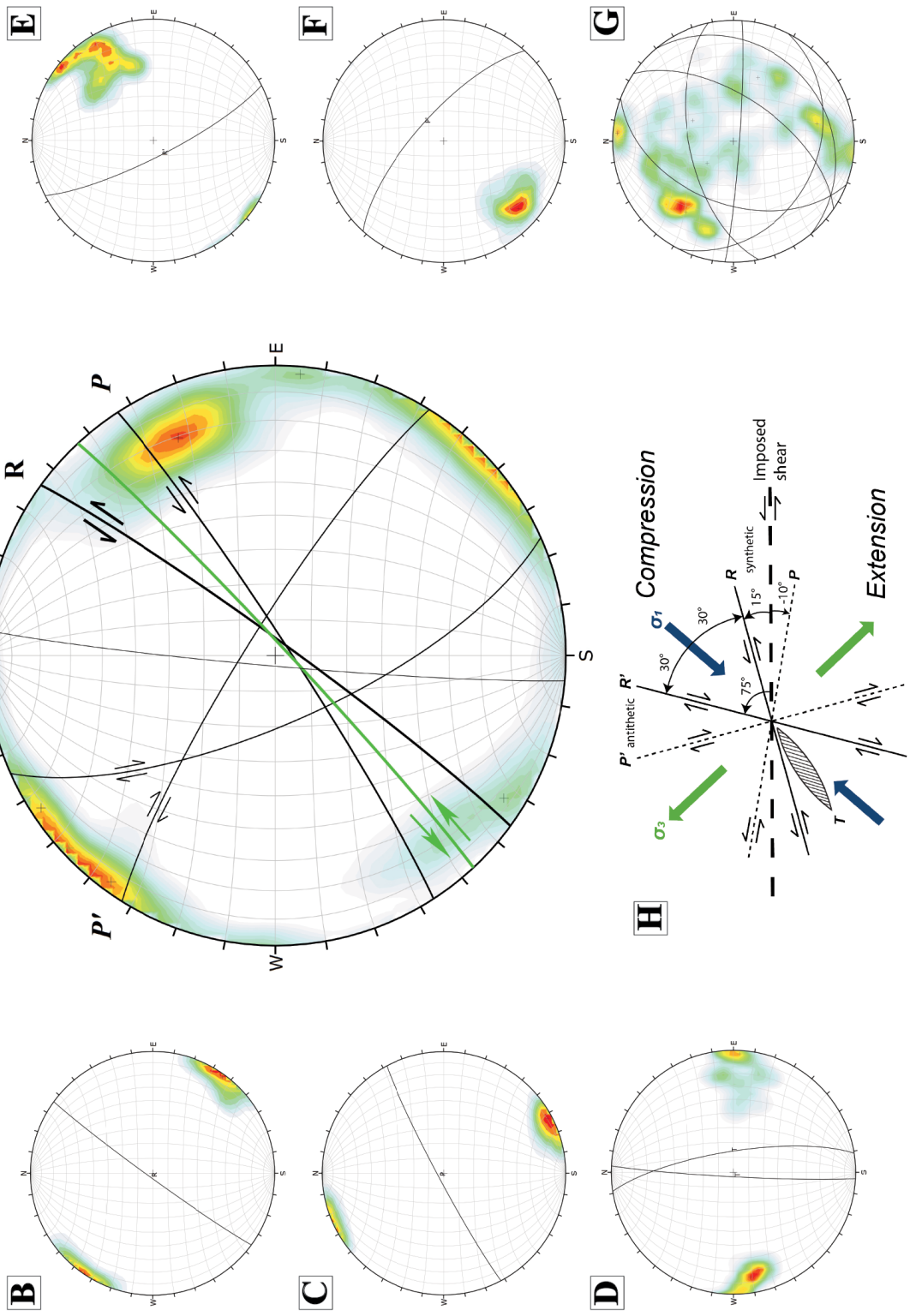


Fig. 13. A) Schmidt equal-area stereonet with statistical mean trends of major brittle structural orientations (shear fractures, faults, cataclasites, fault breccia, and gouge) at Arrow illustrating Riedel geometry and interpreted shear sense. The average attitude of the main foliation (S_1/S_2) is representative of the dominant ductile structural grain (imposed shear), shown in green. Synthetic and antithetic subsidiary structures arranged about the principal flattening surface suggest a dominant sinistral movement as structural evolution continued. n = 8,213. B) Stereonet with domained brittle structure data representing R-shear fractures (n = 2,232). C) Stereonet with domained brittle structure data representing P-shear fractures (n = 1,239). D) Stereonet with domained brittle structure data representing T fractures (n = 1,044). E) Stereonet with domained brittle structure data representing R'-shear fractures (n = 1,303). F) Stereonet with domained brittle structure data representing P'-shear fractures (n = 821). G) Stereonet with domained brittle structure data representing minor low-angle and EW-striking faults and fractures (n = 1,574). H) Schematic diagram of the Riedel shear model and the associated synthetic and antithetic subsidiary structures that may develop from a sinistral dominated movement along a strike-slip shear zone (after Moores and Twiss, 1997).

Downloaded from http://pubs.geoscienceworld.org/segweb/economicgeology/article-pdf/116/2/285/5245035/4797_hillacre_et_al.pdf
by Univ Nebraska Lincoln user

rection of movement and shear sense along the fault zone. The Arrow deformation zone contains abundant fault gouge zones and both cohesive and incohesive cataclasites and breccias (Fig. 14A-H), ranging in scale from a few centimeters to over 10 m in thickness. Most of these brittle structures within the Arrow deformation zone are cohesive types, as the matrices are most commonly composed of quartz, clay minerals, and chlorite, which were precipitated from a hydrothermal fluid (Fig. 14A-H).

Cohesive quartz-healed breccias are numerous at Arrow, often showing evidence for multiple phases of brecciation with matrix-forming quartz subsequently becoming clasts along with wall rock in younger, overprinting breccias. Fault breccia zones have been logged as deep as 1 km and as shallow as the unconformity surface, which averages approximately 110 m below ground surface. They exhibit a variety of alteration assemblages and mineralogical composition based on their proximity to surface and wall-rock interactions. For example, massive quartz-hematite breccias occur at shallower depths (down to approximately 450 m) while chlorite-, graphite-, and sulfide-rich breccias tend to be preserved at greater depths (Fig. 14A, B, D, E). The matrix-forming quartz is commonly euhedral and zoned, and ranges in color from milky white, smoky black to brown, translucent, and translucent pink. Breccias within the Arrow strike-slip shear zone are frequently observed to be mineralized, hosting clasts of mineralized wall rock, disseminated uraniferous minerals, or even completely healed with uraninite (Fig. 14C). As aforementioned, many of these structures exhibit polyphase deformation, and several show evidence for brecciation through fluid overpressuring or hydraulic brecciation.

Cataclasites are dominantly cohesive type within the Arrow deformation zone, with matrices dominantly comprised of clay minerals and clasts of quartz (Fig. 14F, G). They range

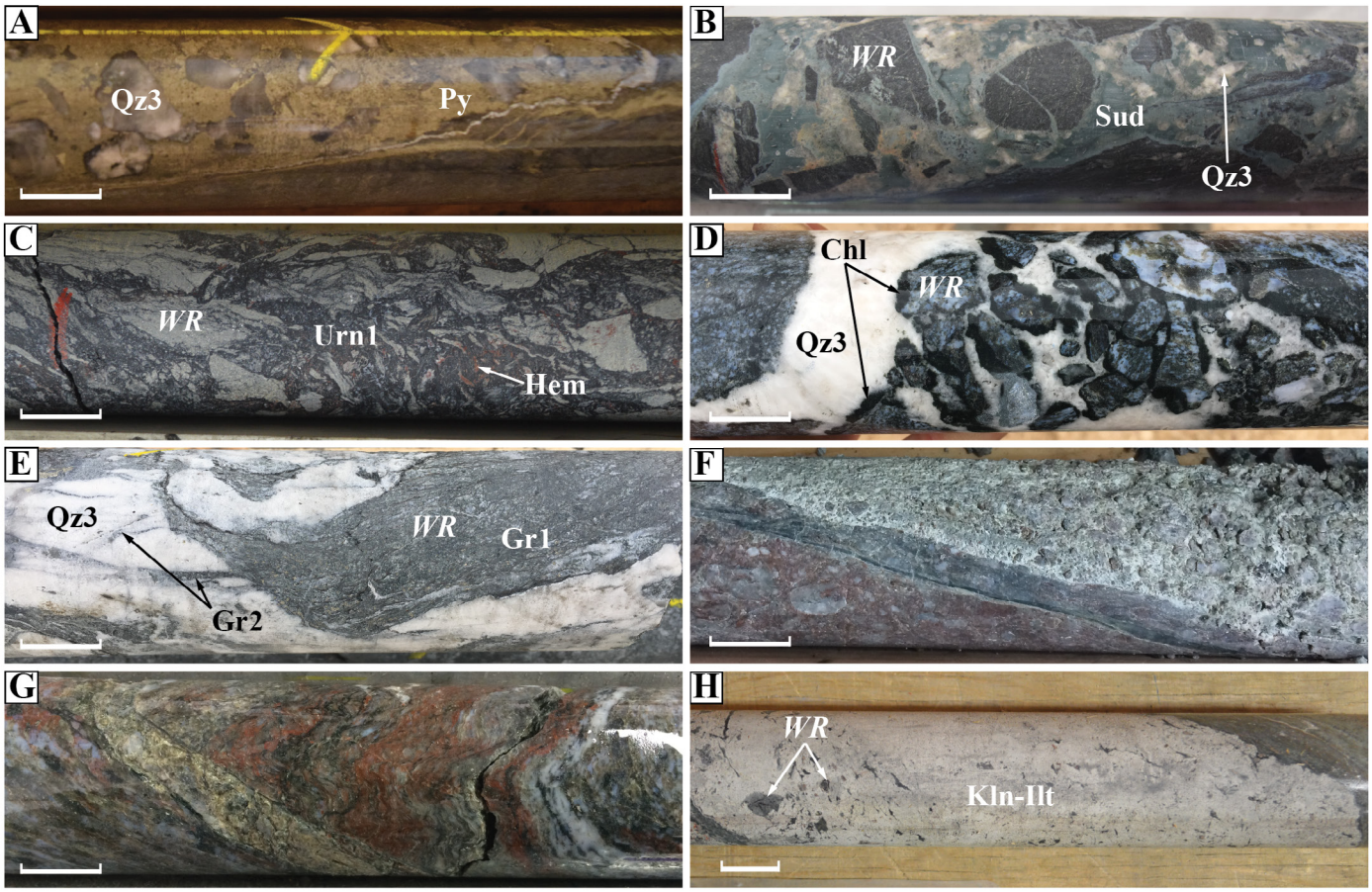


Fig. 14. A) Brecciated milky white translucent quartz vein (Qz3) healed by relatively late massive pyrite (Py) mineralization (AR-16-095c1, 633.3 m). B) Weakly mineralized sudoite (Sud) healed, matrix-supported chaotic breccia hosting angular and subangular clasts of sheared, graphitized, and sericite-altered wall rock (WR) and milky translucent quartz (Qz3)(AR-17-121c2, 661.5 m, up to 980 cps). C) Main-stage uraninite (Urn1) healed matrix-rich mosaic breccia hosting angular clasts of sheared, pervasively sericitized and graphitized wall rock, with trace hematite (Hem) alteration (AR-15-061c2, 780.5 m, up to 55,000 cps). D) Massive milky quartz healed mosaic breccia hosting subangular clasts of altered wall rock mantled by chlorite (Chl) alteration (AR-18-210c3, 865.2 m). E) Massive milky quartz- and graphite (Gr2)-healed breccia overprinting heterogeneous ductile strain, hosting angular clasts of sheared, graphitized (Gr1) wall rock (AR-18-210c3, 870.2 m). F) Decimeter-scale cohesive cataclasite comprised of rounded wall rock and quartz clasts within a fine to very fine grained matrix of clay minerals updip of the A2 shear zone (AR-16-080c2, 400.6 m). G) Centimeter-scale cohesive quartz-clay-chlorite cataclasite in R shear orientation crosscutting sheared and folded wall rock (AR-16-080c2, 416.3 m). H) Mineralized fault gouge consisting of millimeter- to centimeter-scale clasts of sheared, chloritized, and sericitized wall rock within a kaolinite-illite (Kln-Ilt) matrix (AR-17-129c1, 764.7 m, up to 5,400 cps). White scale bars are 20 mm.

Downloaded from http://pubs.geoscienceworld.org/segweb/economicgeology/article-pdf/116/2/285/5245035/4797_hillacre_et_al.pdf
by Univ Nebraska Lincoln user

in size from a few centimeters in thickness (Fig. 14G) up to meter-scale structures (Fig. 14F) and represent zones of prolonged movement and fluid flow evidenced through high degrees of comminution of all mineral grains and strong clay alteration. Cohesive cataclasites are prevalent updip of the major A1 to A5 shear zones (Fig. 14F, G) and commonly host uranium mineralization at greater depths where overprinting mylonitized and/or highly altered rocks within the shears.

Fault gouge zones proximal to and overprinting ductile strain are common, ranging from localized centimeter-scale gouge to meter-scale zones of up to or greater than 90 vol % matrix (Fig. 14H). Matrices most commonly consist of clay minerals (kaolinite, illite), chlorite, and muscovite with negligible clasts of wall rock or quartz (Fig. 14H).

Slickensides are abundant throughout the Arrow deformation zone, most well developed along graphite- and chlorite-lined fractures and along the contacts of incohesive fault rocks. In mineralized zones, slickenstriae are commonly observed on brittle fractures lined with clay, chlorite, and/or hematite, as well as uraninite. Relatively late fractures crosscutting mineralization also exhibit slickenlines, attesting to the prolonged reactivation of major structural zones syn- and postmineralization stages. Multiple generations of slickenstriae are observable on most slickensides at Arrow, recording polyphase brittle deformation and wrench on a local scale (i.e., dip-slip and oblique-slip orientations on conjugate fractures). Orientations of these features range from strike-slip to dip-slip, with near-horizontal oblique-slip orientations being most prominent.

Mineralized structures

Mineralized structures at Arrow range from hydrothermal fluid overpressuring and corrosive replacement-style breccias, massive fault-fill veins or shoots (Fig. 15A, B), shear fracture and extensional vein fills (Fig. 15C), and disseminated uraninite within cohesive gouge or breccia fills (Fig. 15D). Meter-scale uranium fault-fill veins (Fig. 15A, B) hosted within and proximal to the brittle-ductile shears comprise the high-grade domains of semimassive to massive uraninite mineralization, roughly paralleling the high-strain zones with moderate to steep dip. They have great vertical extent (>100 m) and represent dilational zones during slip, with the densest accumulations of uraninite at Arrow hosted within the A2 and A3 shear cores.

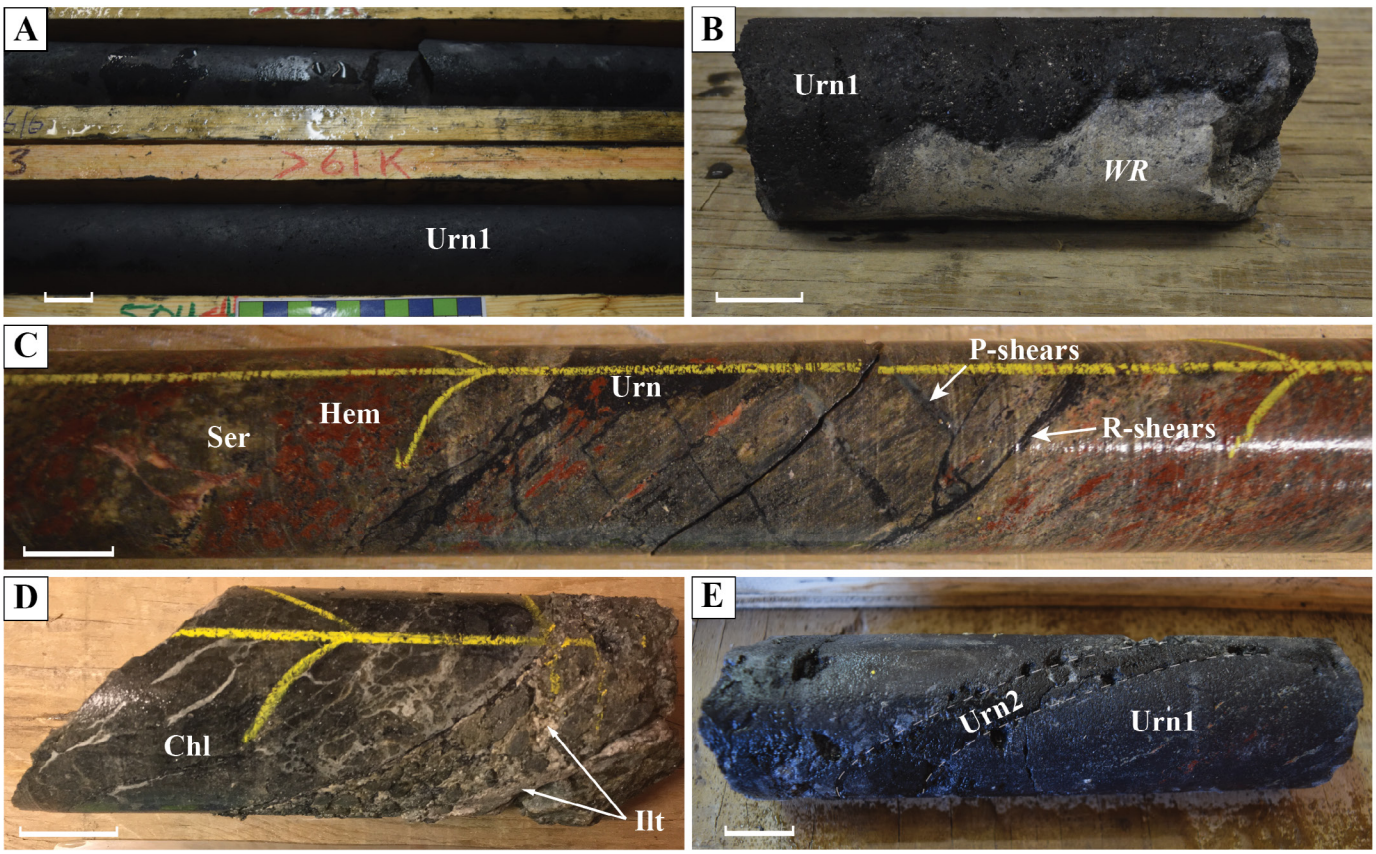


Fig. 15. A) Massive primary uraninite (Urn1) mineralization within a meter-scale extensional fault-fill vein (AR-16-076c1, 502.5 m, up to >61,000 cps). B) Subvertical contact of a massive uraninite (Urn1) vein with strongly altered wall rock (WR) (AR-16-076c3, 516.2 m, up to >61,000 cps). C) Uraninite (Urn1 or 2) mineralization healing multigenerational shear fractures oblique to and at high angles (extensional veins) to ductile shear foliation. Hematite (Hem) alteration associated with mineralization overprints earlier sericitic (Ser) alteration and shows structural and mineral control (AR-17-129c1, 781.15–781.5 m, up to 46,000 cps). D) Mineralized illite (Ilt) and chlorite (Chl) rich cohesive cataclasite (AR-17-129c1, 782.2 m, up to 10,500 cps). E) Younger generation uraninite vein (Urn2) crosscutting older massive uraninite mineralization (Urn1) within the A2 high-grade core (AR-16-098c2, 500.0 m, up to >61,000 cps). White scale bars are 20 mm.

Downloaded from http://pubs.geoscienceworld.org/segweb/economicgeology/article-pdf/116/2/285/5245035/4797_hillacre_et_al.pdf
by Univ Nebraska Lincoln user

Drill core-scale extensional veins (e.g., Fig. 15C) are broadly coeval with the fault-fill veins in competent rock. They may have steep dip oblique to foliation, like the fault-fill zones; however, they are commonly oriented at much shallower dip and high angle to foliation (e.g., Fig. 15C). The extent of the modeled mineral resource at Arrow (O'Hara et al., 2018) represents an envelope of these smaller-scale extensional veins, Riedel shear fractures, and linkages (Fig. 15C), as well as hydraulic breccias and cataclasites healed by kaolinite, illite, chlorite, and/or dravite, which host disseminated uranium mineralization (Fig. 15D). Conversely, uraninite forms the matrix within some brecciated rocks, hosting angular, altered clasts of wall rock (e.g., Fig. 14C). Younger and/or remobilized veins of uraninite are also observed to crosscut prior mineralization phases, evidencing polyphase fluid movement through the structures postprimary mineralization (Fig. 15E). On a millimeter to micrometer scale, uraninite is precipitated along grain and vein boundaries, foliation, and mineral cleavage planes, commonly replacing minerals partially or completely, such as previously altered garnet or feldspar porphyroblasts or muscovite/sericite in the matrix. Although the uranium mineralization at Arrow postdates much of the metasomatism of the wall rocks (i.e., quartz flooding), significant syn- and postmineralization alteration of the host rocks is prominent at Arrow.

Mineral Paragenesis

The structural evolution of the Patterson Lake corridor can be related to uranium mineralization and extensive and varied hydrothermal alteration products (Fig. 16). The host rocks at the Arrow deposit have a complex metasomatic history predating uranium mineralization and exhibit evidence for multistage hydrothermal alteration syn- and postmineralization. Due to the prolonged reactivation and reuse of the Arrow deformation zone by polyphase fluid fluxes, the relative timing and associations between primary mineralogy, alteration mineralogy, and uranium mineralization define a complex relationship. Regional metamorphism of the basement rocks to upper amphibolite to granulite facies, along with intrusion of mafic dike rocks (e.g., pyroxenite) and felsic pegmatite bodies, occurred prior to focused hydrothermal alteration of the basement rocks along the Patterson Lake corridor; however, syn- to postpeak metamorphic metasomatism is evident through formation of biotite at the expense of feldspar and extensive quartz flooding. After these events, several phases of hydrothermal alteration and mineralization have been identified based on structural and textural relationships including a premineralization alteration stage, a main alteration and synprimary uranium mineralization stage, and a posturanium mineralization stage (Fig. 16).

Syn- to postpeak metamorphic metasomatism

Biotitization of feldspars is among the earliest alteration phases of coarser-grained feldspar-rich country rocks proximal to Arrow (Fig. 16). Mineral textures and crosscutting relationships indicate that this nonmetamorphic biotite grew at the expense of feldspar grains and along planar elements in the rock, forming replacement masses and coalescing into veins of black or lustrous brown, crystalline biotite (Fig. 17A). Masses of biotite are locally overprinted and/or replaced by garnet porphyroblasts, and both garnet and biotite were subsequently affected by retrograde chloritization (clinochlore; Figs. 16, 17B). Crystalline biotite commonly forms veins (Fig. 17A) or lines the margins of early crosscutting quartz veins (Qz3; Fig. 16); however, biotite veins and masses are not commonly observed within more intensely altered Arrow wall rocks proximal to uranium mineralization. This suggests an early timing with respect to the dominant syn- and postmineralization alterations.

The competent, relatively undeformed wall rocks within the Arrow zone exhibit pervasive syn- to postpeak metamorphic quartz flooding (Qz2; Fig. 16), often so intense that it replaces more than 80% of the rock (Fig. 17C). The dominant host rock of the Arrow deposit (quartz-feldspar-garnet-biotite gneiss) is particularly affected by this event. Only trace amounts of altered minerals remain in some instances, with faint relict textures of foliation (Fig. 17C). The ensuing quartz is dominantly blue, blue gray, gray purple, or milky blue white in hand specimen. The blue coloration of the quartz is suggested to be derived from Rayleigh scattering of light by ubiquitous submicrometer- and nanometer-sized inclusions of titanium (Ti)-bearing minerals such as rutile/anatase (Fig. 17D), ilmenite, and/or mica, fluid inclusions, or deformation/defects within the crystal lattice (e.g., Zolensky et al., 1988; Seifert et al., 2011). Past studies on blue quartz (e.g., Seifert et al., 2011) have shown that it is generally Ti rich (~100–300 ppm) and that it forms at high temperatures between approximately 700° to 900°C, which is consistent with the high grade of the granulite facies M_1 metamorphic event recorded in the Taltson domain rocks. This therefore suggests that widespread silicification of rocks along the Patterson Lake corridor occurred very early in the evolution of the corridor and is not related to uranium mineralization. Inductively coupled plasma-mass spectrometry (ICP-MS) analyses on select blue quartz samples within the Arrow zone have returned Ti values from 500 to 800 ppm Ti, and EMPA has identified abundant submicrometer inclusions of rutile (Fig. 17D; Hillacre, 2018). Although most of the Arrow deposit host rocks exhibit secondary quartz flooding (i.e., quartz-feldspar-garnet-biotite gneiss), much of the primary metamorphic quartz in the intermediate to felsic orthogneisses also exhibits a blue or purple hue. Therefore, distinguishing between primary metamorphic quartz and secondary silicification through textural and paragenetic relationships is important. While the remobilization and addition of quartz appears to be dominantly postpeak regional deformation, textures indicate that ductile shearing occurred postquartz flooding and thus implies that the quartz flooding occurred below the brittle-ductile transition (Fig. 16) and prior to exhumation and deposition of the overlying Athabasca Supergroup rocks (Fig. 17E, F; Card, 2017). Additionally, in less altered rocks, the metasomatic quartz is commonly transposed with foliation, or the foliation may have helped to focus the silicifying fluid (Fig. 17F). As aforementioned, blue quartz grains exhibit deformation textures indicative of crystal-plastic processes including undulose extinction and dynamic recrystallization along their boundaries through subgrain rotation (Fig. 11A, B).

Altered rocks within the Arrow deformation zone are associated with a variety of hydrous aluminum silicates, includ-

Downloaded from http://pubs.geoscienceworld.org/segweb/economicgeology/article-pdf/116/2/285/5245035/4797_hillacre_et_al.pdf
by Univ Nebraska Lincoln user

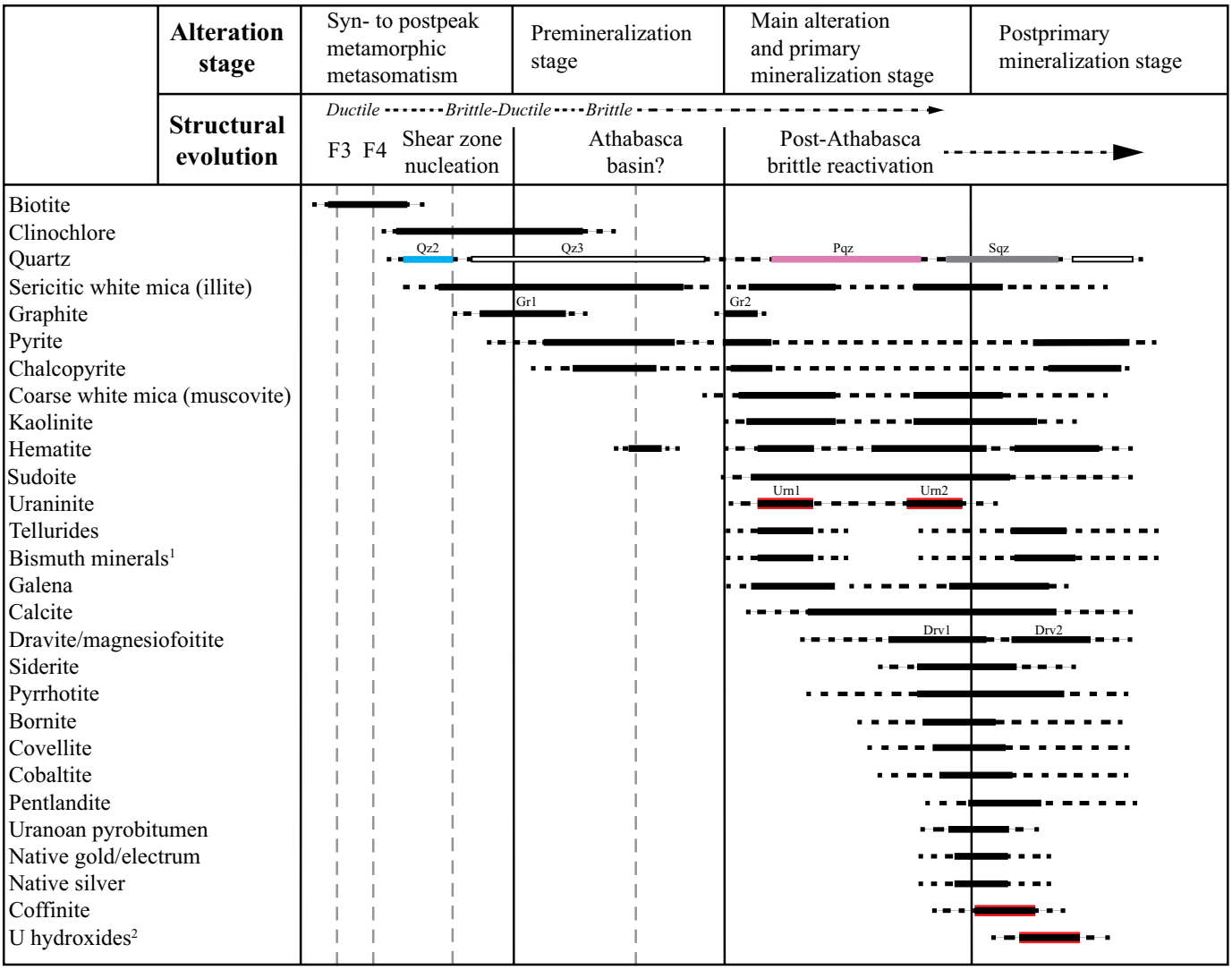


Fig. 16. Generalized alteration mineral paragenesis for basement rocks hosting the Arrow deposit integrating relative timing of U mineral phases, precious metals, and hydrothermal alteration products with identified alteration stages and interpreted structural evolution. Quartz episodes are colorized to represent different phases, and Qz1 (not shown) equates to primary quartz in the rock. Dashed lines indicate uncertainty in the position; uranium minerals are highlighted in red. [1]Native bismuth, bismuthinite, and Bi-Te-Se minerals. [2]Secondary U silicates, including uranophane (Uph), and hydroxides/oxyhydroxides.

ing chlorite group minerals and different generations of white mica (Fig. 16). The most prominent alteration type involving these minerals is early partial to complete sericitization of all preexisting minerals. The abundance of white mica reflects the large quantities of primary K-feldspar in the wall rocks and may suggest the importance of K-bearing hydrothermal fluids. Sericitic white mica (i.e., illite and/or muscovite) dominantly forms as alteration of feldspars and pyroxene but in extreme cases may replace all minerals present in the parent rock, including quartz. White mica is extremely common as a metasomatic alteration in rocks exhibiting strong silicification and is likely one of the products of this reaction (Card, 2017). White-mica grains range from micrometer to centimeter scale and often obliterate any original mineralogy and texture in the wall rock.

Chlorite is not as ubiquitous as white mica; however, there is evidence for multiple episodes of chloritization (Fig. 16). The most common varieties of chlorite at the Arrow deposit are sudoite and clinochlore, based on mineral chemistry, with main-stage sudoite predominant within and proximal to the ore zones (Fig. 16). Retrograde metamorphic Mg-rich chlorite (clinochlore; Figs. 16, 17B) is the earliest identified chlorite phase, commonly rims or completely replaces preexisting biotite and garnet, and commonly defines ductile lineations along foliation planes (e.g., Fig. 7B). The replacement of garnet porphyroblasts by dark-green, fine- to medium-grained clinochlore is particularly distinctive. A mixture of early sericitic white mica and chlorite very commonly forms the matrix in many of the rock samples studied and is clearly overprinted by later alteration phases such as main-stage white-mica alteration (Fig. 17B) and postprimary mineralization tourmaline (i.e., dravite). As aforementioned, mylonitic rocks within the Arrow deformation zone are commonly pervasively chloritized, contributing to softening and

Downloaded from http://pubs.geoscienceworld.org/segweb/economicgeology/article-pdf/116/2/285/5245035/4797_hillacre_et_al.pdf
by Univ Nebraska Lincoln user

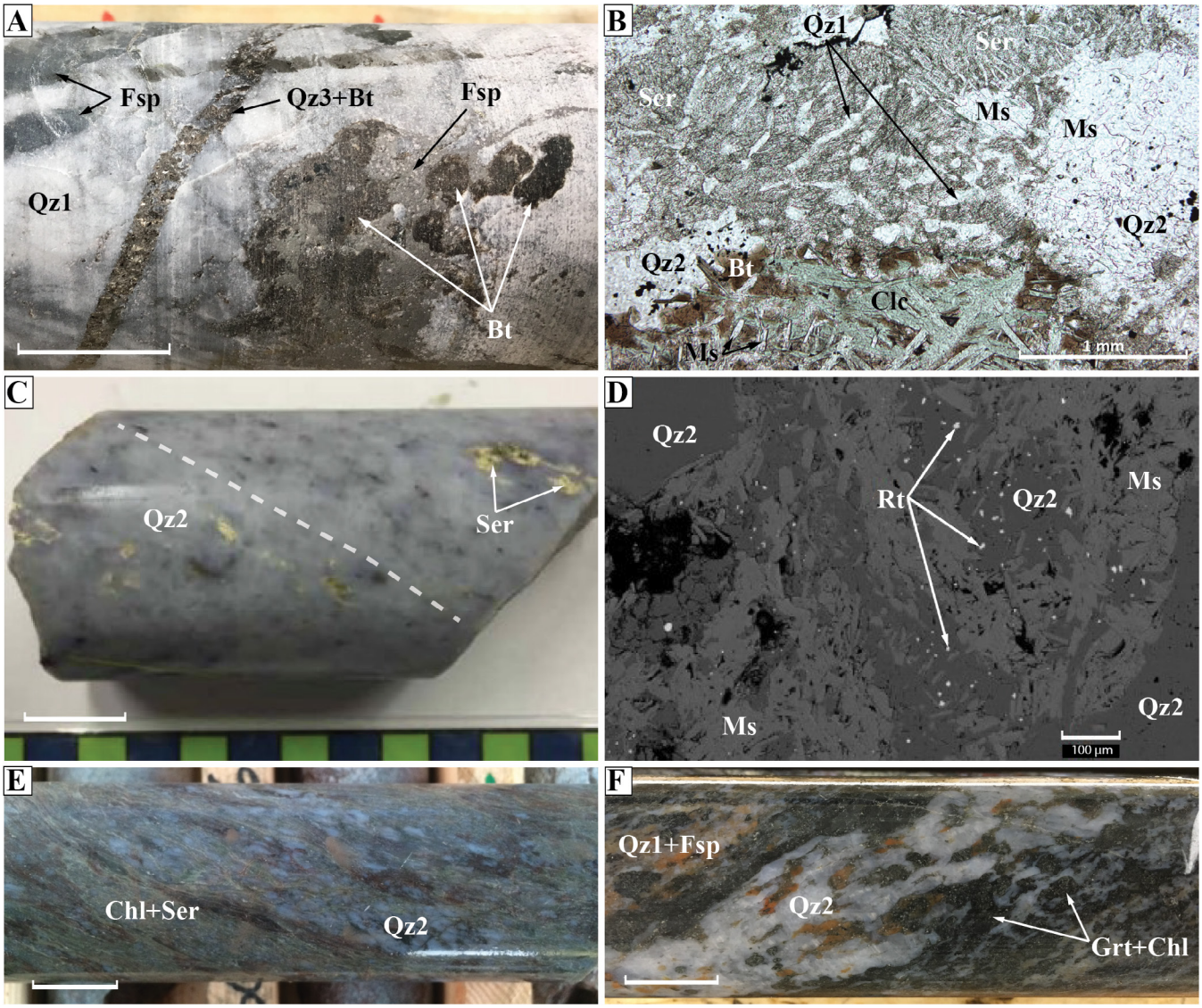


Fig. 17. A) Crosscutting quartz-biotite (Qz3 + Bt) vein in quartz (Qz1)-rich country rock, and early biotitization of feldspar (Fsp) resulting in irregular masses of biotite replacing feldspar grains (NQ, AR-18- 210c3, 769.65 m). B) Early biotite (Bt) being replaced by clinochlore (Clc) and embayed by blue quartz (Qz2). Myrmekitic intergrowths of quartz (Qz1) and sericitized feldspar are visible in the center of the image. Primary feldspar in the rock is almost completely replaced by early sericitic white mica (Ser), which is also embayed by blue quartz (Qz2). Coarse-grained main-stage muscovite (Ms) alteration overgrows all other minerals in the section (AR-16-084c1, 385.1 m). C) Pervasively silicified Arrow host rock containing upward of 80% blue quartz (Qz2) intersected 5 m from uranium mineralization. Extremely silicified instances of the Arrow host rock are extremely common, with sericitized feldspars (Ser) and relict foliation still visible (white dashed line) (AR-16-081c3, 657.9–658.0 m). D) BSE image revealing abundant submicrometer rutile (Rt) inclusions in a blue quartz (Qz2) sample taken near the southwest margin of the Arrow deposit. Muscovite (Ms) alteration has replaced feldspar grains (AR-16-082c2, 717.6–717.65 m). E) Sheared and transposed blue-purple quartz (Qz2) within the upper A1 shear zone, exhibiting early chloritic-sericitic (Chl + Ser) alteration (AR-16-080c2, 251.8 m). F) Blue-gray metasomatic quartz (Qz2) transposed and focused along preexisting foliation in relatively unaltered Arrow wall rock (AR-18-214c1, 464.5 m). White scale bars are 20 mm in A, C, E, F, and 100 µm in B and D.

thus preferential deformation during the formation of the Arrow high-strain zones.

Premineralization alteration stage

Graphite (and/or graphitic carbon where lacking crystallinity) is interpreted to be relatively early in paragenesis, preferentially overprinting previously chloritized mylonitic rocks at the Arrow deposit, preuranium mineralization but post-metasomatic alteration (i.e., biotitization and quartz flooding events) of the host rocks (Gr1; Figs. 16, 18A-C). Premineralization iron sulfide minerals (dominantly pyrite ± chalcopyrite; Figs. 16, 18A-C, E) coprecipitated with graphite (Gr1) at Arrow, and quartz veins and breccias are frequently observed to be associated with graphite. Textural relationships also indicate that graphite was subsequently redistributed via relatively late deformation processes at Arrow (Gr2; Figs. 16,

Downloaded from http://pubs.geoscienceworld.org/segweb/economicgeology/article-pdf/116/2/285/5245035/4797_hillacre_et_al.pdf
by Univ Nebraska Lincoln user

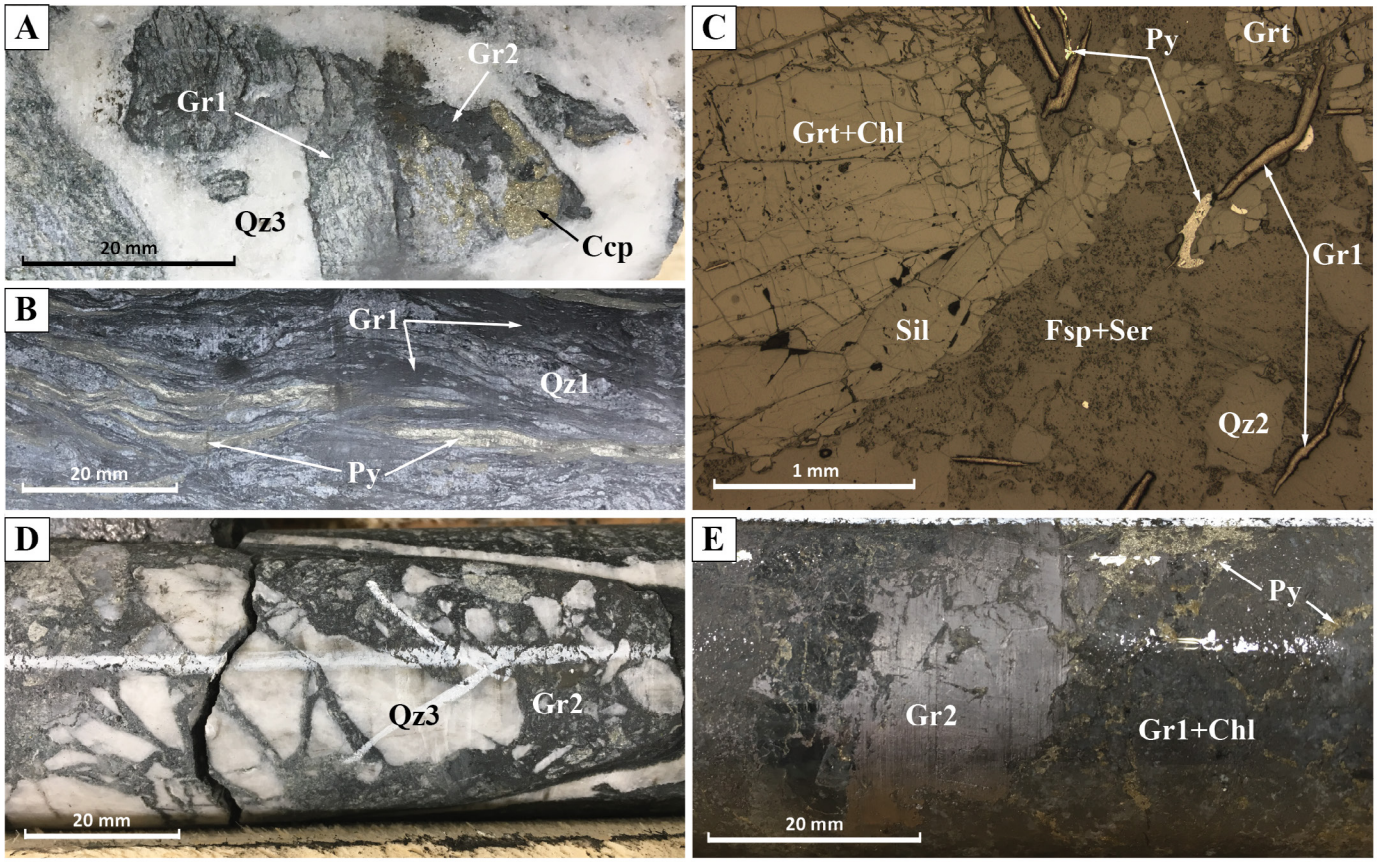


Fig. 18. A) Angular clast of sheared, graphitized (Gr1) wall rock within a milky quartz breccia (Qz3). Younger/remobilized graphite (Gr2) precipitated postbrecciation along fractures in the milky quartz and along clast margins (NQ, AR-18-210c3, 869.4 m). Ccp = chalcopyrite. B) Low-grade mylonite with structurally focused graphitic carbon (Gr1) and premineralization iron sulfide (Py) stringer veins mimicking and crosscutting anastomosing primary shear fabrics (NQ, AR-18-210c3, 805.6 m). C) Metasomatized quartz-feldspar-garnet-sillimanite gneiss within the A1 hanging wall exhibiting chloritized garnet (Grt + Chl) overgrowing sillimanite (Sil), sericitized feldspar (Fsp + Ser), and highly reflective flakes of millimeter-scale graphite (Gr1) associated with finer grains of pyrite (Py) precipitating along grain boundaries and replacing minerals (AR-17-167c2, 689.7 m). D) Clast of graphitized wall rock (Gr1) with contemporaneous premineralization chalcopyrite rimmed by remobilized graphitic carbon (Gr2) within a milky quartz (Qz3) breccia (NQ, AR-18-210c3, 869.8 m). E) Mass of remobilized graphitic carbon (Gr2) overprinting a previously graphitized and chloritized (Gr1 + Chl) high-strain zone with premineralization pyrite (Py) mineralization precipitated interstitially and along fractures (NQ, AR-18-211c1, 1,084.85 m).

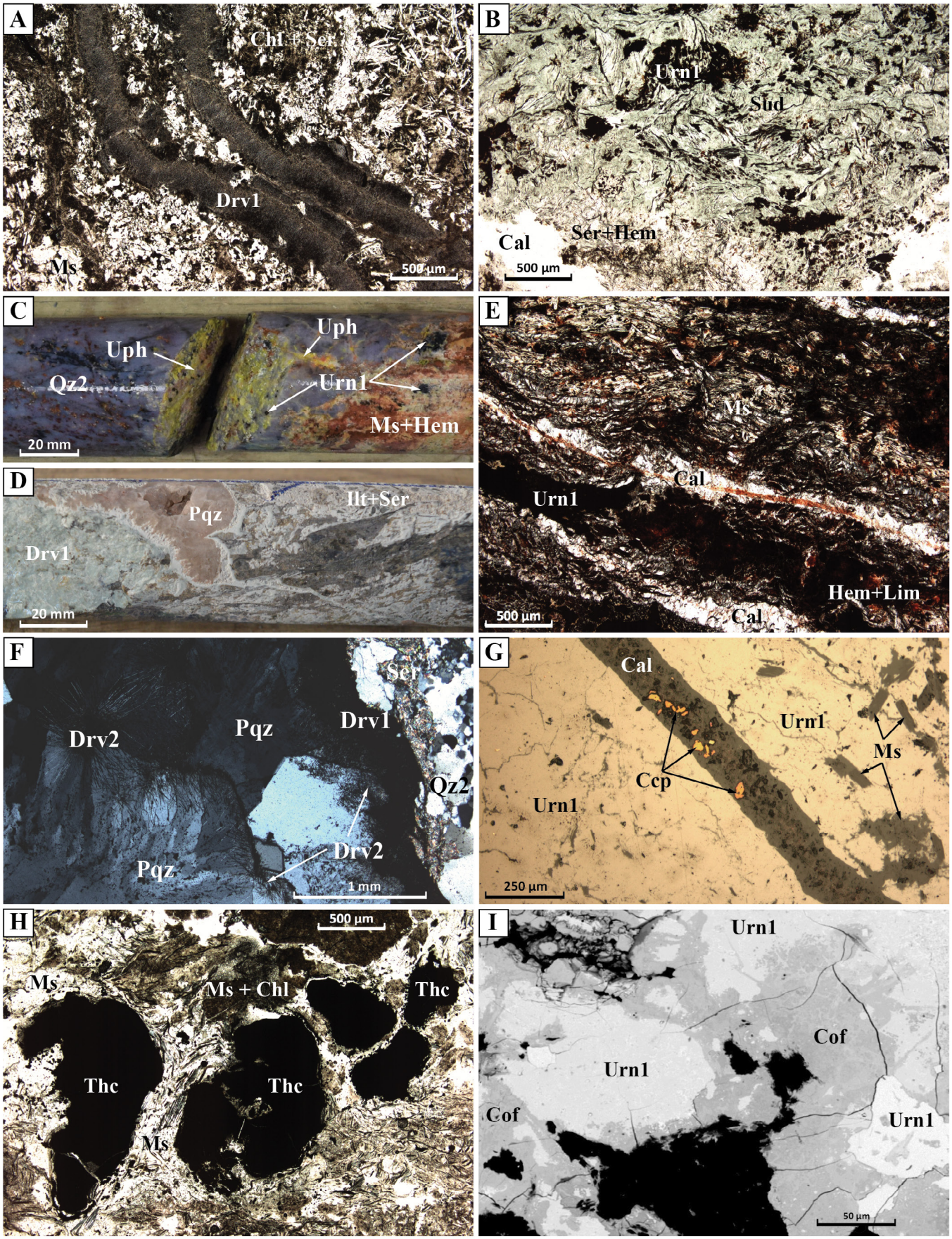
18A, D, E), evidenced by the highly strained and chloritized graphite-bearing rocks being subsequently crosscut by quartz veins and/or healed with quartz via hydraulic fracturing and brecciation (Fig. 18A, D). The paragenetic relationships are complex, however, as relatively early quartz veins (Qz3) are commonly brecciated and hosted within a matrix of graphite (Fig. 18D) or exhibit graphite-healed fractures but also are observed to host clasts of graphitized wall rock within the same structure (Fig. 18A). Disseminated flecks of graphite are also observed in the relatively unstrained, metasomatized wall rocks of the main fault structures, observed to be precipitated along grain boundaries and replacing minerals along with Fe sulfides (Fig. 18C).

Hematite (Fe_2O_3) and limonite ($FeO(OH) \times nH_2O$) alterations are variable, occurring as discrete stains intimately associated with uranium mineralization and overprinting earlier sericite alteration (e.g., Fig. 15C) or contemporaneous with main-stage white-mica alteration and as groundmass alteration of quartz-clastic breccias (e.g., Qz3; Fig. 16). Moderate to strong hematization is also well developed in the upper portion of the crystalline basement rock, interpreted to be part of the red zone paleoweathering profile (Fig. 16).

Main alteration and synprimary uranium mineralization stage

A close relationship between uranium mineralization and white micas is commonly observed throughout the Arrow deposit, with uraninite both replacing early white-mica grains and precipitating along grain boundaries and cleavage planes. Phases of pre-, syn-, and postmineralization white-mica alteration are evidenced by crosscutting and grain boundary relationships (e.g., Fig. 19A). In general, white mica (muscovite) associated with the main alteration stage and that which is syn- to postmineralization is coarser grained than the sericitic white mica (illite) formed premineralization (Fig. 19A). The most common clay minerals encountered at Arrow are kaolinite and illite. Kaolinite is the most common clay mineral proximal to the unconformity, whereas mixtures of illite and muscovite appear to be more commonly associated with

Downloaded from http://pubs.geoscienceworld.org/segweb/economicgeology/article-pdf/116/2/285/5245035/4797_hillacre_et_al.pdf
by Univ Nebraska Lincoln user



Downloaded from http://pubs.geoscienceworld.org/segweb/economicgeology/article-pdf/116/2/285/5245035/4797_hillacre_et_al.pdf
by Univ Nebraska Lincoln user

mineralization, as mentioned. Textural and crosscutting relationships provide evidence of multiple phases of clay alteration, replacing minerals or exhibiting a clear structural control through fracture linings and overprinting of previously sericitized or chloritized structures.

Episodes of main-stage to synmineralization Al-rich hydrothermal chlorite (sudoite; Figs. 16, 19B) form crosscutting fracture linings, small veins, breccia matrices (e.g., Fig. 14B), or mineral replacements. Main-stage sudoite alteration is the most abundant chlorite group mineral at the Arrow deposit and is dominantly structurally focused and commonly associated with mineralization (Fig. 19B). Chloritic slickensides are abundant along brittle fractures, commonly colined with remobilized graphite (Gr2) and exhibiting multigenerational slickenstriae formed during reactivation of previously chloritized and graphitized high-strain zones.

The primary uranium mineralization within the Arrow deposit (Urn1 and 2; Figs. 15E, 16, 19C) comprises dominantly subhedral to euhedral isometric crystals and semimassive occurrences of variably altered uraninite. Uraninite exhibits a bright-white color and relatively clean appearance in BSE images and corresponds to the oldest phases of mineralization based on textural and crosscutting relationships. Many of the uraninite samples from Arrow display largely homogeneous reflectance; however, most samples analyzed show uraninite crystals having zones or mantles of different reflectivity due to alteration or recrystallization. The different uranium mineral groups are clearly visible in drill core (Fig. 19C) and BSE images (e.g., white uraninite vs. gray coffinite; Fig. 19I) and correspond to the paragenetic sequences (Fig. 16) evidenced by textural relationships.

Several phases of younger quartz veins are recognized throughout the Arrow deformation zone (e.g., Pqz and Sqz; Fig. 16). Younger quartz types form druzy veins and cavity fills, breccia matrices, and irregular vein stockworks (Fig. 19D). These younger veins are commonly overprinted and form clasts within breccias healed by clay minerals or yet another phase of quartz. Massive quartz breccias several meters thick are common features overprinting sheared rocks at Arrow. Relatively late quartz phases exhibit a spectrum of colors ranging from translucent to nearly black and often display spectacular zoning. The most common colors include clear to milky white, pink, and smoky gray, brown, or black. The pink quartz-bearing structures have the closest spatial association with uranium mineralization (e.g., Fig. 19D), and appear to be concentrated within the hanging-wall block of the deposit.

At Arrow, telluride minerals containing Pb (altaite?), Bi (tellurobismuthite?), and Cu-Se (bambollaite?) have been identified in thin section and are currently interpreted as syn- to postprimary mineralization stage, based on textural and crosscutting relationships (Mohrbutter et al., 2018). Several main-stage telluride minerals have been identified within the ore zones, commonly associated with bismuth minerals, and postmineralization telluride minerals appear to show a spatial relationship with both bismuth minerals and precious metal mineralization.

Pyrite, chalcopyrite, and galena are among the most common main-stage sulfide minerals and are often observed to be encased in or rimming uraninite or intergrown with uranium minerals. Similarly, main-stage mineralized calcite ($CaCO_3$) veins have been observed within the ore zones, consisting of disseminated uraninite encased within the vein or coprecipitated along the vein margins.

Postprimary uranium mineralization stage

Black or white postmineralization calcite veins are observed crosscutting barren wall rock as well as high-grade uranium mineralization as microstockworks or druzy veins (e.g., Fig. 19E, G). Druzy calcite veins are associated with main-stage and postmineralization-stage sulfide mineralization, frequently showing a contemporaneous relationship (Fig. 19G). Late siderite ($Fe^{2+}CO_3$) veins and druzy void fills associated with post-Athabasca brittle deformation are common within the upper 50 to 100 m of basement rock below the unconformity and crosscut the overlying Athabasca Supergroup sandstones.

Although commonly observed proximal to and within mineralized zones, pale bluish-gray to blue tourmaline, interpreted as dravite and/or magnesiofoitite, forms either in late vein stockworks or larger hydraulic breccias that crosscut the wall rock (Drv1; Fig. 19D) and, in many cases, uranium mineralization. The tourmalines form a substantial alteration halo around the Arrow deposit, extending from over 900-m depth to the unconformity surface. At least two generations of tourmaline minerals have been observed in the matrices of

Fig. 19. A) Plane-polarized light (PPL) photomicrograph of dirty premineralization chlorite-sericite (Chl + Ser) alteration overgrown by coarser clean main-stage muscovite (Ms) alteration, both crosscut by coarse-grained syn- to postmineralization dravite (Drv1) veinlets (AR-16-084c1, A1 shear, 665.0 m). B) PPL image of main-stage sudoite alteration (Sud) overprinting early sericitic white-mica alteration stained with hematite (Ser + Hem). Uraninite mineralization (Urn1) precipitated along grain boundaries and cleavage planes. The assemblage is crosscut by postmineralization calcite veins (Cal) (AR-16-063c1, A2 shear, 446.25 m). C) Canary yellow uranophane (Uph) altering primary uraninite (Urn1) along mineralized fractures in blue quartz (Qz2)-rich wall rock with proximal main-stage muscovite and hematite alteration (Ms + Hem) (NQ, AR-17-147c4, 522.7 m, up to 3,800 cps). D) Druzy pink quartz (Pqz) within an illite-rich hydrothermal breccia (Ilt + Ser) 20 m from A1 shear mineralization, with late blue dravite (Drv1) along fractures (NQ, AR-16-072c2, 418.3 m). E) PPL photomicrograph of calcite (Cal) veins crosscutting main stage muscovite alteration (Ms), uraninite mineralization (Urn1), and associated hematite-limonite (Hem + Lim) alteration (AR-15-059c2, A2 shear, 531.1–531.15 m, up to 52,000 cps). F) Cross-polarized light photomicrograph of a coarse-grained dravite vein (Drv1; in extinction) and younger acicular dravite (Drv2) rimming and precipitating along grain boundaries in a pink quartz vein (Pqz) crosscutting blue quartz (Qz2) and premineralization sericitic alteration (Ser) (AR-16-078c4, A2 hanging wall, 621.25 m). G) Reflected-light photomicrograph of primary uraninite mineralization (Urn1) encompassing earlier main-stage muscovite alteration (Ms) and crosscut by a postmineralization calcite (Cal) and chalcopyrite (Ccp) vein (AR-16-078c3, A2 shear, 471.0 m). H) PPL image of amorphous thucholite grains (Thc) within a matrix of premineralization sericitic white mica (Ser) and chlorite (Chl), and main-stage muscovite (Ms) (AR-16-063c1, A2 shear, 473.25 m). I) Backscattered electron image of heavily altered primary uraninite (Urn1) with mantles of darker gray coffinite (Cof) within the A2 shear wrench zone (AR-16-076c3, 518.85 m).

Downloaded from http://pubs.geoscienceworld.org/segweb/economicgeology/article-pdf/116/2/285/5245035/4797_hillacre_et_al.pdf
by Univ Nebraska Lincoln user

hydrothermal breccias and in veins at Arrow, with the first being relatively coarse grained and the second being dominantly fibrous or acicular (Fig. 19A, F). A study completed by Rosenberg and Foit (2006) showed a similar textural paragenesis at the Rabbit Lake and Key Lake uranium deposits. Quartz veins (especially pink) are very commonly lined with dravite and/or clay minerals (illite, kaolinite, muscovite), clearly illustrating structural control (Fig. 19D). In thin section, the tourmaline commonly exhibits an acicular habit of radiating crystals from vein boundaries or as masses with other minerals (Fig. 19F). Acicular tourmaline crystals (Drv2; Fig. 16) have been observed to occur with both illite and illite-sudoite mixtures. Based on crosscutting relationships observed in thin section and hand sample, the bluish tourmaline is one of the latest alteration phases, dominantly forming postmain mineralization stage at Arrow (Fig. 16). However, some tourmaline may be locally synchronous with the main mineralizing events (Drv1; Fig. 16), such as the suggested case at McArthur River (Adlakha and Hattori, 2016), with a younger stage of magnesiofoitite forming coeval with, or after, late ore remobilization or alteration stages (Drv2; Fig. 16). Although there are variations in the timing of dravite/magnesiofoitite across the basin, the temporal relationship between tourmalines and uranium mineralization at many unconformity-related uranium deposits in the Athabasca basin (e.g., Shea Creek, Kister et al., 2005; Sheahan et al., 2016; and McArthur River, Adlakha and Hattori, 2016) appears to be broadly syn- to posturanium mineralization.

Postmineralization sulfides consist dominantly of pyrite, chalcopyrite (Fig. 19G), and galena, with subordinate pyrrhotite, pentlandite, covellite, cobaltite, and bornite identified in thin section. Postmineralization sulfides occur typically as disseminated blebs or as stringer veins, commonly with quartz and/or carbonate (Fig. 19G), which commonly crosscut the dominant foliation, mineralization, and late alteration phases such as dravite. Postmineralization pyrite and chalcopyrite are the most common as late veins and disseminations. Pyrite is by far the most abundant sulfide mineral overall, forming both contemporaneous with (premineralization stage), and subsequently (syn- to postmineralization stage) to graphitization of the highly strained rocks constituting the Arrow shear zones (Fig. 16). Postmineralization sulfide minerals exhibit a strong spatial association with the preexisting shears, especially those that are graphitic, reusing previous planes of weakness along foliation or fractures, and commonly crosscut earlier fabrics as irregular stringer veins.

Uranium mineralization at Arrow is locally accompanied by uranoan pyrobitumen (thucholite; Fig. 19H); however, instances of pyrobitumen in barren rock proximal to mineralization have also been observed. Thucholite is an unusual mineral, composed of approximately 50% carbon, 25% volatile gases, and 25% ash (Barthauer et al., 1953). The pyrobitumen at Arrow has not been studied in detail; however, it is interpreted to be relatively late in the Arrow paragenetic sequence (Fig. 16), as it is most commonly observed along clay-lined fractures, disseminated through fault gouge, within crosscutting druzy quartz veins, or within voids or vugs.

Secondary uranium minerals at Arrow are constituted by dominantly anhedral, dirty-looking grains, alteration rims, or mantles on uraninite or rutile/anatase. They are far less reflective in BSE images, exhibiting a distinct gray color (e.g., Fig. 19I). Secondary uranium minerals correspond to texturally younger uranium silicates such as uranophane (Fig. 19C) and coffinite (Fig. 19I), as well as other hydroxides/oxyhydroxides (Fig. 16). The presence of several different uraniferous phases indicates postmineralization fluid circulation events affected the primary Arrow orebody over geologic time.

Native gold (containing silver) and bismuth have also been identified in a suite of samples and are commonly associated with telluride minerals. Gold ± silver mineralization occurs as fine-grained (5–250 µm) native gold, which frequently exhibits intergrowth textures with bismuth and telluride minerals. Gold does not appear to be intimately related to sulfide mineralization and appears to postdate initial uraninite mineralization (Fig. 16); however, crosscutting relationships indicate the gold is older than alteration of uraninite to coffinite in the samples studied.

Discussion

Regional- and deposit-scale ductile structural framework

Rocks throughout the Taltson domain, south of the Athabasca basin, underwent multiple metamorphic and deformational episodes ca. 1.94 to 1.8 Ga, resulting in multiple foliations (S_1 to S_3), fold generations (F_2, F_3, and F_4) and the development of deep-seated shear zones (Figs. 2, 3; Card et al., 2008). Intrafolial F_2 folds were refolded by F_3 folds, resulting in an early type 3 fold interference pattern. F_4 folds consist of NNW- to NW-trending folds with subvertical axial surfaces orthogonal to F_3, resulting in a dominant type 1 fold interference pattern observed across the region (e.g., Card, 2009). It is important to determine whether any of these ductile structural features can be observed near the Arrow deposit and to discuss whether they have played a role in the siting of uranium mineralization.

Despite local variability, stretching lineations (Fig. 7) are a useful tool in fold analysis, as they preferentially form colinear to fold axes (i.e., in curtain or sheath folds, which are common in shear zones, especially mylonites; e.g., Cobbold and Quinquis, 1980). The opposing clusters of ductile lineations in Figure 20A bear a strong resemblance to a shift in lineation plunge expected from type 1 dome-and-basin fold geometry produced by F_3 and F_4 folds. This fold geometry is observable at different scales, from drill core and outcrop scale to regional scale (Fig. 20B, C, respectively). Regional airborne magnetic susceptibility and Z-Tipper Electromagnetic (Z-TEM) geophysical surveys reveal patterns that resemble the type 1 fold interference pattern observed at smaller scale in outcrop southeast of Arrow at Turnor Lake (Fig. 20B) and provide corroborating evidence for the fold model on a property scale (Figs. 20C, 21). Regionally, the Clearwater domain represents a deep-seated structure lying axial planar to the interpreted regional NE-plunging synform (Fig. 2), with property-scale parasitic folding in the southeast limb hosting the Arrow deposit, as illustrated in Figure 20C.

Additionally, the wall rocks at Arrow contain a locally pervasive S_1-S_2 fabric that predates the uranium mineralization of the Arrow deformation zone (Fig. 22A). As mentioned, the early S_1-S_2, gently SE-dipping gneissic foliation of the Taltson domain was locally folded by outcrop- and map-scale F_3 folds

Downloaded from http://pubs.geoscienceworld.org/segweb/economicgeology/article-pdf/116/2/285/5245035/4797_hillacre_et_al.pdf
by Univ Nebraska Lincoln user

Downloaded from http://pubs.geoscienceworld.org/segweb/economicgeology/article-pdf/116/2/285/5245035/4797_hillacre_et_al.pdf
by Univ Nebraska Lincoln user

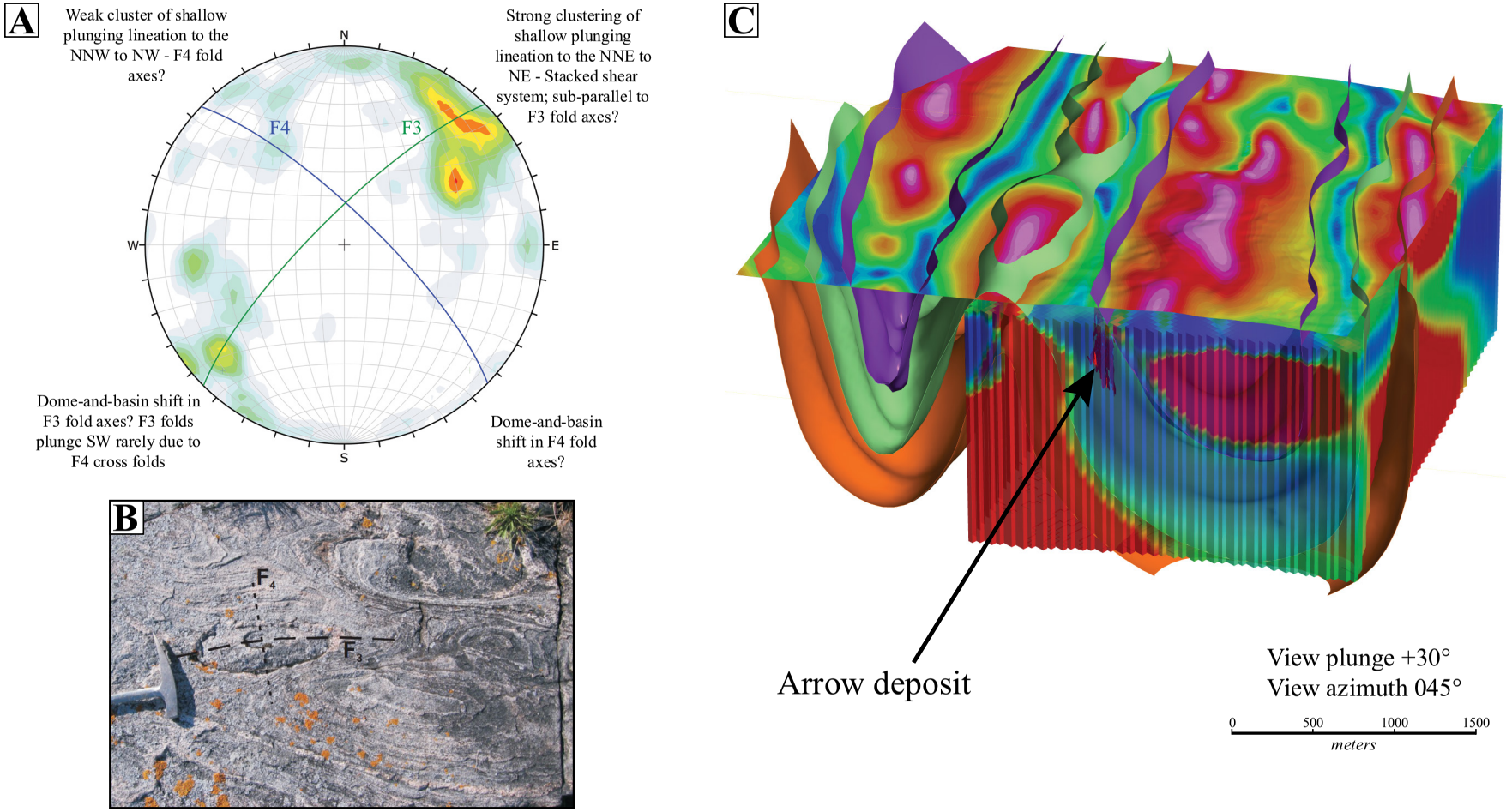


Fig. 20. A) Averaged axial planes constructed from stereographical clustering of Arrow lineations. B) Well-developed type 1 dome-and-basin interference pattern in minor folds at northeast Turnor Lake, approximately 130 km south-southeast of Patterson Lake. F_3 axial traces are parallel to the long-dashed line and F_4 traces to the short-dashed line (from Card, 2009). Data of lineations colinear to axial surfaces display grouping of clusters, resulting in a range of axial plane orientations, which correspond to orientations of regional F_3 and F_4 axial planes of the Lloyd fold domain. These orientations also correlate with larger-scale regional geophysical magnetic fabrics, as well the main structural grains observed at Arrow. C) 3-D schematic based on correlation of airborne magnetic susceptibility and 3-D Z-TEM geophysical surveys, showing the Arrow deposit hosted within the limb of a property-scale F_3 fold, and resulting fold interference patterns within a horizontal slice just above the unconformity surface. Note the scale of the Arrow deposit resource model.

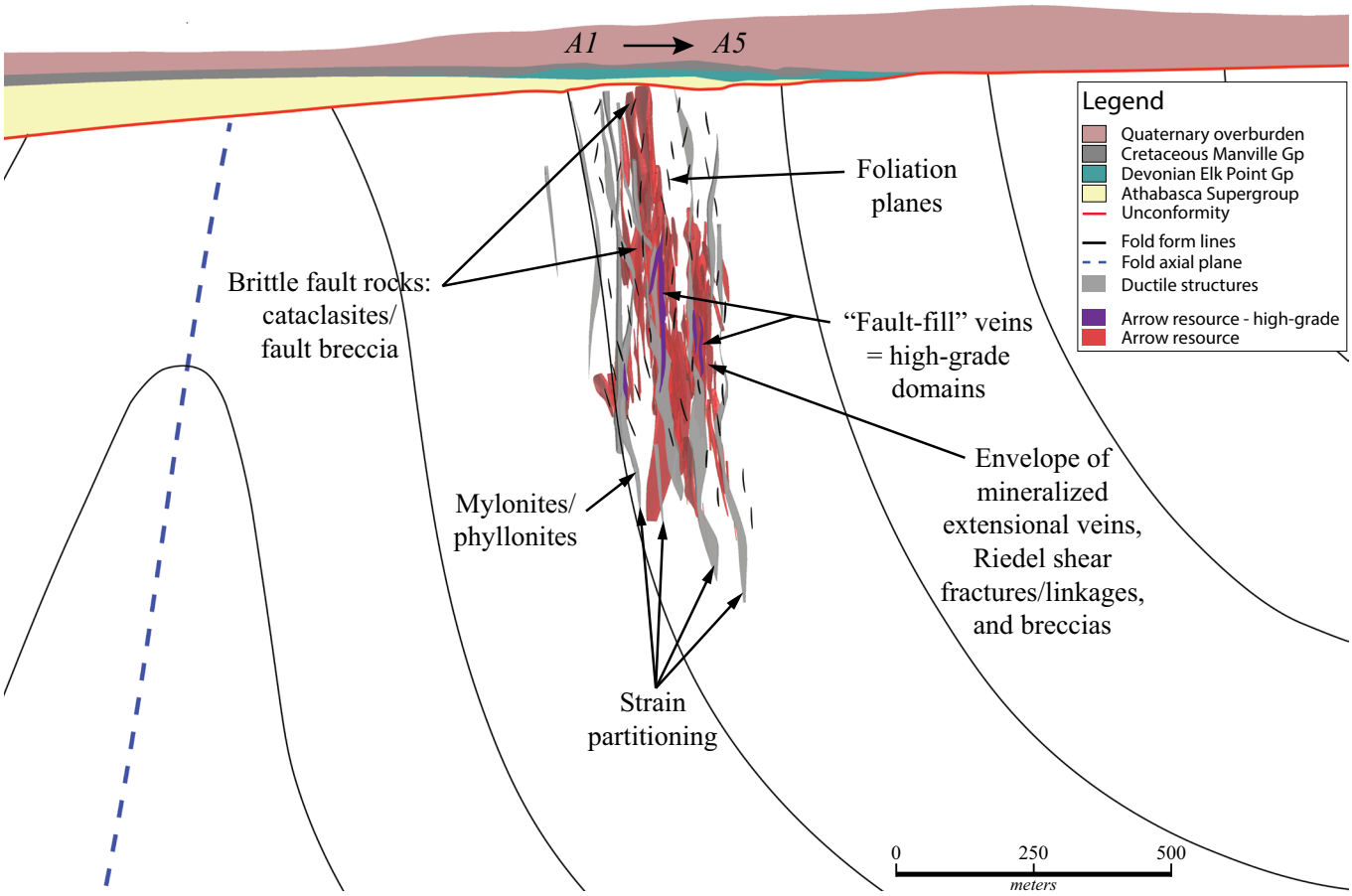


Fig. 21. Schematic cross section looking northeast (052°) of the Arrow strike-slip deformation zone showing the stacked A1 to A5 shears (from left to right) and associated fault rocks, hosted within the limb of an F_3 fold. Note the stacked nature of the ductile structures and mineral resource model (O'Hara et al., 2018), reflecting the partitioned shear system and the overall plunge to the south-southeast.

and is observed to be transposed subparallel to S_3 foliations, especially proximal to and within high-strain zones, which preferentially developed along highly strained F_3 fold limbs (e.g., Fig. 21; Card, 2009). Structural analysis completed at Arrow suggests that regional F_3 and F_4 folds, as described by Card et al. (2008), are common through the study area, resulting in type 3 transitional to type 1 dome-and-basin style folding. This early ductile framework provided limb domains, which became ideal nucleation sites for the formation of high-strain zones, such as the Patterson Lake corridor (Fig. 21). The refolding and fold interference patterns created variability in fold geometry, which played a crucial role in the spatial formation of zones of dilation and zones of compression along high-strain zones. The early ductile structural framework was thus a key factor in the genesis of the Arrow deposit, because it provided constraints on the orientation of the Patterson Lake corridor in the Rook I property, which can act as a limiting or accommodating factor for subsequent shear zone formation, brittle reactivation, fluid movement, and uranium mineralization.

Arrow deformation zone geometry and structural regime

Structural analysis along the ore-hosting portion of the Patterson Lake corridor at Arrow indicates a sequential development of early ductile and brittle-ductile to late brittle episodes of movement along the southeast limb of a regional NE-plunging fold complex (Fig. 2). Structural and metamorphic relationships suggest that mylonitization was initiated in a ductile environment during D_3 deformation, with subsequent overprinting by brittle-ductile and brittle faulting involving widespread cataclasis and brecciation, reflecting the progressive unroofing of the high-strain zones to shallower lithospheric levels. The stacked high-strain zones at Arrow are nearly parallel and are grouped into a deformation zone approximately 200 to 250 m wide (Fig. 21), with mineralization shoots generally plunging to the south-southwest.

The structural system at Arrow is interpreted to have originally developed along near-vertical-dipping NE-to SW-trending heterogeneous high-strain zones (A1-A5 shears) formed under a dominantly transpressional regime along the highly strained F_3 fold limb (Figs. 21, 22B). Under transpressional (and transtensional) conditions, deformation zones commonly develop as steeply dipping or subvertical; however, the strike of the principal flattening surface (i.e., cleavage, schistosity, foliation/gneissosity) may vary with the noncoaxial component of the strain, as is the case at Arrow (Fig. 8). Transpression is strike-slip deformation that diverges from simple shear due to a component of shortening orthogonal to the deformation

Downloaded from http://pubs.geoscienceworld.org/segweb/economicgeology/article-pdf/116/2/285/5245035/4797_hillacre_et_al.pdf
by Univ Nebraska Lincoln user

zone (Dewey et al., 1998). This type of 3-D noncoaxial strain develops chiefly in response to obliquely convergent (or divergent) relative motions across crustal deformation zones at various scales. Characteristic kinematic partitioning of noncoaxial strike-slip and coaxial strains is prominent in situations where the far-field (plate) displacement direction is sufficiently oblique to the deformation zone boundary (Dewey et al., 1998). The angle of obliquity, intensity of finite strain, and degree of kinematic partitioning principally control the orientations of fabrics in transpressional and transtensional zones (Dewey et al., 1998). When the angle of obliquity (α) is small, such as at Arrow, deformation becomes localized on steeply dipping faults (>70°), and associated structures are typical of a strike-slip regime with Riedel faults. As α increases, strain is accommodated by shallow-dipping faults that may result in basins or uplift zones. Subsequent reactivation of preexisting structural weaknesses (shear zones, ductile layers) that are in suitable orientations to minimize work done can facilitate strain partitioning during deformation. The quartz-flooded blocks of wall rock bound by the A1 through A5 high-strain zones likely helped to partition strains into the series of complex displacements, strains, and rotations (Dewey et al., 1998). Dewey et al. (1998) note that in situations where the angle of obliquity is less than 20°, associated stretching and mineral lineations will preferentially form subhorizontally, which is characteristic at Arrow. Such a situation is referred to as "wrench-dominated transpression" (Dewey et al., 1998). Wrench on a deposit scale is evident within the heart of the A2 shear, where the A2 high-grade core lies, marked by a northerly shift in strike and local reverse in dip direction from southeast to northwest. In addition, the separation of pole clusters in the lineation stereonet shown in Figure 20A is likely a reflection of the heterogeneous strain within a partitioned, stacked shear system, with lineation plunge and trend reoriented locally with progressive shearing and strain partitioning during protracted reactivation.

The staircase-like trajectory of the modeled ductile structures in Figure 8 made up of alternating long and straight traces (vertical equivalent to flats) connected by oblique bends and jogs (ramps) is an important map-scale geometry resulting from strike-slip movement. In general, this map-scale geometry reflects the right-stepping C-S–style morphology expected from dextral displacement; however, in this case the modeled north-northeast to south-southwest flexures would represent constraining bends within the shear. During initial right-lateral ductile deformation, the corridor likely developed consisting of northeast to southwest throughgoing straight belts of mylonitic rocks connected by NNE-SSW–trending flexures. The 3-D structural model of the Arrow deposit in Figure 8 illustrates that uranium mineralization is concentrated along the main structural grain and within dilational zones (effectively pull-apart basins) bound by the original restraining bends. With progressive tectonic activity and corresponding changing stress fields, subsequent sinistral reactivation of the corridor would allow for such a situation, effectively turning the NNE-trending constraining bends into releasing bends.

Based on drill core evidence, structural measurements, and deposit-scale structural features, it is suggested that the Arrow deformation zone formed under a partitioned, transpressional regime in which a significant portion of the wrench component was accommodated by the formation of discrete strike-slip shears (i.e., A1-A5) within the overall deformation zone (Figs. 8, 21). Strain partitioning in the Arrow deformation zone was likely facilitated by the reactivation of these preexisting structural weaknesses, which were in orientations suitable to facilitate transpressional strike-slip movement through the development of a stacked shear system (Fig. 21).

Shear zone P-T conditions and alteration

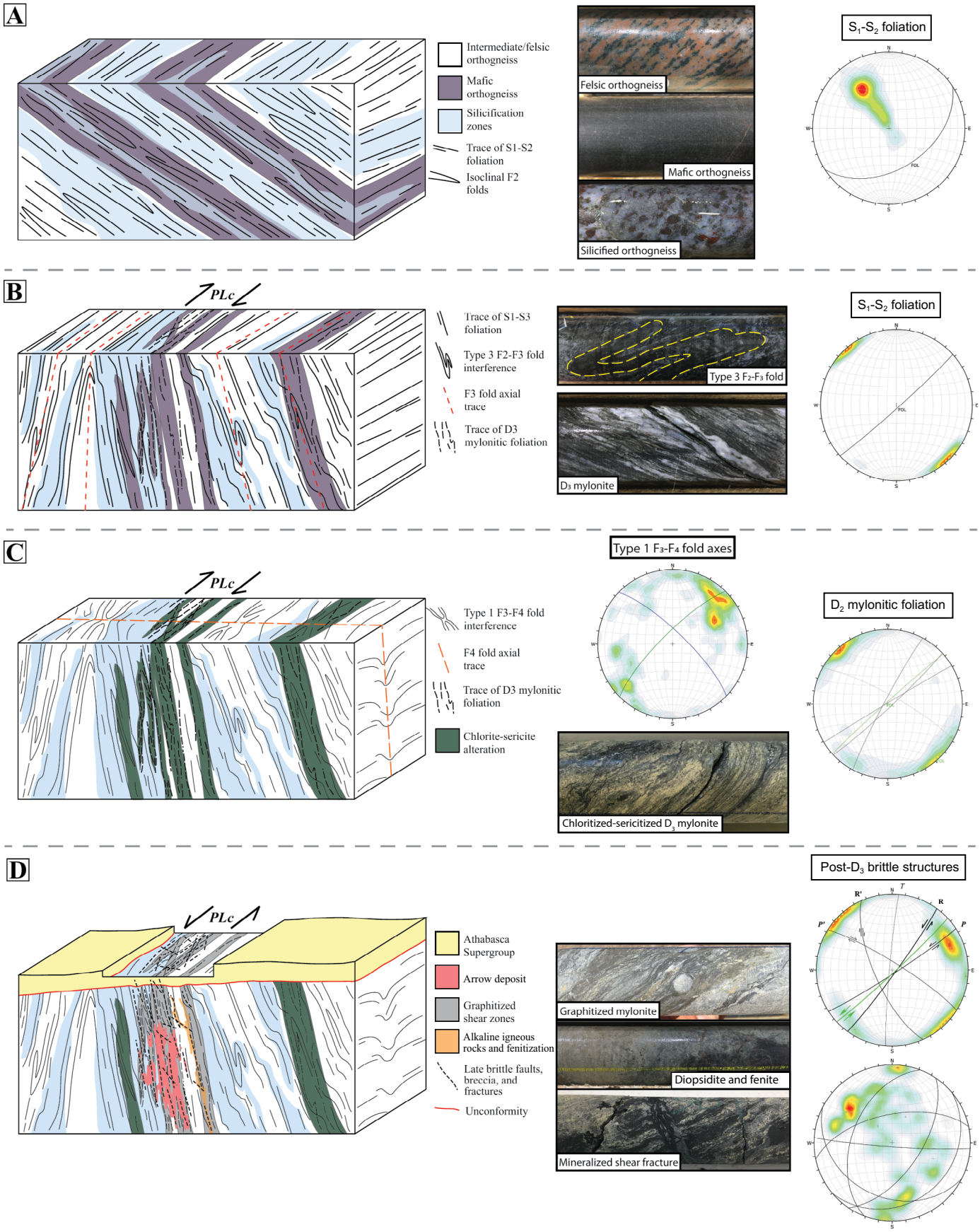
The textural characteristics of microfabrics in shear zone rocks (e.g., crystal-plastic deformation in quartz) may be used to approximate temperature ranges, although the earliest deformational stages may be overprinted and no longer recognizable. The temperature range for low-grade mylonites is thought to be approximately 250° to 500°C (Trouw et al., 2009), with a gradual transition between formation of cataclasites and low-grade mylonites through the brittle-ductile transition zone. The temperature range for the formation of medium-grade mylonites is between 500° and 650°C, in which quartz is commonly fully recrystallized, and gradual transitions to nonmylonitic country rocks are common (Trouw et al., 2009).

Preservation of low- to medium-grade mylonitized rocks at Arrow indicate that they likely formed during intense and/or rapid deformation after peak granulite facies metamorphism, as their textures have generally not been destroyed or overprinted by recrystallization and grain growth associated with any subsequent higher-grade metamorphism. Thin section examination of quartz grains within and proximal to the Arrow high-strain zones reveals evidence for both crystal-plastic and brittle/frictional deformational processes, indicating these zones underwent continued deformation through the brittle-ductile transition zone postpervasive quartz flooding (Figs. 11A, B, 22A-C). Based on analysis of mineral textures and grain boundary relationships and considering the mylonite temperature ranges outlined by Trouw et al. (2009), it is suggested that these high-strain zones initially formed within a ductile regime at around 20-km crustal depth. These zones then further evolved through the brittle-ductile transition, forming low-grade mylonites and phyllonites, followed by cohesive cataclasites and finally incohesive breccias and gouge with prolonged exhumation.

The long-lived evolution of the high-strain zones at Arrow and the relatively high finite strain values reached within mylonitized rocks imply that the strain rate in the shear zones exceeded that in the wall rock for a notable period and that the rocks in the zones were softer than the wall rock (Passchier and Trouw, 2005). Following the nucleation of the structures, changes occur in the rheology of material in the ductile shear zone through an effect known as strain softening, defined simply as decreasing resistance to deformation (Passchier and Trouw, 2005). The A1 through A5 shears exhibit many of the important progressions that contribute to softening, such as grain boundary migration recrystallization, a decrease in grain size, and development of shear bands or shear band cleavage.

In addition to strain softening, measurable volume and porosity changes due to sericitization (dominantly illite) and chloritization, which are important premineralization alteration minerals (Fig. 16), may have played a role in the permeability of the Arrow deformation zone. Alexandre et

Downloaded from http://pubs.geoscienceworld.org/segweb/economicgeology/article-pdf/116/2/285/5245035/4797_hillacre_et_al.pdf
by Univ Nebraska Lincoln user



Downloaded from http://pubs.geoscienceworld.org/segweb/economicgeology/article-pdf/116/2/285/5245035/4797_hillacre_et_al.pdf
by Univ Nebraska Lincoln user

al. (2005) showed that illitization of basement rocks creates space, whereas chloritization consumes space, as the molar volume of chlorite is considerably higher than that of illite. As a result, relatively early sericitic illite alteration of the Arrow high-strain zones likely contributed to the creation of porosity within the zones, thus promoting fluid flow. Furthermore, Alexandre et al. (2005) also suggest that a portion of the potassium liberated during chloritization of early biotite could contribute to the precipitation of a later phase of coarse-grained illite. This interpretive sequence is reinforced by the observed paragenetic relationships at Arrow, which indicate that premineralization sericitic illite was locally formed prechlorite, and coarse-grained illite and muscovite were formed postchloritization during the main alteration and synmineralization stage (Fig. 16). Softening of the shear zones through recrystallization and alteration therefore appears to have resulted in competency and permeability changes within the basement, weakening and breaking up the rocks and thus creating significant rheology contrast between the shears and the quartz-flooded wall rock and effectively preparing the shear zones for ongoing deformation and fluid movement.

Post-Athabasca brittle reactivation

The heterogeneous high-strain zones hosting the Arrow deposit further evolved through episodic reactivation events, creating various small-scale brittle fault linkages oblique to and connecting the main fault zone (Figs. 21, 22D). During the period of fault reactivation, heterogeneity in the rheological characteristics of the basement rock types, ductile fabric elements of D_3 transposed foliations, and anastomosing shear planes appear to have mechanically controlled the locale and geometry of brittle structures that host uranium mineralization.

Drill core evidence reveals that as strain progressed through the brittle-ductile transition, brittle fracturing of rock prevailed and allowed the deformation zone to grow and organize into dense elongated networks through the process of individual shear and extension fractures forming and ultimately linking up (e.g., Figs. 12E, 15C), similar to the process described by Katz et al. (2004). The complex arrangement of shear fractures within the Arrow strike-slip deformation zone carries kinematic information about the evolution of the fault system as a whole. Experiments conducted by Riedel in the early 1900s and numerous other experiments using clay-cake models (e.g., Tchalenko, 1968, 1970; Naylor et al., 1986; Lazarte and Bray, 1996; Atmaoui, 2005) have revealed a consistent timing and faulting sequence of these prominent features in strike-slip fault zones. This led to the discovery that strike-slip faults often do not develop a single clean fault but a zone of deformation involving an array of small fractures and linkages (Fig. 13H; e.g., Tchalenko, 1968; Davis et al., 2000; Haakon, 2010). In deep-seated wrench-dominated faulting, synthetic and antithetic Riedel shear fractures are among the primary features to appear in strike-slip zones and evolve as a series of linked displacement surfaces (Davis et al., 2000). Sets of subsidiary shear fractures that propagate a relatively short distance out from the main fault or shear, but are coeval with it, are termed Riedel shear fractures and develop in zones of simple shear during the early stages of fault formation (Katz et al., 2004). Riedel shear fractures developed along a fault or slip surface show distinct geometric arrangements that carry information about the movement sense on the fault plane (Passchier and Trouw, 2005). These relatively small-scale fractures have been given different names based on their orientations and kinematics (Riedel, 1929). In large-scale fault patterns, Riedel fractures may refer to as many as six direction groups (R, R', P, P', Y, T) of associated synthetic or antithetic smaller-scale fractures (Fig. 13H).

Riedel shears can be used as shear sense indicators, through observation of deflection of foliation or of older Riedel shears by younger shears (e.g., P by R; Y by R; Passchier and Trouw, 2005). The attitude of the composite foliation planes is representative of the general strike of the Arrow strike-slip deformation zone, shown in green in Figure 13A, while the most prominent orientations of the aforementioned structures represent the development of a Riedel-style brittle geometry. The most prominent orientation of brittle structures (Fig. 13B) represents formation of subsidiary Riedel shear fractures oblique to the northeast-southwest imposed shear angle at acute angles. A dominantly sinistral displacement is suggested by the counterclockwise orientation of R and R' shears (Fig. 13E) with respect to the main shear orientation, overprinting earlier dextral displacement during ductile shearing.

Interpretation of the major structural trends, kinematic indicators in hand specimen, and fault and fracture offsets suggests a predominantly oblique-reverse, wrench-dominated transpressional, sinistral strike-slip fault system of complex Riedel-style geometry was active during brittle reactivation

Fig. 22. Block diagram schematic (NW-SE cross-section face) illustrating the structural evolution of the Patterson Lake corridor and related metasomatism, hydrothermal alteration, and formation of the Arrow uranium deposit. A) Development of composite gneissic S_1-S_2 foliation and intrafolial F_2 folds, coincident with M_1 granulite facies metamorphism. Preferential pervasive silicification of intermediate orthogneiss units and growth of overprinting garnet porphyroblasts occurs syn- to post-peak metamorphism. B) Early D_3 deformation characterized by upright NE-SW–striking F_3 folds leading to development of S_1-S_3 transposition foliation (F_3 axial planar) along the newly forming Patterson Lake corridor and type 3 F_2-F_3 fold interference. Subvertical, right-lateral anastomosing ductile shear zones begin to develop along highly strained F_3 fold limbs = PLc. C) Late D_3 deformation characterized by formation of NW-SE–striking F_4 cross folds leading to type 1 F_3-F_4 fold interference. D_3 ductile to brittle-ductile high-strain zones (A1-A5) evolve subparallel to S_1-S_3 transposition foliation in F_3 fold limb; concentrated in softened mafic units. Replacement of granulite facies assemblages by M_2 amphibolite facies metamorphism (biotite, amphibole), followed by development of midgreenschist facies M_3 assemblages including widespread chloritization and subsequent ubiquitous sericitization. D) Graphitization of major shear zones through the brittle-ductile transition coeval with sulfide mineralization, followed by local intrusion of alkaline dike rocks and associated fenite alteration. Later brittle sinistral reactivation of the Patterson Lake corridor forming arrays of fault rocks including cataclasite, breccia, fault gouge, and Riedel shear fractures, postdating Athabasca Supergroup deposition. Primary uranium mineralization along reactivated shear zones and within arrays of brittle fault rocks in hanging-wall and footwall blocks. Syn- and postmineralization quartz-carbonate veins, tourmaline, sulfides, and precious metals, followed by alteration of the Arrow orebody.

Downloaded from http://pubs.geoscienceworld.org/segweb/economicgeology/article-pdf/116/2/285/5245035/4797_hillacre_et_al.pdf
by Univ Nebraska Lincoln user

of the earlier right-lateral ductile high-strain zones. The primary and subsidiary R, R', P, P', and T shear fractures experienced multiple episodes of brittle structural reactivation and fluid migration, during which the primary uranium mineralization was emplaced (Fig. 22D) and subsequently remobilized and/or recrystallized. The dilatant areas and extensional fault bends and jogs opened through wrench-dominated movement and Riedel brittle reactivation acted as favorable structural sites for fluid flow. Additionally, the A1 through A5 high-strain zones at Arrow are broadly similar in orientation and geometry to type IV fault structures in the southern Shea Creek area, as described by Lorilleux et al. (2002).

The prevalence of oblique-slip slickenstriae orientations measured in Arrow drill core (Fig. 23A) corroborates the deformational model in terms of dominant strike-slip movement with a minor overall dip-slip component. Measurements of these structures in numerous drill holes (Fig. 23A, B) allow for this general description of the fault system at Arrow. To perform an accurate paleostress reconstruction through inversion of fault-slip data and reconstruct the major characteristics of the deformation over a large area, however, more kinematic data is required to definitively interpret the overall shear sense (e.g., Angelier, 1984). Furthermore, due to the heterogeneity of the Arrow deformation zone, paleostress analysis is difficult, as heterogeneous fault-slip data will likely result in a composite stress state representing an aggregate of the stress states corresponding to multiple superimposed tectonic events.

Bearing this in mind, all available slickenline data has been compiled and compared with fracture data to give a general sense of shear along the Arrow deformation zone, considering the orientations of shear fracture families and any available kinematic information. Additionally, because of the amount of reactivation along the shear zone, care was taken in interpretation of slickenstriae data, as the slickensides often only preserve the most recent reactivation episode. Plotting slickenstriae measurements on a 2-D rose diagram reveals patterns that reflect the fracture network geometry (Fig. 23C) and the contractional or extensional nature of specific fracture sets (i.e., contractional orientations [e.g., P fractures] exhibit a higher abundance of slickenstriae, while extensional fractures lack slickenstriae). Slip on conjugate polished fracture sets in en echelon arrays throughout the Arrow shear zone and wall rocks results in equal and opposite sets of slickenlines, which are apparent in Figure 23C. Idealized principal stress directions interpreted based on Figure 23C correspond to the orientations of fracture sets and the principal flattening surface at Arrow; however, more detailed kinematic analysis and paleostress reconstruction is warranted.

Paragenesis, origin of graphite, and parallels with other Athabasca basin uranium deposits

The alteration mineral assemblages observed at Arrow record multiple hydrothermal-metasomatic events affecting the Patterson Lake corridor prior to uranium mineralization at ca. 1.45 Ga (Hillacre et al., 2018), such as metamorphism (retrograde metamorphic assemblages), pre-Athabasca Supergroup weathering, magmatism (Clearwater domain, Patterson Lake Alkaline Igneous Complex), and extensive hydrothermal al-

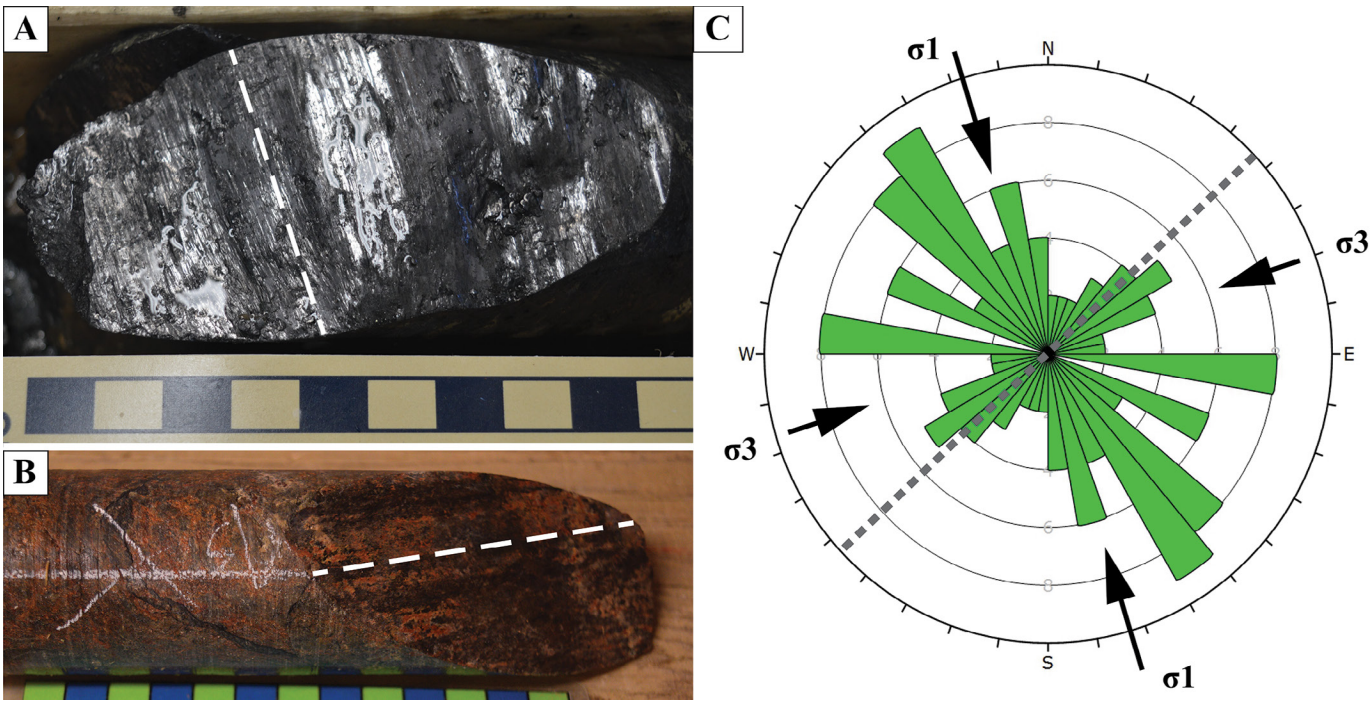


Fig. 23. A) Near strike-slip slickenstriae on a graphitic slickenside within the A3 shear zone (AR-16-094c1, 410.1 m). B) Near dip-slip slickenstriae on a mineralized fracture face with associated hematite-limonite alteration (AR-17-171c3, 768.0 m, up to 8,000 cps). Scale bar divisions in A and B are 1 cm. C) Rosette plot (n = 74) of slickenstriae gamma measurements from slickensides in Arrow drill core, including generalized trend of the Arrow deformation zone (gray dashed line) and possible corresponding principal stress directions (σ_2 is ~vertical). Slip on conjugate fracture sets can create equal and opposite sets of linear features.

Downloaded from http://pubs.geoscienceworld.org/segweb/economicgeology/article-pdf/116/2/285/5245035/4797_hillacre_et_al.pdf
by Univ Nebraska Lincoln user

teration phases. These events resulted in widespread and pervasive quartz flooding, preferential sericitization and chloritization of quartz-poor mylonitic rocks, and graphite and sulfide veining (Card and Noll, 2016; Card, 2017). As the A1 through A5 shears evolved through the brittle-ductile transition and became sites for focused fluid flow, they were overprinted with abundant graphite contemporaneous with iron sulfide mineralization and quartz veins (Fig. 22D). The vein- and breccia-hosted pink quartz contains the most radiation-induced defects (Cerin et al., 2017), suggesting this phase crystallized from uraniferous fluids contemporaneously with the main mineralization event at ca. 1.45 Ga (Hillacre, 2018). Smoky quartz exhibits less homogeneous radiation defects, displaying α particle-induced cathodoluminescence rims, which crosscut the growth zoning and thus appear to record late uranium remobilization events (Cerin et al., 2017).

Graphite is interpreted to be relatively early in alteration paragenesis, preuranium mineralization but postmetasomatic alteration (i.e., quartz-flooding events) of the host rocks. Crosscutting and grain boundary relationships indicate graphite and sulfides were introduced into the Arrow shear structures postsericitization and chlorite alteration as the fluid evolved through modifications in response to alteration processes and/or during younger fluid flux events. This process further weakened the rocks, setting up ideal pathways and potentially providing a reductant for subsequent uraniferous fluids. The interpretation that the graphite along the Patterson Lake corridor is of hydrothermal origin rather than derived from metamorphism of carbon-rich deformed sedimentary horizons contrasts with the literature on unconformity-related uranium deposits in the eastern Athabasca basin. Graphitic pelites occur within the Wollaston Supergroup (Annesley et al., 2005; Yeo and Delaney, 2007), and many of the deposits are spatially associated with these rocks (e.g., Hoeve and Sibbald, 1978; Hoeve and Quirt, 1984). Nevertheless, Card (2012b) suggested from detailed textural examination of drill core in the eastern Athabasca basin that much of the graphite was also hydrothermal in origin. In addition, a variety of reductants, other than graphite, have been proposed for many of the deposits (Yeo and Potter, 2010). At the Arrow deposit, the paragenetic relationships and complete lack of any known sedimentary source rocks support that the graphite was introduced into the Arrow deformation zone via hydrothermal processes under brittle-ductile conditions (Figs. 18B, 22D). Studies have shown that graphite may precipitate from carbon-bearing fluids or melts and often forms veins that are structurally controlled within granulites or igneous rocks (e.g., Beyssac and Rumble, 2014; Luque et al., 2014; Rumble, 2014). Carbon in granulite-hosted graphite veins is derived from sublithospheric sources or from decarbonation reactions of carbonate-bearing lithologies and is transported chiefly in CO_2-rich fluids from which it can precipitate (Luque et al., 2014). Based on mineral textures and crosscutting relationships in thin section and hand specimen (Fig. 18A-E), it is suggested that the graphite along the Patterson Lake corridor at Arrow is of secondary origin, precipitated from fluids that were channeled through brittle fracture systems, both conformable to and crosscutting preexisting ductile structures. Textural relationships also indicate that graphite was subsequently redistributed via relatively late deformation processes at Arrow. Premineralization iron sulfide minerals (dominantly pyrite ± pyrrhotite and chalcopyrite) coprecipitated with graphite at Arrow, and quartz veins and breccias are frequently observed to be associated with graphite. Hydrothermal fluids restricted to the C-O-H system are not capable of causing coprecipitation of other minerals with graphite, nor are they effective in dissolving and replacing silicate minerals in the wall rocks (Rumble, 2014). However, solutions containing sulfur- and chloride-bearing species would account for the coprecipitation of sulfides and other noncarbonaceous minerals, as well as enhancing the solubility of silicate minerals in the country rock (Rumble, 2014).

The intensity of the metasomatism and alteration that predates the formation of the Athabasca basin at the Arrow deposit, including quartz flooding, chloritization, sericitization, and the formation of graphite and early sulfides (Fig. 16), contrasts markedly with the volumetrically less significant premineralization alteration described for basement-hosted uranium deposits in the eastern Athabasca basin (e.g., Eagle Point, Millennium; Alexandre et al., 2005; Cloutier et al., 2009, 2011). Nevertheless, the association between primary uranium mineralization, muscovite, and sudoite, followed by later dravite, carbonates, sulfides, and secondary uranium-bearing minerals is comparable. This implies that the fluids involved in the formation of the basement-hosted deposits were likely similar, as were those involved in the subsequent vein and alteration events. The importance of the intense early metasomatic events was that they record the presence of a long-lived, deep-seated structure that focused fluids and assisted in providing the chemical and structural preparation for the development of the Arrow deposit.

Overall structural controls on mineralization at the Arrow deposit

The intimate relationship between brittle reactivated faults and unconformity-related uranium deposits has been recognized since the classic reports on the Rabbit Lake deposits by Hoeve and Sibbald (1978) and Hoeve et al. (1980) and are the starting point for nearly all exploration targeting in the Athabasca basin (Jefferson et al., 2007). Other structural studies on uranium deposits in the Athabasca basin (e.g., Lorilleux et al., 2002; Harvey and Bethune, 2007; Tourigny et al., 2007) have illustrated the importance of the development of subsidiary structures (e.g., cross structures, splays, bifurcations, extensional and compressional flexures, and breccia/cataclasite zones) within basement fault complexes for the focusing of fluid flow and ore deposition. For example, the various polyphase hydrothermal breccias associated with uranium mineralization in the southern part of the Shea Creek area mapped and described by Lorilleux et al. (2002) are similar to those encountered within the basement rock at the Arrow deposit and exemplify the importance of basement fault reactivations and ensuing development of permeable damage zones. The structural connections created through subsequent seismic events affecting preexisting basement and sandstone faults help induce fluid circulation and interaction and thus uranium mineralization.

The ductile structural framework (i.e., foliation development and folding), shear zone formation, alteration, and subsequent development and linkage through brittle reactivation and reuse of major structures are all integral components in

Downloaded from http://pubs.geoscienceworld.org/segweb/economicgeology/article-pdf/116/2/285/5245035/4797_hillacre_et_al.pdf
by Univ Nebraska Lincoln user

the genesis of the Arrow deposit (Fig. 22A-D). Each factor contributes to the production of favorable chemical conditions (i.e., reducing environment through deposition of graphite/sulfides and/or chloritization), as well as accommodation space and structural conduits through which hydrothermal fluids were able to deposit and remobilize uranium ore.

The initial formation of the uranium veins at Arrow is related to the reactivation and reuse of large- and small-scale primary and subsidiary structures formed through the prolonged evolution and post-Athabasca reactivation of the major A1 through A5 shears (Fig. 22D). Heterogeneous strain and partitioning during deformational episodes are observed through the stacked nature of the structural and mineral resource models (Figs. 8, 21), indicating a structural control on mineralization facilitated by the reactivation of preexisting structural weaknesses that are in suitable orientations to minimize work done (i.e., structures that may reactivate more easily based on their orientations relative to the active stress fields; e.g., oblique to the principal flattening surface). Oblique, crosscutting faults therefore most likely provided the necessary pathways for uranium-bearing fluids to penetrate and move along the reactivated brittle-ductile structural grain. Fluid flow and reactivation of mineralized structures then further concentrated, remobilized, and altered ore within previously established and newly formed subsidiary fractures, cataclasis zones, and shear and mylonite zones.

Implications for development of the Patterson Lake corridor

The present research at the Arrow deposit provides insights for the understanding of the overall structure and other uranium occurrences along the Patterson Lake corridor. The corridor is characterized by heterogeneous strain evidenced by fault rocks exhibiting characteristics reflecting multiple perturbation events. Thus, because of the heterogeneity in rheology related to alteration/metasomatism, the style and intensity of deformation and formation of suitable zones of dilation (e.g., reactivated constraining bends becoming releasing bends, Riedel fractures, and pull-apart basins) are not consistent along the corridor. Along the portion of the Patterson Lake corridor contained within the Rook I property, the highest concentrations of uranium appear to be associated with zones of higher structural disturbance, indicated by increased transposition of regional foliation due to shearing (i.e., steeper dip at Arrow; Figs. 6, 22B) and increased brittle reactivation of ductile structures and formation of Riedel shear fracture arrays (i.e., brecciation, cataclasis, and extensional fractures). The locations of the Triple R deposit and Spitfire discovery (Fig. 3) are also likely the result of heterogeneity (i.e., extent of brittle overprint and thus permeability) and periodicity of the deformation style (i.e., extensional vs. compressional, fault bends) along the Patterson Lake corridor. Overall, the fault/shear architecture appears to play a large role in the distribution of uranium mineralization along the Patterson Lake structural corridor, with fluid flux potentially highest in zones of widespread, permeable damage zones, in the core of which significant volumes of fluids precipitated uranium minerals (i.e., the A2 and A3 fault-fill high-grade cores; Fig. 21). The highly prospective Patterson Lake corridor represents only one of many subparallel corridors of heterogeneous strain in the southwest Athabasca region, with others such as the Derkson corridor (Fig. 3) remaining largely untested to date. The overall northeast-southwest orientation of the Patterson Lake corridor and others in the area also provides implications for the prospectivity of the corridors in the region, as a large majority of fault orientations hosting known uranium mineralization in the Athabasca basin strike northeast-southwest (Thomas et al., 2018).

This study provides the geologic, structural, and paragenetic framework for ongoing studies at the Arrow deposit and along the Patterson Lake corridor. The discovery of the Arrow and Triple R deposits, and this research, has sparked other work in the area, including structural studies of some of the other deposits along the Patterson Lake corridor (Abdelrazek et al., 2019; Johnstone et al., 2019) and regional geophysics, age, fluid inclusion, and isotopic studies (Potter et al., 2019; Rabiei et al., 2019).

Conclusions

The geologic relationships and structural history of the Patterson Lake corridor is exceedingly complex, spanning at minimum from the Paleoproterozoic (crystallization age of ca. 2.46 Ga; Card et al., 2014) to the Mesoproterozoic (U mineralization at ca. 1.45 Ga; Hillacre et al., 2018). The Patterson Lake corridor displays evidence of episodic structural reactivation and exhumation at progressively shallower crustal levels, related to the protracted tectonic evolution of the Precambrian shield in this region, and accompanied by various episodes of hydrothermal fluid flow with associated alteration and uranium mineralization, recrystallization, and remobilization. Arrow is a structurally controlled uranium deposit, hosted within a NE-SW–striking brittle-ductile deformation zone approximately 250 m wide, over 1 km in strike length, and more than 1 km in depth extent, which cuts Paleoproterozoic granulite facies rocks of the Taltson domain. Foliations within the Arrow deformation zone have been deflected and transposed, and the resulting anastomosing transposition foliation (S_1-S_3) accommodated protracted deformation along the zone, allowing for uranium mineralization to penetrate the reactivated shears. Plastic deformation within the major high-strain zones (A1-A5) provides evidence for early shearing under a ductile to brittle-ductile regime, whereas formation of Riedel shears and incohesive fault rocks indicates ongoing deformation through the brittle-ductile transition into a brittle regime. The prominence of these brittle rocks indicates prolonged reuse and reactivation of the preexisting A1 to A5 shear zones pre-, post-, and synmineralization, overprinting ductile deformational fabrics and incorporating angular clasts of ductile-deformed wall rock into their structure. Furthermore, highly altered and evolved fault gouge structures demonstrate that the portion of the Patterson Lake corridor hosting the Arrow deposit likely acted as a conduit for the movement of a significant volume of fluid over a substantial period of geologic time. Overall, there are aspects of the alteration stages identified through the paragenetic sequence at Arrow that are similar to other basement-hosted deposits in the eastern Athabasca basin. These include the presence of premineralization clinochlore and white mica, synmineralization muscovite, and syn- to postmineralization sudoite and dravite. In addition, the primary uraninite has been altered, and secondary uranium minerals precipitated in subsidiary

Downloaded from http://pubs.geoscienceworld.org/segweb/economicgeology/article-pdf/116/2/285/5245035/4797_hillacre_et_al.pdf
by Univ Nebraska Lincoln user

structures. However, we suggest the processes active within the portion of the Patterson Lake corridor hosting the Arrow deposit, such as softening of shear zones and metasomatism and/or hydrothermal alteration of host rocks, were a critical factor in preparing the ground for the formation of world-class, high-grade uranium deposits, such as Arrow.

Acknowledgments

The project was supported by NexGen Energy Ltd., and Natural Sciences and Engineering Research Council of Canada (NSERC) via a Collaborative Research and Development grant to Kevin Ansdell, and a Graduate Student Fellowship to Sean Hillacre from the Society of Economic Geologists Canada Foundation and Barrick Gold Corporation. Thanks to Robert Millar and Angela Cooper at Saskatchewan Research Council for thin section preparation and for providing laboratory space for mineralized sample sorting and preparation, and to Tom Bonli at the University of Saskatchewan Electron Microprobe Laboratory. NexGen Energy Ltd. provided unlimited access to drill core stored at the Arrow deposit and to their logging and geochemical database. The technical staff at the company, past and present, are thanked for insightful discussions and support. Colin Card and Dave Thomas are also thanked for discussions regarding the regional geology and structural interpretations, the latter serving as the external examiner for the thesis defense of Hillacre. James Sykes is thanked for his guidance and discussion during the early stages of this project, and Courtney Onstad, Jill Johnson, Robert Mohrbutter, and Sean Cross for their enthusiasm with supporting B.Sc. projects. The manuscript benefited greatly from the comments provided by the reviewers, Irvine Annesley, an anonymous referee, and Associate Editor Jonathan Cloutier, and the editorial suggestions of Larry Meinert. This paper is part of a Master of Science thesis completed by the senior author at the University of Saskatchewan.

REFERENCES

Abdelrazek, M., Benedicto, A., Ledru, P., and Gerbeaud, O., 2019, First insights on permeability development associated with uranium-rich mineralization of the Spitfire orebody, in the Patterson Lake corridor in western Athabasca, Canada: Geological Association of Canada-Mineralogical Association of Canada, Volume of Abstracts, v. 42, p. 52.

Adlakha, E.E., and Hattori, K., 2016, Paragenesis and composition of tourmaline types along the P2 fault and McArthur River uranium deposit, Athabasca basin, Canada: The Canadian Mineralogist, v. 54, no. 3, p. 661–667.

Adlakha, E.E., Hattori, K., Zaluksi, G., Kotzer, T., and Potter, E.G., 2014, Alteration within the basement rocks associated with the P2 fault and the McArthur River uranium deposit, Athabasca basin: Geological Survey of Canada, Open File 7462, 35 p., doi: 10.4095/293364.

Alexandre, P., Kyser, K., Polito, P., and Thomas, D., 2005, Alteration mineralogy and stable isotope geochemistry of Paleoproterozoic basement-hosted unconformity-type uranium deposits in the Athabasca basin, Canada: Economic Geology, v. 100, p. 1547–1563.

Alexandre, P., Kyser, K., and Jiricka, D., 2009, Critical geochemical and mineralogical factors for the formation of unconformity-related uranium deposits: Comparison between barren and mineralized systems in the Athabasca basin, Canada: Economic Geology, v. 104, p. 413–435.

Angelier, J., 1984, Tectonic analysis of fault slip data sets: Journal of Geophysical Research, v. 89, no. B7, p. 5835–5848.

Annesley, I.R., Madore, C., and Portella, P., 2005, Geology and thermotectonic evolution of the western margin of the Trans-Hudson orogen: Evidence from the eastern sub-Athabasca basement, Saskatchewan: Canadian Journal of Earth Sciences, v. 42, p. 573–597.

Ashton, K.E., Hartlaub, R.P., Heaman, L.M., Morelli, R.M., Card, C.D., Bethune, K., and Hunter, R.C., 2009, Post-Taltson sedimentary and intrusive history of the southern Rae province, along the northern margin of the Athabasca basin, western Canadian Shield: Precambrian Research, v. 175, p. 16–34.

Atmaoui, N., 2005, Development of pull-apart basins and associated structures by the Riedel shear mechanism: Insight from scaled clay analogue models: Unpublished Ph.D. thesis, Germany, Ruhr-University of Bochum, Institute of Geology, Mineralogy and Geophysics, 94 p.

Barthauer, G.L., Rulfs, C.L., and Pearce, D.W., 1953, Investigation of thucholite: American Mineralogist, v. 38, no. 9–10, p. 802–814.

Beyssac, O., and Rumble, D., 2014, Graphitic carbon: A ubiquitous, diverse, and useful geomaterial: Elements, v. 10, p. 415–420.

Bickford, M.E., Collerson, K.D., and Lewry, J.F., 1994, Crustal history of the Rae and Hearne provinces, southwestern Canadian Shield, Saskatchewan: Constraints from geochronologic and isotopic data: Precambrian Research, v. 68, p. 1–21.

Bosman, S.A., 2017, Uranium potential of Phanerozoic rocks: Stratigraphy and potential traps in the Patterson Lake region [abs.]: Saskatchewan Geological Survey (SGS), Saskatchewan Ministry of the Economy, Open House 2017 Abstract Volume, Miscellaneous Report 2017-3, p. 3.

Bosman, S.A., and Ramaekers, P., 2015, Athabasca Group + Martin Group = Athabasca Supergroup? Athabasca basin multiparameter drill log compilation and interpretation, with updated geological map: Saskatchewan Geological Survey, Miscellaneous Report 2015-4.2, Paper A-5, 13 p.

Bosman, S.A., Card, C.D., and Delaney, G., 2018, Phanerozoic stratigraphy of the Patterson Lake area, southwest margin of the Athabasca basin Saskatchewan: Implications for uranium exploration [abs.]: Resources for Future Generations, Vancouver, June 16–21, 2018, Technical Session EN14, Abstract 1807.

Bucher, K., and Frey, M., 1994, Petrogenesis of metamorphic rocks: Berlin, Springer-Verlag, 318 p.

Card, C.D., 2002, New investigations of basement to the western Athabasca basin: Saskatchewan Geological Survey, Saskatchewan Energy and Mines, Summary of Investigations 2002, v. 2, Miscellaneous Report 2002-4-2, Paper D-12, 17 p.

——2009, Cree South project 2009: Reconnaissance bedrock mapping in the Lloyd domain and Virgin River shear zone: Saskatchewan Geological Survey, Saskatchewan Ministry of Energy and Resources, Summary of Investigations 2009, v. 2, Miscellaneous Report 2009-4.2, Paper A-7, 21 p.

——2012a, A proposed domainal reclassification for Saskatchewan's Hearne and Rae provinces: Saskatchewan Geological Survey, Saskatchewan Ministry of the Economy, Summary of Investigations 2012, v. 2, Miscellaneous Report 2012-4.2, Paper A-11, 9 p.

——2012b, The origins of anomalously graphitic rocks and quartzite ridges in the basement to the southeastern Athabasca basin: Saskatchewan Geological Survey, Saskatchewan Ministry of the Economy, Summary of Investigations 2012, v. 2, Miscellaneous Report 2012-4.2, Paper A-6, 15 p.

——2017, Distribution and significance of crystalline rocks in the Patterson Lake uranium exploration corridor of northwest Saskatchewan: Saskatchewan Geological Survey, Saskatchewan Ministry of the Economy, Summary of Investigations 2017, v. 2, Miscellaneous Report 2017-4.2, Paper A-11, 18 p.

——2018, The Patterson Lake alkaline igneous complex: evidence for deep-seated structural control in the Patterson Lake corridor, and implications for mineral exploration: Saskatchewan Geological Survey, Saskatchewan Ministry of Energy and Resources, Summary of Investigations 2018, v. 2, Miscellaneous Report 2018-4.2, Paper A-9, 19 p.

Card, C.D., and Bosman, S.A., 2007, The Cree Lake South project: Reconnaissance bedrock mapping in the Mudjatik and Virgin River domains, and the Virgin River shear zone near the southwest margin of the Athabasca basin: Saskatchewan Geological Survey, Saskatchewan Ministry of Energy and Resources, Summary of Investigations 2007, v. 2, Miscellaneous Report 2007-4-2, Paper A-7, 22 p.

Card, C.D., and Noll, J., 2016, Host-rock protoliths, pre-ore metasomatic mineral assemblages and textures, and exotic rocks in the western Athabasca basin: Ore-system controls and implications for the unconformity-related uranium model: Saskatchewan Geological Survey, Summary of Investigations 2016, v. 2, Miscellaneous Report 2016-4.2, Paper A-8, 19 p.

Card, C.D., Pana, D., Stern, R.A., and Rayner, N., 2007, New insights into the geological history of the basement rocks to the southwestern Athabasca basin, Saskatchewan and Alberta: Geological Survey of Canada, Bulletin 588, p. 119–133.

Card, C.D., McEwan, B., and Bosman, S.A., 2008, The Cree Lake South project 2008: Regional implications of bedrock mapping along the Virgin

Downloaded from http://pubs.geoscienceworld.org/segweb/economicgeology/article-pdf/116/2/285/5245035/4797_hillacre_et_al.pdf
by Univ Nebraska Lincoln user

River transect: Saskatchewan Geological Survey, Miscellaneous Report 2008-4-2, Paper A-2, 23 p.
Card, C.D., Bethune, K.M., Davis, W.J., Rayner, N., and Ashton, K.E., 2014, The case for a distinct Taltson orogeny: Evidence from northwest Saskatchewan, Canada: Precambrian Research, v. 255, p. 245–265.
Card, C.D., Bosman, S.A., and Delaney, G., 2018, Are uranium deposits of the Athabasca basin more closely related to unconformities or to deep-seated structural control? [abs.]: Resources for Future Generations, Vancouver, June 16–21, 2018, Technical Session EN14, Abstract 1793.
Cerin, D., Götze, J., and Pan, Y., 2017, Radiation-induced damage in quartz at the Arrow uranium deposit, southwestern Athabasca basin, Saskatchewan: The Canadian Mineralogist, v. 55, p. 457–472.
Cloutier, J., Kyser, K., Olivo, G.R., Alexandre, P., and Halaburda, J., 2009, The Millennium uranium deposit, Athabasca basin, Saskatchewan, Canada: An atypical basement-hosted unconformity-related uranium deposit: Economic Geology, v. 104, p. 815–840.
Cloutier, J., Kyser, T.K., Olivo, G.R., and Brisbin, D., 2011, Geochemical, isotopic, and geochronologic constraints on the formation of the Eagle Point basement-hosted uranium deposit, Athabasca basin, Saskatchewan, Canada and recent remobilization of primary uraninite in secondary structures: Mineralium Deposita, v. 46, p. 35–56.
Cobbold, P.R., and Quinquis, H., 1980, Development of sheath folds in shear regimes: Journal of Structural Geology, v. 2, p. 119–126.
Davis, G.H., Bump, A.P., Garcia, P.E., and Ahlgren, G., 2000, Conjugate Riedel deformation band shear zones: Journal of Structural Geology, v. 22, p. 169–190.
Dewey, J.E., Holdsworth, R.E., and Strachan, R.A., 1998, Transpression and transtension zones: Continental transpressional and transtensional tectonics: Geological Society, London, Special Publication 135, p. 1–14.
Fayek, M., and Kyser, T.K., 1993, Petrography, chemical ages, stable isotopic compositions, and REE contents of three stages of uranium mineralization from the Athabasca basin: Saskatchewan Geological Survey, Saskatchewan Energy and Mines, Summary of Investigations 1993, Miscellaneous Report 93-4, p. 166–173.
Fayek, M., Harrison, T.M., Ewing, R.C., Grove, M., and Coath, C.D., 2002, O and Pb isotopic analyses of uranium minerals by ion microprobe and U-Pb ages from the Cigar Lake deposit: Chemical Geology, v. 185, p. 205–225.
Fission Uranium Corporation, 2018, Fission increases indicated resource; doubles inferred resource: Press release, February 20, 2018, www.fission-uranium.com/project/triple-r-deposit/news/index.php?content_id=629.
Haakon, F., 2010, Structural geology: New York, Cambridge University Press, 463 p.
Harvey, S.E., and Bethune, K.M., 2007, Context of the Deilman orebody, Key Lake mine, Saskatchewan: Geological Survey of Canada Bulletin 588, p. 249–266.
Hillacre, S., 2018, Structural analysis, paragenesis, and geochronology of the Arrow uranium deposit, western Athabasca basin, Saskatchewan, Canada: Implications for the development of the Patterson Lake corridor: M.Sc. thesis, Saskatoon, Saskatchewan, University of Saskatchewan, 163 p.
Hillacre, S., Ansdell, K., and McNamara, G., 2018, Uraninite geochronology of the Arrow uranium deposit, Patterson Lake corridor, Saskatchewan: Resources for Future Generations, Vancouver, June 16–21, 2018, Technical Session EN14, Abstract 2095.
Hoeve, J., and Quirt, D., 1984, Mineralization and host rock alteration in relation to clay mineral diagenesis and evolution of the Middle Proterozoic Athabasca basin, northern Saskatchewan, Canada: Saskatchewan Research Council, Technical Report 187, 186 p.
Hoeve, J., and Sibbald, T.I.I., 1978, On the genesis of Rabbit Lake and other unconformity-type uranium deposits in northern Saskatchewan, Canada: Economic Geology, v. 73, p. 1450–1473.
Hoeve, J., Sibbald, T., Ramaekers, P., and Lewry, J., 1980, Athabasca unconformity-type uranium deposits: A special class of sandstone-type deposits? *in* Ferguson, S., and Goleby, A., eds., Uranium in the Pine Creek geosyncline: Proceedings of the International Uranium Symposium on the Pine Creek Geosyncline: Vienna, International Atomic Energy Agency (IAEA), p. 575–594.
Hoffman, P.F., 1988, United plates of America, The birth of a craton: Early Proterozoic assembly and growth of Laurentia: Annual Review of Earth and Planetary Sciences, v. 16, p. 543–603.
Holcombe Coughlin and Associates (HCA), 2007, Oriented core manual: www.holcombecoughlin.com/HCA_downloads.
Imber, J., Holdsworth, R., Smith, S.A.F., Jefferies, S.P., and Collettini, C., 2008, Frictional-viscous flow, seismicity and the geology of weak faults: A review and future directions: Geological Society, London, Special Publication 299, p. 151–173.
Jeanneret, P., Goncalves, P., Durand, C., Poujol, M., Trap, P., Marquer, D., Quirt, D., and Ledru, P., 2017, Geochronological constraints on the trans-Hudsonian tectono-metamorphic evolution of the pre-Athabasca basement within the Wollaston-Mudjatik transition zone, Saskatchewan: Precambrian Research, v. 301, p. 152–178.
Jefferson, C.W., Thomas, D.J., Gandhi, S.S., Ramaekers, P., Delaney, G., Brisbin, D., Cutts, C., Portella, P., and Olson, R.A., 2007, Unconformity-associated uranium deposits of the Athabasca basin, Saskatchewan and Alberta: Geological Survey of Canada, Bulletin 588, p. 23–68.
Johnstone, D., Bethune, K., and Tschirhart, V., 2019, The structural and lithological evolution of the Patterson Lake corridor, southwestern Athabasca basin: Geological Association of Canada-Mineralogical Association of Canada, Volume of Abstracts, v. 42, p. 117.
Katz, Y., Weinbergerb, R., and Aydinc, A., 2004, Geometry and kinematic evolution of Riedel shear structures, Capitol Reef National Park, Utah: Journal of Structural Geology, v. 26, p. 491–501.
Kister, P., Vieillard, P., Cuney, M., Quirt, D., and Laverret, R., 2005, Thermodynamic constraints on the mineralogical and fluid composition in a Proterozoic clastic sedimentary basin: The Athabasca basin (Saskatchewan, Canada): European Journal of Mineralogy, v. 17, p. 325–342.
Kotzer T., and Kyser, T.K., 1995, Petrogenesis of the Proterozoic Athabasca basin, northern Saskatchewan, Canada, and its relation to diagenesis, hydrothermal uranium mineralization and paleohydrogeology: Chemical Geology, v. 120, p. 45–89.
Lazarte, C.A., and Bray, J.D., 1996, A study of strike-slip faulting using small-scale models: Geotech Testing Journal, v. 19, p. 118–129.
Lewry, J.F., and Sibbald, T.I.I., 1977, Variation in lithology and tectonometamorphic relationships in the Precambrian basement of northern Saskatchewan: Canadian Journal of Earth Sciences, v. 14, p. 1453–1467.
Lorilleux, G., Jebrak, M., Cuney, M., and Baudemont, D., 2002, Polyphase hydrothermal breccias associated with unconformity-related uranium mineralization (Canada): From fractal analysis to structural significance: Journal of Structural Geology, v. 24, p. 323–338.
Luque, F.J., Huizenga, J-M., Crespo-Feo, E., Wada, H., Ortega, L., and Barrenechea, J.F., 2014, Vein graphite deposits: geological settings, origin, and economic significance: Mineralium Deposita, v. 49, p. 261–277.
MacDonald, C.C., 1980, Mineralogy and geochemistry of a Precambrian regolith in the Athabasca basin: M.Sc. thesis, Saskatoon, Saskatchewan, University of Saskatchewan, 151 p.
Mercadier, J., Richard, A., Bioron, M-C., Cathelineau, M., and Cuney, M., 2010, Migration of brines in the basement rocks of the Athabasca basin through microfracture networks (P-Patch U deposit, Canada): Lithos, v. 115, p. 121–136.
Mohrbutter, R., Hillacre, S.E., Ansdell, K.M., and Batty, M., 2018, Precious metals in the Arrow uranium deposit, Patterson Lake corridor, southwestern Athabasca basin, Saskatchewan, Canada [abs.]: SEG Conference 2018: Metals, Minerals, and Society, Keystone, Colorado, September 23, 2018, Poster P.197, www.segabstracts.org/abstract_summary.php?mode=public&abs_id=1429.
Moores, E.M., and Twiss, R.J., 1997, Tectonics: Long Grove, Illinois, Waveland Press, Inc., p. 403.
Naylor, M.A., Mandl, G., and Sijpesteijn, C.H.K., 1986, Fault geometries in basement-induced wrench faulting under different initial stress states: Journal of Structural Geology, v. 8, p. 737–752.
Norris, A.W., 1963, Devonian stratigraphy of northeastern Alberta and northwestern Saskatchewan: Geological Survey of Canada, Memoir 313, 168 p.
O'Hara, P., Cox, J., Robson, D.M., and Mathisen, M., 2018, Pre-feasibility study of the Arrow deposit, Rook I property, Saskatchewan, Canada: NI 43-101 Technical Report prepared by Wood and RPA for NexGen Energy Ltd., effective date November 5, 2018, 269 p.
Onstad, C., Hillacre, S.E., Ansdell, K.M., McEwan, B., and McNamara, G., 2017, Geochemical analysis of host rock lithologies at the Arrow uranium deposit, Athabasca basin, Saskatchewan: Interpretation of protolith and alteration [abs]: Prospectors and Developers Association of Canada-Society of Economic Geologists (PDAC-SEG) Student Minerals Colloquium 2017, Toronto, Ontario, March 6, 2017, Poster Presentation.
Passchier, C.W., and Trouw, R.A.J., 2005, Microtectonics, 2nd ed.: Heidelberg, Springer Verlag, 366 p.
Peterson, T.D., Van Breemen, O., Sandeman, H., and Cousens, B., 2002, Proterozoic (1.85–1.75 Ga) igneous suites of the Western Churchill province:

Downloaded from http://pubs.geoscienceworld.org/segweb/economicgeology/article-pdf/116/2/285/5245035/4797_hillacre_et_al.pdf
by Univ Nebraska Lincoln user

Granitoid and ultrapotassic magmatism in a reworked Archean hinterland: Precambrian Research, v. 119, p. 73–100.
Potter, E., Tschirhart, V., Powell, J., Rabiei, M., Johnstone, D., Kelly, C., Pehrsson, S., Chi, G., Bethune, K., Craven, J., et al., 2019, Formation of unconformity-related uranium deposits: Insights from integrated multidisciplinary studies of the Patterson Lake corridor, northern Saskatchewan: Saskatchewan Geological Survey, Saskatchewan Ministry of Energy and Resources, Miscellaneous Report 2019-3, p. 3.
Quirt, D., 1999, The significance of green sandstones and illite-chlorite mixed-layer clay-bearing sandstones of the Athabasca Group in the Close Lake-McArthur River area (NTS 74H): Saskatchewan Geological Survey, Saskatchewan Energy and Mines, Summary of Investigations 1999, v. 2, Miscellaneous Report 99-4.2, p. 121–131.
Rabiei, M., Chi, G., Potter, E., Tschirhart, V., Feng, R., MacKay, C., Frostad, S., McElroy, R., Ashley, R., and McEwan, B., 2019, Evolution of hydrothermal fluids in the Patterson Lake corridor, southwestern Athabasca basin: Significance for uranium mineralization: Geological Association of Canada-Mineralogical Association of Canada, Volume of Abstracts, v. 42, p. 163.
Ramaekers, P., 1979, Stratigraphy of the Athabasca basin: Saskatchewan Geological Survey, Summary of Investigations 1979, Miscellaneous Report 79-10, p. 154–160.
——1980, Stratigraphy and tectonic history of the Athabasca Group (Helikian) of northern Saskatchewan: Saskatchewan Geological Survey, Summary of Investigations 1980, Miscellaneous Report 80-4, p. 99–106.
Ramaekers, P., Jefferson, C.W., Yeo, G.M., Collier, B., Long, D.G.F., Catuneanu, O., Bernier, S., Kupsch, B., Post, R., Drever, G., et al., 2007, Revised geological map and stratigraphy of the Athabasca Group, Saskatchewan and Alberta: Geological Survey of Canada, Bulletin 588, p. 155–191.
Reid, K.D., Ansdell, K., Jiricka, D., Witt, G., and Card, C.D., 2014, Regional setting, geology, and paragenesis of the Centennial unconformity-related uranium deposit, Athabasca basin, Saskatchewan, Canada: Economic Geology, v. 109, p. 539–566.
Riedel, W., 1929, Zur mechanik geologischer Brucherscheinungen: Zentralblatt Mineral Geol Paläont B, p. 354–368.
Rosenberg, P.E., and Foit, F.F., 2006, Magnesiofoitite from the uranium deposits of the Athabasca basin, Saskatchewan, Canada: The Canadian Mineralogist, v. 44, no. 4, p. 959–965.
Rumble, D., 2014, Hydrothermal graphitic carbon: Elements, v. 10, p. 427–433.
Saskatchewan Ministry of Energy and Resources, 2019, Saskatchewan mining and petroleum GeoAtlas: https://gisappl.saskatchewan.ca/Html5Ext/index.html?viewer=GeoAtlas, accessed October 18, 2019.
Schmid, S.M., and Handy, M.R., 1991, Towards a genetic classification of fault rocks: Geological usage and tectonophysical implications, *in* Müller, D.W., McKenzie, J.A., and Weissert, H., eds., Controversies in modern geology: Evolution of geological theories in sedimentology, earth history and tectonics: London, Academic Press, p. 339–361.
Seifert, W., Rhede, D., Thomas, R., Forster, H.J., Lucassen, F., Dulski, P., and Wirth, R., 2011, Distinctive properties of rock-forming blue quartz: Interferences from a multi-analytical study of submicron mineral inclusions: Mineralogical Magazine, v. 75, no. 4, p. 2519–2534.
Sheahan, C., Fayek, M., Quirt, D., and Jefferson, C.W., 2016, A combined ingress-egress model for the Kianna unconformity-related uranium deposit, Shea Creek project, Athabasca basin, Canada: Economic Geology, v. 111, p. 225–257.
Sibbald, T., 1974, La Loche (north) area: Reconnaissance geological survey of 74C-NW and 74C-NE: Summary Report of Field Investigations by the Saskatchewan Geological Survey, Saskatchewan Department of Mineral Resources, p. 38–45.
——1985, Geology and genesis of Athabasca basin uranium deposits: Summary of Investigations 1985, Saskatchewan Geological Survey, Saskatchewan Energy and Mines, Miscellaneous Report 85-4, p. 133–156.
Stern, R.A., Card, C.D., Pana, D., and Rayner, N., 2003, SHRIMP U-Pb ages of granitoid basement rocks of the southwestern part of the Athabasca basin, Saskatchewan and Alberta: Geological Survey of Canada, Radiogenic Age and Isotopic Studies, Report 16, Current Research 2003-F, 20 p.
Sykes, J., Rozdilsky, S., Kocay, J., Browne, A., and Ainsworth, G., 2014, Arrow: A new high-grade uranium discovery in an emerging district [abs.]: Saskatchewan Geological Survey Open House 2014, Saskatoon, December 1–3, 2014, Abstract Volume, p. 34.
Tchalenko, J.S., 1968, The evolution of kink-bands and the development of compression textures in sheared clays: Tectonophysics, v. 6, p. 159–174.
——1970, Similarities between shear zones of different magnitudes: Geological Society of America Bulletin, v. 81, p. 1625–1640.
Terzaghi, R.D., 1965, Sources of error in joint surveys: Geotechnique, v. 15, p. 287–304.
Thomas, D., Aubin, A., and Zaluski, G., 2018, What does an Athabasca basin uranium deposit footprint look like? [abs.]: Resources for Future Generations, Vancouver, June 16–21, 2018, Technical Session EN14.
Tourigny, G., Quirt, D.H., Wilson, N.S.F., Wilson, S., Breton, G., and Portella, P., 2007, Geological and structural features of the Sue C uranium deposit, McLean Lake area, Saskatchewan: Geological Survey of Canada, Bulletin 588, p. 229–247.
Tremblay, L.P., 1982, Geology of the uranium deposits related to the sub-Athabasca unconformity, Saskatchewan: Geological Survey of Canada, Paper 81-20, 56 p.
Trouw, R.A.J., Passchier, C.W., and Wiersma, D.J., 2009, Atlas of mylonites and related microstructures: Heidelberg, Springer Verlag, 322 p.
Tschirhart, V., Pehrsson, S., Card, C., Potter, E., Powell, J., and Pana, D., 2020, Interpretation of buried basement in the southwestern Athabasca basin, Canada, from integrated geophysical and geological datasets: Geochemistry: Exploration, Environment, Analysis, doi: 10.1144/geochem2019-061.
Whitney, D.L., and Evans, B.W., 2010, Abbreviations for names of rock-forming minerals: American Mineralogist, v. 95, p. 185–187.
World Nuclear Association, 2018, Uranium in Canada: www.world-nuclear.org/information-library/country-profiles/countries-a-f/canada-uranium.aspx, updated November 2018, accessed November 18, 2018.
Yeo, G.M., and Delaney, G., 2007, The Wollaston Supergroup, stratigraphy and metallogeny of a Paleoproterozoic Wilson cycle in the Trans-Hudson orogen, Saskatchewan: Geological Survey of Canada, Bulletin 588, p. 89–97.
Yeo, G.M., and Potter, E.G., 2010, Review of reducing mechanisms potentially involved in the formation of unconformity-type uranium deposits and their relevance to exploration: Saskatchewan Geological Survey, Saskatchewan Ministry of Energy and Resources, Summary of Investigations 2010, v. 2, Miscellaneous Report 2010-4.2, Paper A-12, 13 p.
Zolensky, M.E., Sylvester, P.J., and Paces, J.B., 1988, Origin and significance of blue coloration in quartz from Llano rhyolite (llanite), north-central Llano County, Texas: American Mineralogist, v. 73, p. 313-323.



Sean Hillacre has worked as an exploration geologist in the Athabasca basin uranium district in Saskatchewan for the last five years since receiving his B.Sc. (High Honors) degree in geology in 2015 from the University of Saskatchewan. In 2018, he obtained his M.Sc. degree while working full time for NexGen Energy Ltd. as part of the team progressing the Arrow uranium deposit toward production. With his supervisor, he led several research projects contributing to the understanding of uranium ore genesis in the southwestern Athabasca basin while completing his graduate studies focused on the structural and paragenetic characteristics of the Arrow deposit and Patterson Lake corridor. His research focuses on structural geology and controls on ore deposits, taking an interdisciplinary approach to develop applications toward mineral exploration.

Downloaded from http://pubs.geoscienceworld.org/segweb/economicgeology/article-pdf/116/2/285/5245035/4797_hillacre_et_al.pdf
by Univ Nebraska Lincoln user

Downloaded from http://pubs.geoscienceworld.org/segweb/economicgeology/article-pdf/116/2/285/5245035/4797_hillacre_et_al.pdf
by Univ Nebraska Lincoln, user